A NOVEL MICROFABRICATION TECHNIQUE FOR DEVELOPMENT OF A 3D PYRAMIDAL POROUS MEMBRANE

SHASHI RANJAN

(B.Eng., Birla Institute of Technology, Ranchi, India)

A THESIS SUBMITTED

FOR THE DEGREE OF DOCTOR OF PHILOSPHY

DIVISION OF BIOENGINEERING

NATIONAL UNIVERSITY OF SINGAPORE

2011

Acknowledgements

A spark of Philosophy got ignited in my mind when I gratefully wanted to acknowledge every drop of effort that has made my long cherished dream of being a part of great scientific adventure come true through this Doctorate of Philosophy study. When I started collecting these drops together it became an ocean, in which I swam back to the antiquity of "Big Bang" that set a new beginning of our Universe and to the Creation that started at the 'Time zero' to bring forth all that exist at this moment. I feel grateful to the creation of 'The Planet Earth' in which 'Mother Nature' gave birth to 'the life' that began its greatest journey on the steps of evolution to manifest a wonderful treasure in from of 'Human Mind'. The Mind which is endowed with the power of thought and enquiry that led to all scientific discoveries and inventions. I also feel grateful to the long history of human beings with immense amount of knowledge accumulated over time that has shaped the current scenario of research and developments. Then I feel grateful to everyone who has contributed to science in some or other way to shape the current state-of-art of research. Furthermore, I recognize the value and efforts of all schools, colleges and teachers who have educated me and have made me suitable for conducting research.

With special regard I heartily acknowledge National University of Singapore, Faculty of Engineering and Division of Bioengineering for providing me uninterrupted financial, technical and administrative support during the course of my PhD study. I would also like to express my gratefulness towards Institute of Materials Research and Engineering (IMRE) for providing me research facilities.

Now, let me gratefully acknowledge support and valuable guidance from my supervisor A/P Zhang Yong. He has played a special role in during my PhD training by putting his time, energy and efforts to cautiously guide me in right direction. I am indebted for his contributions towards my PhD study. I am also grateful to Dr. Tamil Selvan Subramanian who has guided me as my co-supervisor and has provided me highly sophisticated research facilities.

I would like express my gratitude towards Prof. Lim Chwee Teck, Asst. Prof Zhou Guangya and Prof. Seeram Ramakrishna for allowing me to use research facilities in their laboratory. I also express my due regard to Asst. Prof. Partha Roy and Asst. Prof. Evelyn Yim for being examiners for my written as well as oral Qualifying examination and I appreciate their suggestions that they gave me during these exams.

My special thanks to Dr. Lim Chee Tiong for teaching me microfabrication techniques, sharing his experience, giving me suggestions and for many insightful discussions. I am very thankful to all members of my lab who have helped in a lot during course of my PhD study. Their contribution is appreciated.

It is a grateful moment that fills my heart with gratitude to end my acknowledgement letter by expressing my deepest regard to my parents who have been my source of inspiration throughout my life and my warmest gratitude to my family and friends for their constant support in all aspects of my life.

Shashi Ranjan,

12 August 2011

List of Publications and Awards

Journal Publications:

- **Ranjan, S.**, Zhang,Y., 3D microlithography based on partial activation in materials, *Sensors and Actuators A- Physical*, 2012, *Under Review*

- **Ranjan, S**., Selvan, ST, Zhang,Y**.,** An anti-clogging 3D Porous Membrane for sorting and pattering of micro-entities, *Advanced Healthcare Materials, 2012, Accepted*

Patents:

- **US Provisional Application No. 61/491,395**
  "A Novel 3D Pyramidal Porous Membrane and its Applications Thereof"

Presentations:

- **Ranjan, S.**, Zhang,Y., A micro-fluidic device for cell and bead-based biosensor, *4th East Asian Pacific Workshop on Nano-Biomedical Engineering*, Dec. 2010 (Oral Presentation)

- **Ranjan, S.**, Subramanian, T. S., Zhang,Y., A novel finding of remarkable cross-linking behavior of a photo-sensitive material, *IMRE PG student poster presentation*, Sep. 2010 (Poster Presentation)

- **Ranjan, S.**, Tiong, C.T., Subramanian, T. S., Zhang,Y Fabrication of 3D Structures by Photolithography to Create Single Bead Micro-array, *IMRE PG student poster presentation*, July, 2009 (Poster Presentation)

- **Ranjan, S.,** Zhang, Y., Novel three-dimensional porous film for single-cell microarray applications, *Techconnect world, Santa Clara, CA, USA*. 2012

- **Ranjan, S.,** Zhang, Y., Capture of circulating tumor cells (CTCs) using a novel micro-device, *Techconnect world, Santa Clara, CA*, USA. 2012

Awards:

- Oral Presentation Award in the 4th East Asian Pacific Workshop on Nano-Biomedical Engineering, Dec. 2010

Table of Contents

Summary

Three-dimensional (3D) microfabrication has a niche role in emerging technologies as essential components of various MEMS and biomedical applications such as micro-lens array, photonic crystals, micro-filters, cell sorters, bio-sensing and tissue engineering. However, the 3D microfabrication is quite challenging as it requires simultaneous control over fabrication of lateral as well as vertical dimensions of microstructures. To achieve such control, highly localized light exposure in photosensitive materials is sought in existing 3D microfabrication techniques. The exposed regions cross-link and microstructures are fabricated according to pattern of the exposure. However, this strategy is complicated, expensive and slow as it employs point-to-point or layer-by-layer exposure pattern which requires highly sophisticated and expensive equipments. Herein, it is hypothesized that controlling the cross-linking instead of the exposure would help in developing a simple 3D microfabrication technique. The cross-linking in lateral dimensions can be easily controlled by exposing photosensitive material through a binary coded photo-mask (as in photolithography). Nonetheless, controlling the light exposure or cross-linking in vertical dimension is not possible by using a normal photo-mask due to 'all-or-none' exposure pattern leading to complete cross-linking of the exposed region. Hence, a new strategy involving partial activation (PA) has been developed in this study for controlling cross-linking in both dimensions using photo-mask based exposure system. PA represents a state of material in which slight activation of cross-linking initiators is generated but the amount of such initiators is not enough for inducing cross-linking reaction. In such a state, cross-linking can only take place under certain special conditions. The cross-linking in the PA is different from normal cross-linking and is

favored in certain configuration (anisotropic). Such a cross-linking pattern can provide opportunities for 3D microfabrication which can be modulated by simple parametric control such as exposure energy or baking temperature. Thus, this strategy allows fabrication of 3D microstructures besides retaining the speed and the simplicity of photo-mask exposure scheme. Different types of 3D microstructures have been fabricated by using a single inexpensive photo-mask at high throughput in this project. To the best of our knowledge, the study on the PA as well as the 3D microfabrication based on materials' properties has not been reported in past.

The purpose of the 3D microfabrication technique in this project is to develop a functional micro-device for sorting and patterning of micro-entities such as cells or beads which is useful for disease diagnosis and treatment. Cell-sorting and patterning is an essential step in various diagnosis and prognosis applications such as sorting blood cells from the plasma, sorting rare cells (tumor or epithelial) from the blood, sorting stem cells from amniotic fluid and single cell studies. Bead-sorting and patterning is useful for immunoassays. The existing techniques for sorting or patterning of micro-entities using external forces such as dielectrophoretic, magnetic, optical however, are expensive, requires tagging of micro-entities and living cells are subjected to electromagnetic field with unknown implications. Other simpler alternative is the use of micro-filters, but their drawback is low throughput or unclean sorting. Amongst micro-filters, porous membrane presents the simplest option besides having high throughput performance. However, pore clogging is a common drawback in using porous membrane which adversely affects its performance. Herein, a unique anti-clogging three-dimensional (3D) pyramidal porous membrane (3DPPM) with multiple functionalities for enhanced performance has been

developed by using newly developed 3D microfabrication technique. The 3DPPM consists of an array of funnel-like pores, wherein each pore is surrounded by four 3D pyramidal micro-structures. The fabrication of such an arrangement of structures requires integration of different 3D microstructures which is challenging. To overcome these problems, a method involving non-uniform distribution and self-polymerization of the PA in micro-space has been developed in this study. The 3DPPM thus developed in this project has been integrated with a micro-channel to develop a functional microfluidic device.

The design of the 3DPPM developed in this project confers four useful features. 1) It is anti-clogging and therefore allows uninterrupted sorting of micro-entities continuously; 2) Simultaneous sorting and patterning of micro-entities can be achieved for downstream analysis of the patterned micro-entities; 3) Inhomogeneous cell population of different sizes can be patterned or trapped between the 3D microstructures for single-cell studies; 4) Bi-directional sorting can be achieved, both in the direction of fluid-flow through the pores as well as that perpendicular to it, for high sorting efficiency. All these four features of 3DPPM have been studied in this project by using cells and micro-beads. Moreover, the cell viability has also been studied to prove that the 3DPPM is useful for cell-based applications.

List of Tables

List of Figures

List of Illustrations

List of Acronyms

CCD: Charged Coupled Device

DEP: Dielectrophoresis

DLD: Deterministic Lateral Displacement

DMEM: Dulbecco's Modified Eagle's Medium

DI: De-ionized

FBS: Fetal Bovine Serum

FTIR: Fourier Transfrom Infra Red Spectroscopy

HMDS: Hexamethyldisilazane

IPA: Iso-propyl Alcohol

IR: Infra Red

PBS: Phosphate Buffer Saline

PDMS: Poly(dimethylsiloxane)

PEB: Post Exposure Bake

PI: Porpidium Iodide

PA: Partial Activation

SEM: Scanning Electron Microscopy

UV: Ultra Violet

2D: Two Dimensional

3D: Three Dimensional

3DPPM: 3D Pyramidal Porous Membrane

Chapter-1: Introduction

Chapter-1: Introduction

1.1 OVERVIEW

The advancement in micro-technology has presented various techniques for fabrication of microstructures [1]. Among these microstructures, three-dimensional (3D) microstructures have an important niche in micro-technologies. 3D microstructures are defined as structures in which lateral dimensions vary with vertical dimension. These structures are being used in various research fields such as MEMS, Optical systems and biomedical devices. The fabrication of such structures require simultaneous control over lateral as well as vertical dimensions of microstructures formed and thus 3D microfabrication is challenging [2]. Though, a number of techniques have been reported for 3D microfabrication, but, these are limited by high cost, low throughput and need for highly sophisticated equipment. Such limitations surface due to current approach in which highly localized light exposure in a photosensitive material is sought to control position or distribution of the light exposure in lateral and vertical dimensions. The exposed region cross-links and microstructures are fabricated according to pattern of the exposure. However, this method requires highly sophisticated and expensive equipment which limits their wide spread acceptance. Also, such techniques have low throughput. For example, Two-photon photo-polymerization employs point-to-point exposure (slow) by using highly controlled light exposure system (expensive) for 3D microfabrication. Other laser-based techniques such as polymerization, ablation or deposition of materials by laser, holographic lithography or stereolithography are also slow and complicated as they employ layer-by-layer fabrication approach. Gray-scale lithography is another alternative but need for a special and expensive photo-mask is the limiting factor for this

technology (details of these techniques have been covered in chapter-2). Other unconventional 3D microfabrication techniques, like inclined/rotated photolithography or silicon micro-machining are limited to the fabrication of few types of 3D microstructures and it may require special fabrication arrangements. Thus, the need for a simple, inexpensive and high throughput technique for 3D microfabrication is evident. Herein, a novel 3D microfabrication technique has been developed. This method is based on the partial activation (PA) of material which does not require sophisticated equipment or facilities.

The development of 3D microstructures can be useful if they can be integrated in a functional micro-device to solve some technical or scientific problems. One such problem would be pore clogging in porous membranes. The porous membranes are being used commonly for filtration and separation applications in different areas of research and industrial processes such as waste-water treatment, cell-separation and sterilization. However, pore clogging or fouling is drawback in using porous membranes, which greatly affects their performance by decreasing productivity and by increasing operational and maintenance cost [3-5]. The pore clogging is caused due to blockage of the pores by filtered particles which drastically reduce fluid flow through pores. This causes increase in flow-resistance and fluidic pressure over the membrane. The increasing pressure may have adverse effects on the filtered materials such as living cells, besides decreasing filtration efficiency. To overcome this, there is a need for anti-clogging porous membrane such that filtered particles do not block the pores. Herein, an anti-clogging 3D porous membrane has been developed for sorting and patterning of micro-entities (cells and beads).

1.2 THE IDEA AND THE HYPOTHESIS

As mentioned in the previous section that the existing 3D microfabrication techniques are complicated, expensive and slow. The main challenge in the 3D microfabrication is to simultaneously control the cross-linking in vertical as well as lateral dimensions. Nevertheless, the cross-linking in lateral dimensions alone can be easily controlled by exposing a photosensitive material through a binary coded photo-mask (normally used for photolithography). A 2D pattern drawn on the photo-mask allows control of the light exposure in lateral dimensions, but it is not possible to control it in vertical dimension due to 'all-or-none' pattern of exposure through such photo-masks. Thus, controlling cross-linking in vertical dimensions in this situation by some simple means, without requiring control over the exposure in vertical dimension, may allow fabrication of 3D microstructures by simpler methods. However, the exposed region cross-links completely that makes it rigid, restricting further manipulation in the cross-linked regions. Hence, complete cross-linking should be avoided in the exposed region which may allow manipulation or alteration of the cross-linking in the exposed region. Herein, it is hypothesized that 'partial activation' (PA) would provide opportunity to manipulate the pattern of cross-linking in the exposed region which may allow control over the fabrication in vertical dimension besides lateral dimensions. PA represents a state of partial activation of the material which is not enough for initiating cross-linking reaction and unstable bonding or connection between cross-linking molecules may exist. Such weak connections between molecules may allow anisotropic cross-linking into some

stable or favorable configurations. If such anisotropic cross-linking is modulated by simple methods, a new technique for 3D microfabrication may be developed.

The hypothesis for developing 3D microfabrication technique:

1. The partial activation may allow control over the cross-linking of the exposed material.
2. Partially activated material may allow anisotropic cross-linking into certain favorable configurations which may be helpful in the fabrication of 3D microstructures.

The next aim of this project is to develop an anti-clogging 3D porous membrane for simultaneous sorting and patterning of micro-entities. The 3D microstructures can be integrated in the porous membrane in such a way that each pore in the porous membrane is surrounded by these structures. Such integration would create micro-traps over pores. The micro-entities such as cells or beads can be trapped in the micro-traps during filtration which would not block the pore leaving an interstitial-gap between trapped micro-entity and the pore. Such interstitial-gap would allow fluid or smaller micro-entity to pass through without clogging the pore. Moreover, such membrane would also allow patterning of micro-entities.

The hypothesis for integration of 3D microstructures in a porous membrane:

1. A novel anti-clogging 3D porous membrane can be fabricated by integrating 3D microstructures developed by the partial activation method.

2. The 3D porous membrane thus developed can be integrated in microfluidic device for developing a new device for patterning and sorting of micro-entities (Cells/beads).

1.3 OBJECTIVES AND SPECIFIC AIMS

Main Objective: To develop a 3D microfabrication technique for the fabrication of an anti-clogging 3D porous membrane for sorting and patterning of micro-entities.

Specific Aims: The main objective of this project can be accomplished by completing three specific aims of this project. Each specific aim is divided in few milestones that gauge their completion.

Specific aim 1: To develop a 3D microfabrication technique based on the PA in a photo-sensitive material.

Milestone-1: To study the characteristics partially activated material.

Milestone-2: To develop new methods to control such cross-linking for fabrication of different 3D microstructures.

Specific-aim 2: To design and fabricate 3D pyramidal porous membrane by the technique developed in specific aim 1.

Milestone-1: To develop a method for integration of 3D pyramidal microstructures in a porous membrane.

Milestone-2: To integrate this membrane in a micro-fluidic device.

Specific-aim 3: To study multi-functionality of the micro-device developed in specific aim 2.

Milestone-1: To study the anti-clogging of the membrane integrated in the micro-device.

Milestone-2: To study simultaneous sorting and patterning of micro-entities in the micro-device.

Milestone-3: To study patterning of micro-entities of different sizes in the micro-device.

1.4 THE SCOPE

This project incorporates study of the PA in materials and its application in developing a new technology. The PA and its properties have not been reported in past. This study has demonstrated a unique property of molecular re-arrangement within the PA, which has helped in devising a new 3D microfabrication technique. The 3D microfabrication technique can be adapted in different laboratories that do not require access to advanced resources. It may be exciting for scientists working in the optical-MEMS field for development of new class of micro-lens array and micro-lens with different properties. It may also be useful to researchers working in the MEMS field for developing devices with flexible and movable parts. The research can especially be useful to bioengineers for cell-based applications such as studying cell-surface interaction, cell-growth on 3D topographies. Thus, we believe that this work should have wide scope in different fields of science and technology.

The second part of the work involves the development of a unique 3D pyramidal porous membrane. One of the interesting features of this porous membrane is its 'anti-clogging' characteristics. This porous membrane can be an interesting tool for studying the fundamental filtration process as it draws attention to a new concept of 'anti-clogging'. The other exciting feature of this porous membrane is its ability to simultaneously sort and pattern micro-entities. It has been used for bead/cell sorting and patterning in this project. Beads patterning is gaining importance in multiplex detection and in-vitro diagnosis. Cell sorting is clinically important while patterning of cells is important for understanding cells behavior and for single-cell studies. Thus, this 3D porous membrane can have different applications such as sorting cancerous cells from blood, separation of blood cell subtypes and single-cell studies. Moreover, the patterned array beads can be useful for multiplex disease diagnosis. Thus, the achievement of this project can be useful for biological studies as well as biomedical applications.

Chapter-2: Literature Review

Chapter-2: Literature Review

2.1 THE OVERVIEW:

This chapter on literature review deals with technical know-how related to various aspects of this project. The purpose of this literature review is to provide a general overview of works that have been published in the past and are related to the work done in this project. The review presented here is not exhaustive and does not claim to include all related articles. This review starts with discussing the state-of-art and other techniques that have been used for 3D microfabrication. Problems and short-comings of existing techniques have also been discussed here with the aim of highlighting the gap in the current technological developments. The literature review then takes a quantum leap to discuss about different techniques currently being used for the sorting/separation of particles escaping a review on porous membrane which seems to be the next step. There are few reasons for bypassing the porous membrane review and that are: 1) The porous membrane technology is very traditional and this has become part of various book chapters; 2) The focus of this project is to develop an 'anti-clogging' strategy for porous membrane and to develop a new tool for biomedical application, but literature available for porous membrane mainly deals with materials or techniques for the fabrication of porous membranes; 3) No new concepts, like 3D or anti-clogging porous membrane, have been developed in the porous membrane technology that should be reviewed. Hence, justifying reasons for this escape and keeping in mind the word limits for this thesis, a jump from 3D microfabrication techniques to the separation techniques has been taken here. As the micro-device developed in this project has been applied for the separation and patterning of micro-entities, this review smoothly transits from the

separation techniques to patterning techniques followed by a review on techniques used for simultaneous separation and patterning of particles.

2.2 3D MICROFABRICATION

2.2.1 APPLICATIONS OF 3D MICROFABRICATION TECHNOLOGY

3D microfabrication has been used for the fabrication of micro-lens [6, 7] or micro-lens array[8-10], which constitute the essential part of the modern optical systems or for some interesting applications, like artificial eyes [11]. Another interesting and widely used application of the 3D microfabrication is the fabrication of photonic crystals and waveguides [12-15]. 3D microfabrication has also been used for optical data storage [16]. The fabrication of 3D micro-filters and micro-fluidic devices are other applications of this technology[17, 18], besides being used for cell-sorting applications [19] as well as for bio-sensing [20-22]. Tissue-engineering is another field in which use of 3D topographies for tissue-regeneration and implant applications is appealing [23, 24]. Recently, stem-cell research is also gaining interest in using 3D topographies to modulate gene-expression and protein-localization in cells [25, 26]. Other exciting applications of 3D microfabrication technology is for miniaturized drug delivery system [27, 28] and for developing non-fouling coatings [29].

2.2.2 THE TECHNIQUES FOR 3D MICROFABRICATION

Microfabrication is a recent science which has received an unprecedented popularity due to its increasing demand for various industries, especially electronics industries. Core of this science is developments in material science and parallel sophistication of techniques

for high resolution fabrication in micro-scale. The combination of these two and some other expertise gave rise to the field of microfabrication which involved use of new materials and techniques for transferring a pattern or a design from a dataset to a substrate. These techniques are referred as patterning or lithographic techniques which involve few key steps, (i) design of a pattern, (ii) an appropriate method of transferring pattern, (iii) a functional material responsive to the pattern transfer process and (iv) suitable tools that ensure pattern transfer [30]. Probably, the most popular means of pattern transfer is the light in from of optical lithography such as Photolithography which are popular due to its simplicity, speed and its ability to transfer pattern to virtually any practical dimension without changing the process. Though popular and efficient, optical lithography is not suitable for the fabrication of 3D microstructures due to their inherent limitation of all-or-none scheme of exposure. Therefore, many alternative techniques have been developed for 3D microfabrication. The literature review on 3D microfabrication techniques has been categorized here as; i) controlled cross-linking in 3D micro-space by high energy radiation, ii) layer-by-layer fabrication of 3D microstructures, and iii) unconventional strategies. The above said review is as follows:

2.2.2.1 CONTROLLED CROSS-LINKING IN 3D MICRO-SPACE BY HIGH ENERGY RADIATION

High-energy radiations such as UV-light, e-beam have been used for 3D microfabrication [31]. The high-energy radiation can change the property of a sensitive material by either initiating the cross-linking or by breaking the cross-linking between polymers chains. This causes a change in the property of the exposed region, which is harnessed for selective removal of either one of them. The microstructures are formed based on the

pattern of the exposure which is controlled in lateral as well as vertical dimensions of micro-space. Either position or distribution of the exposure is controlled by the existing 3D microfabrication techniques. Different techniques that have been used for such control are discussed as follows:

Gray-scale lithography: The distribution of light exposure can be controlled in the micro-space by using a special photo-mask which is referred as gray-scale mask and the process is called gray-scale lithography [32-35]. The special mask used for the gray-scale lithography can vary the illumination intensity of the light over the photo-sensitive material and generates an optical density counter that determines the shape of the micro-structures formed. Many types of gray-scale mask have been used. Half-tone masks are one of the popular choices [36-40]. Half-tone masks are usually fabricated by varying thickness of chromium on glass which creates the gray–scale level. The pattern on such mask is carved by using e-beam lithography. The high-energy beam-sensitive (HEBS) glass mask is another example of the gray-scale masks. The HEBS masks are fabricated by incorporating metal ions in the glass and the density of the metal ion determines the gray scale level in the mask [41, 42]. The pattern writing in HEBS glass is also usually accomplished by the electron beam. The use of HEBS gray-scale mask can be used for fabrication of 3D microstructures, like micro-lens or waveguide [43-46]. Similar approach has also been used for fabrication of gray-scale mask by direct writing of pattern in thin metallic film by using Laser [47]. There are other innovative approaches available in the literature for producing gray-scale level during exposure of the photo-sensitive material by light. Micro-lens projection lithography using gray-scale micro-lens array is one of them [48]. Microfluidic photo-mask is another innovative approach for

creating gray-scale level [49, 50]. The use of fluid as the light absorbing element is innovative and the opacity of such mask can be tailored by tailoring this ability of the fluid. Use of liquid crystal display as gray-tone mask is another example of innovative approach in the field of gray-scale lithography [51]. Figure-2.1 depicts pyramidal microstructure fabricated using gray-scale lithography.

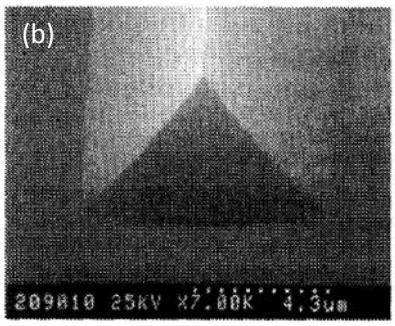

Fig: 2.1: 3D microstructures fabricated by gray-scale lithography: SEM image of pyramids obtained by gray-tone lithography [40]. (Copyright permission obtained from publisher)

E-beam/ Proton-beam lithography: Electron-beam (e-beam) lithography is being used as direct write technique for the 3D lithography [52-54]. The e-beam lithography requires precisely controlled e-beam to locally expose the e-beam sensitive material (resist). The distribution of exposure energy dose determines the developing rate distribution and final structure fabrication. The intensity of e-beam needs to be calibrated to expose the corresponding depth of the resist material. The surface relief is then converted into the intensity data according to the calibrated plot by using some software. The resist is scanned according to the intensity data to produce 3D profile. The secondary electron generated by electron beam has low energy distribution which helps in achieving high resolution fabrication [55]. Figure-2.2 shows saw-tooth structure fabricated by e-beam

lithography. Proton-beam has also been used for 3D lithography with high resolution, but mostly for nanofabrication rather than microfabrication [56].

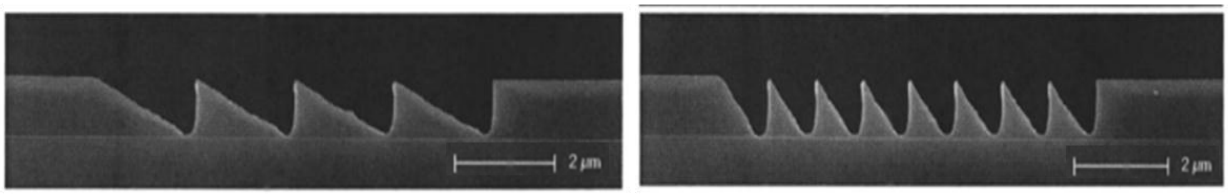

Fig. 2.2: Micro-structures fabricated by e-beam lithography: SEM images of the saw-tooth structures of different dimensions, fabricated by e-beam lithography [52]. (Copyright permission obtained from publisher)

Direct writing by focused laser beam: Laser is the popular tool for microfabrication due to the high control it can provide. Focused beam of laser has been used as the direct-write technique for 3D microfabrication. Mask-less fabrication of 3D microstructures using UV-laser has been realized (Fig.2.3) [57-59]. The principle of structure fabrication by focused beam of laser is similar to that of e-beam lithography. The beam of laser induces cross-linking in the photo-sensitive resist in a controlled manner. Usually, a photo-mask is not required, but a special exposure system is required. A computer aided design of the pattern data is obtained in digital format. The pattern data is converted into exposure data and is fed into the exposure system in from of image frames. The exposure system continuously generates the image frames by exposing pixel-by-pixel 2D dot pattern on a light-sensitive material coated on a substrate. Other laser-based techniques use laser for serially ablating or depositing materials for controlled fabrication of 3D microstructures [60, 61] and photo-induced polymerization of liquid pre-polymer by laser.

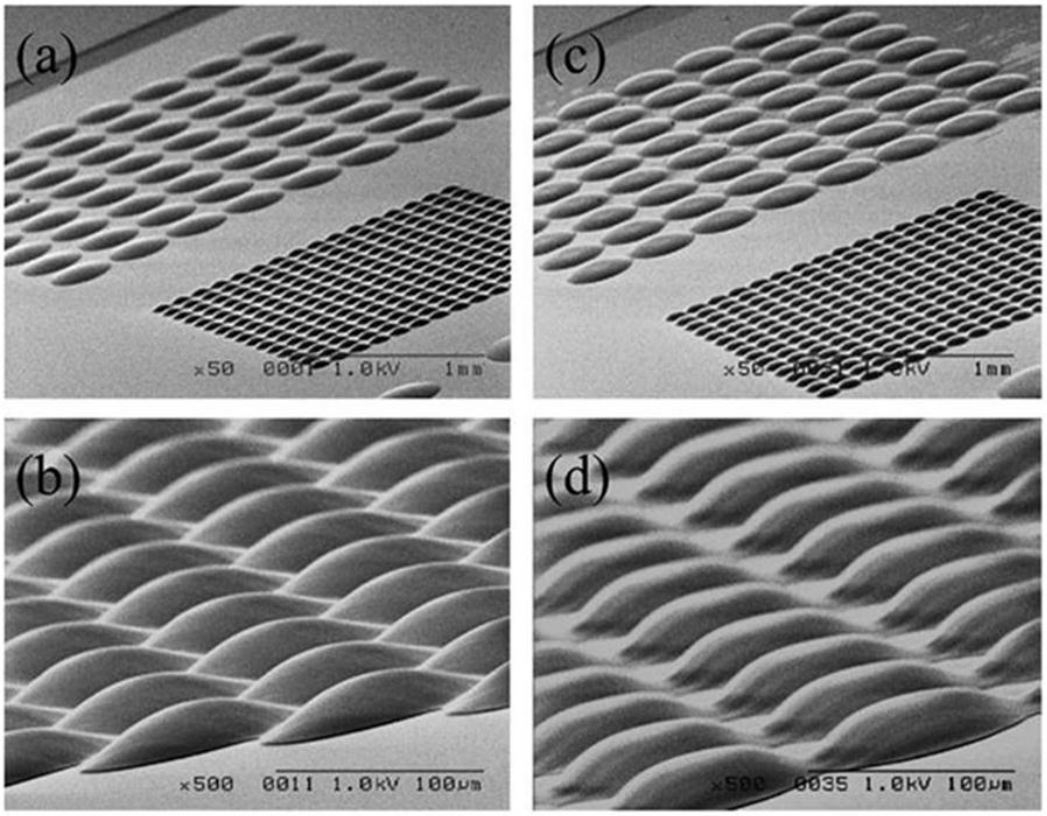

Fig. 2.3: 3D microlens fabricated by laser-beam lithography: 3D microlense are fabricated here by using UV-laser and a mask-less exposure system. SEM pictures of fabricated spherical micro-lens array (a & b) and aspherical micro-lens array (c & d) [58]. (Copyright permission obtained from publisher)

Two photon photo-polymerization: One of the most popular techniques for the 3D microfabrication is the two photon photo-polymerization by using focused beam of lasers [62, 63]. The technique depends on the use of a photo-sensitive material that absorbs light of certain energy to initiate photo-cross-linking or photo-polymerization. The required energy is provided by simultaneous absorption of two-photon from either one or two focused laser beams. The laser-light is focused at a point in the 3D micro-space to cross-link a small volume of material. The photo-polymerization takes place in the vicinity of

the focused beam only and thus creates a 3D micro-voxel around that point. The fabrication procedure is performed by scanning the focused laser according to the pre-programmed voxel matrix generated from the 3D image of microstructures by using software. The dimension of the voxel mainly depends on the spot-size and the pulse-energy of lasers used which determines the spatial resolution of spots fabricated. The exposure can be controlled due to two-photon capability of the material and the material can be exposed at different points to from the real three-dimensional objects [62, 64-66]. The two-photon photo-polymerization is similar to the focused-beam of laser, but can achieve high spatial resolution due to reducing un-necessary cross-linking. The technique can also surpass the diffraction limit. The experimental set-up for two-photon polymerization or focused laser-beam based fabrication is similar. Mainly, the set-up consists of a laser-source which can be focused on the resist using an objective lens. Different depths can be achieved by shifting the focus by moving the objective lens up and down. The scanning is performed by the movement of the computer controlled stage. Figure-2.4 shows some 3D microstructures fabricated by this technique.

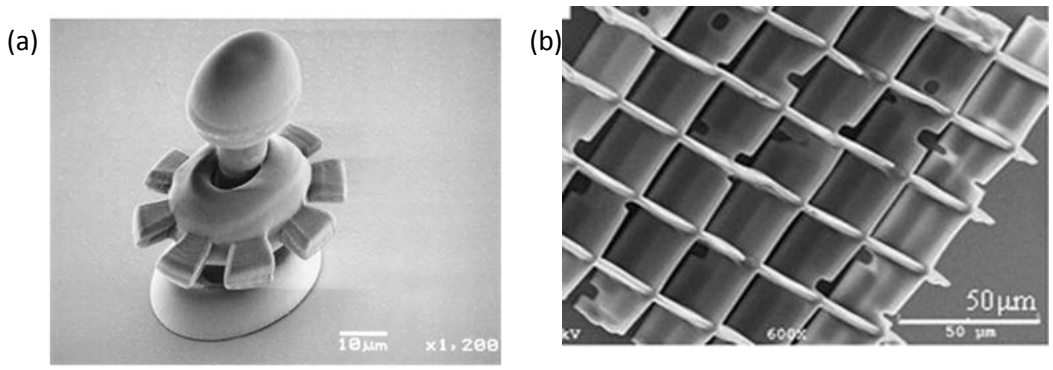

Fig. 2.4: Fabrication of 3D microstructures by two photon photo-polymerization: Micro-SEM images of (a) 3D microstructure fabricated by single-photon focused laser beam [59] while (b) the three-layer pattern of micro-porous structures with random holes in all layers fabricated by two-photon photo-polymerization technique [65]. (Copyright permission obtained from publisher)

2.2.2.2 HOLOGRAPHIC 3D MICROFABRICATION

The holographic microfabrication is based on the exposure pattern created by interference between two coherent beams of laser. This technique is also known as interference lithography. The resultant interference intensity pattern is recorded in the thin film of photo-sensitive resist [67, 68]. The complex 3D pattern can be fabricated by either intersecting more than two lasers at one time or exposing the same substrate multiple times with different interfering patterns. Complex 3D lattice has been fabricated as photonic crystals by exposing with four coherent beams of laser and selective removal by dissolution [69]. The pattern can be predicted using theoretical calculations in advance. The technique is particularly suited for the fabrication of 3D photonic crystals. The advantage of this technique is that it is relatively fast and simple and is suited for high throughput applications. The drawback of this technique is that only low refractive index materials can be used which may not be suitable for photonics applications.

2.2.2.3 LAYER-BY-LAYER FABRICATION OF 3D STRUCTURES

The layer-by-layer fabrication approach is simple to comprehend but difficult to accurately realize. In layer-by layer approach, 2D microstructures are fabricated in a layer and then another layer is coated. The 2D microstructures are again fabricated in the second layer by precisely locating the positions from the first layer and subsequently another layer is coated and structures are fabricated again. The process is repeated to fabricate the desired microstructure. Simply this is the technique for accumulation of 2D

microstructures from different layers to fabricate 3D microstructures. Few different strategies have been developed for the fabrication of 3D microstructures by this method. Layer-by-layer etching is one of the simpler techniques for fabrication of 3D micro-structures. The technique can be useful for fabrication of 3D photonic crystals by using standard microfabrication facilities [70]. In this technique, a layer of substrate is usually coated and is patterned to selectively etch it. The etched part is covered by another material (like polycrystalline silicon) and is polished to make it flat. Then another layer is coated and the procedure is repeated to fabricate repeating units of stacked layers.

Micro-stereolithography is another important technique for layer-by-layer fabrication of micro-structures. In micro-stereolithography, a layer of photo-sensitive material is coated on a substrate and is exposed to light either through a photo-mask or by a beam of light. The fabrication for the first layer is completed by post-exposure processing and then the second layer is coated and then the procedure is repeated for several times for the complete fabrication of the desired micro-structure. The micro-stereolithography is different from the fabrication done through layer-by-layer scanning through the focused beam of laser. In the later, actually the sub-layers within a single layer are scanned through focusing the beam in the single plane whereas in the former different layers are coated and exposed. To increase the spatial resolution and precision in fabrication of very complex structures by this technique, two photon micro-stereolithography has been used [71, 72]. Different variants of this technology have been demonstrated in the literature for fabrication of 3D microstructures, like the micro-stereolithography combined with UV-lithography [73]. Recently multi-material micro-stereolithography has also been demonstrated [74].

Other than these two layer-by-layer approach, other methods, like layer-by-layer deposition of material using robotic arm [75, 76] and self-assembly of the micro-particle [77, 78] have also been demonstrated in the literature.

2.2.2.4 UNCONVENTIONAL METHODS

Other than the conventional approaches, few interesting strategies can be found in the literature for which have been used for fabrication of 3D micro-structures. One such strategies is the inclined or rotated exposure to a photo-sensitive material by X-ray or UV-light [79, 80]. The strategy is simple and can be used for fabrication of few types of 3D micro-structures. The idea behind this technique is inclined exposure of the photo-resist through a photo-mask by light. Depending on the angle of incidence or the angle of rotation, the slope of the fabricated structures is decided. Other than that, silicon micromachining can also be used for 3D microfabrication [81].

2.2.3 THE SCOPE AND LIMITATIONS OF EXISTING TECHNIQUES

The current techniques used for the fabrication of 3D micro-structures have their own advantages and disadvantages. The use of electron beam or proton beam can provide better resolution than the UV-light, but their use is expensive due to high cost of equipment and maintenance. The e-beam lithography is suitable for sub-micron fabrication, but it is difficult to apply this technique for high-aspect ratio 3D microfabrication due to low penetration depth of the e-beam. Proton-beam is also used for nano-fabrication and may not be a good choice for microfabrication. The e-beam

lithography also suffers from low throughput and use of multiple layers. Also, the e-beam lithography required lot of calibration and optimization before developing the relation between the depth profile and the exposure-dose [82].

The laser-based techniques provide better control over the fabrication process and can achieve high spatial resolution. With introduction of the two-photon fabrication the spatial resolution as well as complexity of microstructures has substantially increased [72]. Though the use of laser has come with a popular tool for the 3D microfabrication, the cost, the through-put and the need for special and expensive equipment has not been resolved. The problem of the 3D microfabrication by the focused beam of light is the roughness of the 3D profile due to residual cross-linking and improper joining of structures from each 2D pattern. The use of two-photon needs materials with special characteristics. The two-photon micro-stereolithography is capable of precisely controlling the exposure in the 3D micro-space but the coating of resist limits its use. The coating of resist depends on the surface tension and the viscosity of the material which limits the spatial resolution. Also, two-photon stereolithography suffers from accumulation of errors during layer-by-layer fabrication. Also, it requires long time and effort as it employs layer-by-layer accumulation based on 2D sliced data obtained from 3D computer aided design. Other laser-based techniques including photo-induced polymerization of liquid pre-polymer by laser and serially ablating or depositing materials using laser also suffers from low through-put, and are complicated for fabrication of complex 3D structures. The drawback of the holographic microfabrication is that only materials with low refractive indices are suitable for direct patterning by this method.

The gray-scale lithography has been used as another alternative fabrication of 3D micro-structures. The technique can be useful, but the disadvantage of this approach is the requirement of a special or an expensive photo-mask, the design of which may need a lot of calibration or simulation steps. Also, it is not suitable for fabrication of complex 3D microstructures with high aspect-ratio. The inclined or rotated exposure to a photo-sensitive material by X-ray or UV-light also has limitations. The access to X-ray is generally restricted and also, only limited types of shapes can be fabricated. Silicon micromachining can also be used for 3D microfabrication, but it requires access to harsh chemicals or expensive equipment. Thus, most of techniques used for 3D microfabrication are expensive, time-consuming and are mostly performed in specially maintained clean-room lab environment which adds-up to the cost and restricts the use.

2.3 SORTING OF MICRO-ENTITIES IN MICRO-DEVICE

2.3.1 THE OVERVIEW

The past decade has seen a rapid progress in the use of micro-fluidic devices encompassing various fields of science and technology. Since their advent, micro-fluidic devices have shown great promises for developing "lab-on-a-chip" devices. Sorting/separation of micro-entities (like beads or cells) using micro-fluidic devices is one such achievement [83, 84]. The development of micro-fluidic devices with ability to filter micro-entities such as cells or beads has found its application in immunological & biological assays and for performing cell studies. Bead-sorting can be used for performing immunoassays. Beads can be conjugated with some ligand molecules and can

interact with target molecules present in the sample for efficient and multiplex detection [85, 86]. The cell-sorting is another major application of micro-fluidic devices [87]. Separation of rare cells such as circulating tumor cells (CTCs) from blood is used for diagnosis and prognosis of cancer [88], and thus the need to develop simple and effective tools for this purpose is medically important [89]. Enumeration of circulating epithelial cells from blood [90] and isolation of mesenchymal stem cells from blood are few other medically important applications of the cell separation which have been achieved by using micro-fluidic devices [91]. The micro-fluidic devices have also been applied for fractionation of blood cell subtypes, for example separation of leukocytes from whole blood (leukapheresis) which is clinically important for removing white-blood cells (leukocytes) from blood of leukemic patient or from blood used for transfusion [92]. With increasing consensus for analyzing cells at single-cell level, micro-fluidic devices have been used for sorting of single-cell for studying each cell individually [93, 94].

2.3.2 SORTING TECHNIQUES

The review presented here for the sorting of micro-entities is divided in terms of different technical principles that are used for this purpose. Different techniques have been discussed here with their scope and limitations.

2.3.2.1 ACTIVE SEPARATION TECHNIQUES INVOLVING EXTERNAL FIELD OR FORCE:

Many techniques that have been used for sorting of micro-entities in micro-fluidic devices are based on the use of external field to exert differential force on different micro-entities. The amount of the force exerted on a micro-entity depends on degree and kind of interaction with the external field. The net force on a particle affects its

trajectories while it flows through a micro-channel. Different types of micro-entities experience different amounts of force and hence their trajectories are different. This principle has been used for the separation of micro-entities in micro-fluidic devices. Different techniques based on this principle have been discussed here.

Electric field for sorting of micro-entities: Electricity has popularly been used for the separation of micro-entities based on either intrinsic charge or polarisability. The charge-based separation is less preferred due to small differences in the charge among different types of micro-entities. The polarisability of micro-entities has extensively been used for their separation. When a dielectric particle, like cell, is placed in an electric field, it is polarized to create a dipole. If the electric field is uniform, the net force on the micro-entity induced by electric field is zero due to equal and opposite forces exerted by the electric field. However, if a micro-entity is placed in a non-uniform electric field, the net force on the particle is not zero and hence a net movement is observed. This phenomena is called as Dielectrophoresis (DEP) [95]. The principle of DEP was first demonstrated in 1951 by *Pohl. et al* [96]. DEP has been used for the separation of different types of micro-entities such as cells and beads. The force exerted in the non-uniform electric field by DEP depends on the electrical properties of micro-entities, their surrounding medium, their shape and size, and frequency as well as gradient of the electric field. Based on the movement of and in the electric field, the DEP can be classified as positive-DEP (p-DEP) or negative-DEP (n-DEP). When electrical polarisability (or permeability) of a micro-entity is greater than the surrounding medium, the net movement would be towards high intensity of electrical field (i.e. towards electrode) and is called as Positive-DEP or p-DEP. If the electrical polarisability (or permeability) of a micro-entity is lower than their

surrounding medium, the net movement of particle is towards low intensity of the electrical field (i.e. away from electrodes) and is called as negative-DEP or n-DEP.

Different strategies have been presented in the literature for producing non-uniform electric filed in micro-devices for performing DEP-based sorting of micro-entities. In some of these strategies, insulating obstacles, such as ridges [97], narrowing wedges [98, 99] or array of posts [100] are incorporated in a micro-channel and a voltage is applied. The electric field in the vicinity of these obstacles becomes non-uniform and DEP is generated on micro-entities that flow near these obstacles. In another strategy, electrodes of different shapes and sizes have been used for generating non-uniform electric field [101].

DEP has been applied for different cell separation application, such as the bacterial cell separation, separation of live and dead yeast cells [102, 103], separation of malaria infected cells from blood [104], cancer cell separation from blood [105-107] separation of white blood cells from blood [108] and stem cell separation from blood [109] etc. Though dielectrophoresis has been used for efficient separation of micro-entities, the need for special media with particular electrical properties is its drawback. Also, the effect of electric field on living cells is unknown and this technique may not be suitable for very sensitive cells.

Magnetic field for sorting of micro-entities: Like electric field, magnetic field can also be used for the separation of magnetically susceptible particles or magnetically labeled cells [110]. When a non-uniform magnetic field is applied perpendicular to the flow direction of micro-entities, a magnetic force is experienced by them which can pull them away

from the flow. The micro-entities are subjected to two forces, the hydrodynamic force in the direction of the flow due to the pumping of the fluid in the device and the magnetic force perpendicular to the flow velocity. The vector sum of these two forces determines the final trajectories of micro-entities, which experiencing different forces due to different magnetic properties or sizes are separated from each other. This principle has been applied for the separation of micro-particles or cells in micro-fluidic devices [111, 112]. The simplest design for such systems is depicted in the Figure-2.5. The micro-fluidic device in such a design consists of a flow channels with two inlets and two outlets. One inlet is used for the delivery of the sample and the other inlet is used for the flow of buffers. The sample and the buffer flow in the micro-channel as two laminar flows. The magnetic field is applied perpendicular to the flow direction in the channel. The particles experiencing magnetic force are deviated from the sample channel to the buffer channel and are collected at the buffer outlet. The magnetically unsusceptible particles are collected at the sample outlet. More complicated designs for improved separation have also been reported, for example a device for size-based separation of micro-particles with multiple inlets and outlets have been realized [113].

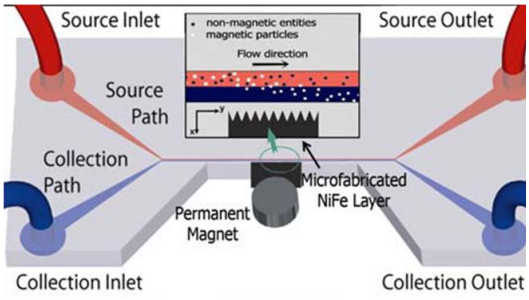

Fig. 2.5: Magnetic separation of particles: The sample is introduced in the source inlet which travels in the source path. The magnetically susceptible particles are deflected from the source path to the collection path under the influence of the magnetic field and are collected at the collection outlet [111]. (Copyright permission obtained from publisher)

Separation of magnetic micro-entities has been used extensively for different applications. Magnetic micro-particles are conjugated with some ligand or target molecule (like antigen or antibody). The corresponding counterpart is then allowed to adhere to these particles which can be separated by using magnetic micro-fluidic device. The magnetic separation of micro-entities has been used for various applications such as separation of biomolecules [114, 115], pathogen detection and disease treatment [116, 117]. The magnetic separation has also been used widely for separation of cells such as separation of magnetically labeled cells [118], immuno-magnetic separation of specific cells from blood [119], separation of red-blood cells from white-blood cells by using intrinsic magnetic properties of red-blood cells [120].

Magnetic separation has few distinct advantages over electrical separation. Magnetic separation is applied externally and no contact with liquid is required. The magnetic field is hardly affected by environmental factors like ionic strength and PH. Magnetic forces may also be milder than electrical forces. However, cells rarely have intrinsic magnetic properties and the use of magnetic separation is limited by the need for magnetic labeling of cells. The throughput of the magnetic separation may also be low.

Optical techniques for sorting of micro-entities: Optical micromanipulation techniques have been developed in recent past for the trapping and/or sorting of micro-entities [121, 122]. The radiation force of the Laser can be used to accelerate or move micro-entities to trap or to sort them. The concept of optical trapping of micro-entities in optical potential wells using focused beam of Laser was first introduced by Ashkin *et al*. in 1970, where

two counter propagating Laser-beams were used for trapping particles [123]. The particles can also be trapped by using single focused beam of Laser which is popularly known as optical tweezers. The principle of optical trapping or acceleration of particles under a beam of Laser can simply be modeled as the continuous momentum transfer from photons to particles during particle-photon interaction. Particles with higher refractive index are attracted towards the center of the focused beam (i.e. towards high intensity of light beam) due to larger momentum transfer by intense beam compared to less intense beam at boundary. The refracting light also transfers momentum in the direction against the direction of light propagation and once the particle is in center of focused beam, the net momentum transfer is against the direction of light propagation which induces motion of particle against photon's movement. The net momentum transfer from scattered light is in the direction of light propagation which moves particles in the direction of the beam. The particle is trapped when net force arising from all momentum transfer is zero. This model doesn't hold well for explaining the trapping of particles smaller than the wavelength of light. This can be explained by strong electric field generation in the narrowest part of the beam where smaller dielectric particles act as a dipole and move towards the most balanced electric field region i.e. center of focused beam of light.

Optical trapping of micro-entities has been used for various applications related to particle or cell manipulation. Trapping of individual viruses and bacteria has been demonstrated by using single-beam gradient force traps of optical-tweezers[124]. Optical forces has also been used for damage-free trapping and manipulation of single living cells including bacteria, yeast, protozoa and even red blood cells [125]. Optical sorting techniques have also been used for sorting cells in micro-fluidic devices which are based

on the principle similar to electrostatic sorting performed in FACS. Instead of using an electrostatic field to deflect a cell in FACS, radiation force is used to deflect a desired particle. The technique has been used for sorting mammalian cells and macrophages using a micro-fluidic cell-sorting system [126, 127]. Optical tweezers have also been used for studying mechanical properties of red blood cells which is clinically relevant [128, 129].

Optical micromanipulation offers several advantages such as high through-put, complex manipulation at single particle/cell level, label-free manipulation, but the use of Laser and high power beams limits its use.

Acoustic forces for sorting of micro-entities: Acoustic forces generated from ultrasonic waves can be a useful tool for separation of micro-particles and cells from liquid sample. Recently, acoustic manipulation techniques have received increased attention for designing chip-based micro-systems for separation and manipulation of micro-particles or cells due to advancement in micro-technology which enable integration of ultrasonic resonator in a micro-chip [130]. Ultrasonic standing wave exerts force on micro-entities that can affect their motion. The ultrasonic wave is generated orthogonal to the direction of flow over the cross-section of a micro-channel. Usually, it is tuned in such a way that a node is positioned in the center of micro-channel and two anti-nodes are located at two ends of the channel. The particles or cells experience a force either towards a node or towards an anti-node depending on the acoustic properties of micro-entities and their surrounding medium. To generate ultrasonic sound waves, different types of ultrasonic wave generator, like piezoelectric transducers, can be used. It can be generated by using either two counter sound waves or a single sound wave facing a sound reflector.

The acoustic force on the particle in ultrasonic standing wave depends on the properties of the ultrasonic waves, properties of micro-entities and their surrounding medium [131]. The acoustic force is determined from the amplitude and frequency of the acoustic wave. The higher the frequency of a wave, the higher is the acoustic force. Acoustic force on a micro-entity depends on its density and compressibility relative to the surrounding medium. The acoustic force on a micro-entity is also dependent on its volume. These properties decide motion of a micro-entity in ultrasonic standing wave field. Micro-entities differing in size, density, compressibility or their combination can be sorted by the acoustic force.

Acoustic forces have been used for separation of micro-particles and cells from a fluid flow into a stream of particle flow [132-134]. The technique has been used for the separation of particles of same size with different density and separation of red blood cells and platelets [134]. One of the interesting applications of the acoustic force based cell separation that has been shown in literature is separation of lipid droplets from blood. Red blood cells in plasma is pushed to the nodes and lipid droplets are pushed to the anti-nodes [135]. The technique can be used for separation of lipid from blood during an open heart surgery.

Acoustic manipulation of micro-particles or cells is attractive tool due to non-contact manipulation of particles. The acoustic forces are not affected by surface properties or ionic properties of liquid. The throughput is reasonably high and has not been reported to damage cells. However, the need for suitable surrounding medium limits its use.

Split field thin fractionation (SPLITT): SPLITT is another active method for sorting of micro-entities. In this method, particles are pushed from one sample stream to another stream by applying an external field. The force affects different micro-entities differently which cause separation of one type of micro-entity from another [136]. The external field may be gravitational, electrical or magnetic. It is a continuous flow process and has been used for separation of cells or micro-particles. The general design of SPLITT can be useful for separation of micro-entities based on different properties.

2.3.2.2 PASSIVE SEPARATION TECHNIQUES WITHOUT INVOLVING EXTERNAL FORCES

There are different techniques that do not use external field or force for sorting of micro-entities in micro-devices, instead they depend on the micro-fluidic phenomena or interaction of micro-entities with structures or obstacles in a micro-channel. The separation is mainly based on the flow based differences which arise from either channel design or from micro-structures in a micro-fluidic device. Such techniques are discussed here as follows:

Pinched flow fractionation: The pinched flow fractionation is an elegant example of use of simple micro-fluidic principles for particles or cell separation [137]. The technique is based on the laminar flow and negligible diffusion in a micro-channel. The sample stream (containing micro-entities to be sorted) is pushed through a narrow channel along with a carrier stream (containing only buffers) through two inlets. The flow rate of the carrier stream is usually higher than the sample stream which pushes away the sample stream towards one side wall. The sample stream is kept thinner in comparison to the carrier

stream. In such situation smaller particles remain in the sample stream whereas some portion of bigger particles comes in the carrier stream. When the pinched stream is allowed to open up in a wider channel the laminar flow helps in separating these particles in different flow streams (Fig.2.6). The separated particles can be collected further downstream. Based on this concept, other similar devices has been demonstrated for sorting of micro-entities [138]. The method has successfully been applied for the separation of 1-5micron particles as well as separation of erythrocytes from blood [139].

The pinched flow fractionation technique is simple and yet effective for size-based separation of particles or biological cells. The through-put can be reasonably high. However, it is limited to size-based separation only and it requires lot of fine tuning of parameters before accurate separation is achieved.

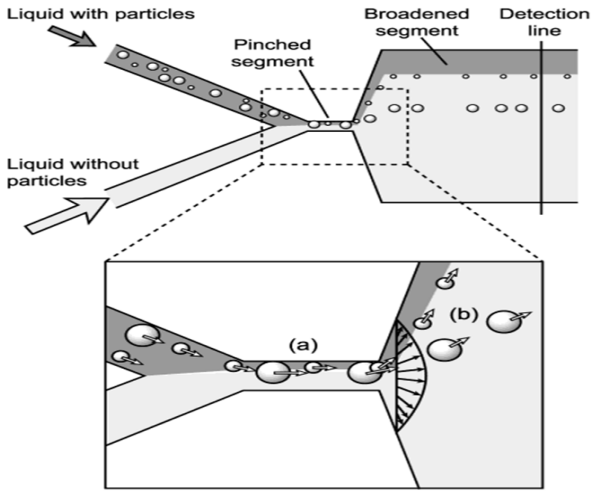

Fig. 2.6: Principle of pinched flow fractionation: It based on laminar flow and negligible diffusion in a micro-channel: a sample stream (dark-colored in the diagram) is pushed through a pinched micro-channel along with another buffer stream. (a) Particles are aligned to one sidewall in the pinched segment of the channel by controlling the flow rates from two inlets; (b) particles are separated according to their sizes by the spreading flow profile at the boundary of the pinched and the broadened segments [Yamada et.al, 2004].

2.3.2.3 MICRO-FILTRATION

The significance of micro-filtration has been well recognized and different types of micro-filters for different applications have been demonstrated. Few strategies that have been applied for micro-filtration are Cross-flow filtration [140], porous membrane micro-filtration [141] and micro-filtration using different types of micro-structures such as pool-dam based micro-filtration [142], wire-type filtration [143], micro-pillar based filtration [144] and micro-filtration by using 'C' or U-shaped structures [88]. The filtration principle is based on the size and deformability differences in different types of micro-entities.

Wire-type or pool-dam type filters are simpler but less efficient and are not suitable for trapping rare cells from blood. Cross-flow filtration is efficient but complete separation is difficult to achieve and it may not be suitable for separating very low number of cells. Pillars arranged in one dimension are limited to separate low number of cells and are also prone to clogging. Pillars arranged in 'C' or U-shaped structures can act as trapping sites and such structures can be arranged asymmetrically in two-dimensional space to increase the effectiveness of separation. The problem with such arrangement is that efficiency of trapping depends on cell-size and flow speed which limit their use [88]. Membrane micro-filters with uniform pore-size can achieve very high efficiency of cell or particle separation but membrane filters suffer from pore-clogging and pore fouling and are not suitable for continuous filtration of large number of cells [5, 145]. The efficiency of cell trapping may depend on flow-speed or applied pressure for most micro-filters. In some, efficiency may directly be related to the flow-speed. Increased speed or pressure may cause trapped cells to squeeze through microstructures or pores as cells are flexible

entities. This may decrease the throughput and would not be suitable for handling large volume of biological sample (e.g. blood) in micro-fluidic devices. Increasing filter area may not be a good solution as it may decrease the detection efficiency and may also use large quantities of expensive reagents used for detection. Another problem with many of above mentioned micro-filters is unclean separation of cells. As these devices have plain empty spaces near filtering structures, so there can be accumulation of undesired cells and this may affect the detection specificity of desired cells. Hence, micro-filtration is simple and easy to use, but suffers from clogging and unclean sorting, which limits their use for continuous separation.

Micro-filtration have been used for filtering tumor cell from whole blood [88, 141], for fractionating white-blood cells from red-blood cells [146] and separation of plasma from blood [147] to name a few.

Hydrodynamic filtration: Another interesting approach for sorting of micro-entities is hydrodynamic filtration which relies on laminar flow in a micro-fluidic device [148, 149]. The principle of hydrodynamic filtration is similar to cross-flow filtration, but unlike cross-flow filtration hydrodynamic filtration allows concentration and alignment of micro-entities before separation. The dimensions of the main channel and the side channel determine the flow-rate distribution in side channels. The narrower the side channel, the lesser is the flow. When the relative flow in the side channel is low, only small amounts of fluid is removed from the main channel. Micro-entities which are larger than flow line are not removed even if the size of these micro-entities is smaller than the cross-section of the side channel. Though particles are not removed, fluid is removed

which helps in concentrating particles and continuous removal of fluid also helps in alignment of particles near side-walls. As the flow distribution on side-channels is increased particles of particular size are removed through side channels. Micro-entities can be concentrated, aligned and classified by using hydrodynamic filtration.

The hydrodynamic fitters have been demonstrated to enrich white blood cells (WBC) and red blood cells (RBC). The hydrodynamic fitters are simple to use and are effective for concentration of particles. The through-put can also be high. However, complete separation of particles or 100% efficiency is difficult to achieve by this technique.

Other cell separation techniques based on the hydrodynamic principles have also been demonstrated. One of them is based on an interesting behavior of blood flow in capillaries. RBC tends to flow in the center of capillaries. This principle has been used for the depletion of RBC from whole blood using a simple and high through-put micro-fluidic device [150] and for enrichment of WBC flowing at side-walls in a micro-channel [151]. Another one is based on the 'bifurcation law' or 'Zweifach–Fung effect' which states that particles tend to move in the channel at higher flow-rate and particle-free fluid tends to flow in a channel with lower flow-rate at a bifurcation of a channel. This property has been used for separation of blood plasma from the blood or blood-cell enrichment [152]. Few more separation principles can be found in literature, like cell-separation using multi-stage multi-orifice flow fractionation in micro-channel and is referred to as MS-MOFF [153]. The method has been used for capturing circulating tumor cells or rare cells from blood.

2.3.2.4 SEPARATION BY SELECTIVE GUIDED MOVEMENT USING OBSTACLES

Micro-entities can be separated by selectively guiding their motion in micro-channels. An elegant example of this type of separation is 'Deterministic Lateral Displacement' (DLD) where motion of micro-entities in laminar flow are guided or affected by an array of pillars arranged in a particular manner [154]. DLD is suitable for size-based continuous separation of micro-entities. In DLD, symmetrical pillars are arranged in a number of rows where each row is shifted by a small distance or angle relative to the previous row. The distance between each pillar and the distance or angle of shift determines the critical size for sorting [155]. Micro-entities, smaller than the critical size, are not affected by pillars and flow in the same streamline whereas particles larger than the critical size are 'bumped' on pillars and shifts to the adjacent streamline. The shift of a larger particle is according to its size and the angle of shifted rows. The shift of larger particles pushes them away from the laminar flow streamline whereas smaller particles remain in the original streamline and thus particles are separated from each other (Fig.2.7).

DLD has been practically successful in separation of biomolecules, micro-particles and cells with high efficiency and at high speed. Separation of blood components from whole blood has been demonstrated by using DLD device [156, 157]. It has also been used for enrichment of a particular cell types, like larger cardiomayocytes cells from a population of cells, for tissue-engineering purposes [158]. An innovative use of DLD has been demonstrated in determining the hydrodynamic size of cells and even predicts properties, like healthy verses malignant, based on the size-determination, thus performing separation and measurement tasks within a microfluidic device [159].

DLD is an elegant example of using passive means for effective separation. The method does not require any pre-labeling of cells or particles. The separation parameters can be tuned to suit different needs. The DLD has capability to achieve high efficiency separation with high through-put. However, the technique is only limited to size-based separation.

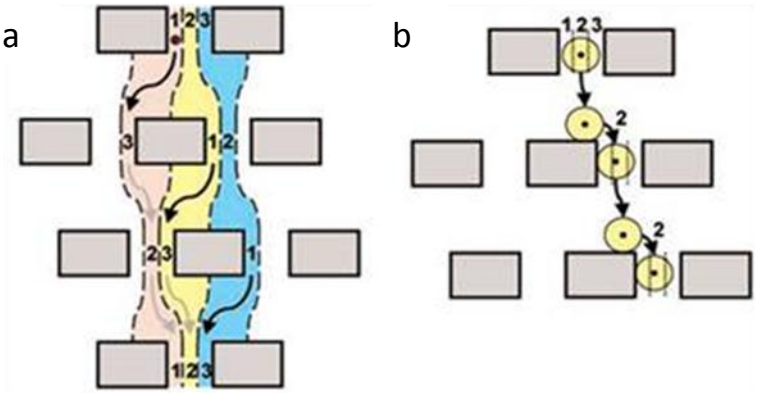

Fig. 2.7: Deterministic Lateral Displacement (DLD): (a) the smaller particles follow the streamline of the laminar flow and is not affected by the arrangement of pillars whereas (b) bigger particles shifts according to the shift in pillars arrangement [154]. (Copyright permission obtained from publisher)

Another technique using obstacles for sorting micro-entities is hydrophoretic separation by using slanted obstacles in a micro-channel [160]. The slanted obstacles are placed on the top and the bottom of the channel in an alternating manner. Lateral pressure gradient is generated in the micro-channel due to these obstacles which induce transverse flow in direction perpendicular to the direction of flow. Different micro-entities are affected differently due to such flow and get separated over time. The technique has been used for separation of WBC from RBC [161]. The hydrophoretic separation technique utilizes

pressure gradient induced by intrinsic means instead of generating force gradient by using external force, like electrical or magnetic force.

2.3.2.5 SEPARATION BY INERTIAL FORCES IN MICROFLUIDICS

Microfluidics has usually been associated with negligible inertial forces. However, inertial forces have recently been used for separation of micro-particles in micro-fluidic devices. Inertial lift forces can induce movement of micro-entities from one streamline to another streamline of the laminar flow. Position of a micro-entity in the flow is determined by the equilibrium of inertial and shear forces induced due to flow of fluid. Under effect of these forces, micro-entities with different sizes can be located in different streamlines and can be separated by using flow splitters [162]. When particles flow in a spiral micro-channel, dean-drag is also active apart from inertial lift force. The balance of forces determines the streamline along which a particle is located. Larger particles are located near side walls while smaller particles are located in the outer half of the channel. Hence, particles are located along different streamlines which is based on the size of particles. Streamlines can be separated which can achieve particle separation [163].

2.4 PATTERNING OF MICRO-ENTITIES IN MICRO-DEVICE

Patterning of micro-entities is a term used for obtaining micro-entities in a pre-designated area on a substrate or space. If the patterning is achieved in a micro-device or by using micro features, it is termed as micro-patterning. Bead-based (micro-particles) immunoassay is an emerging tool for solid-phase detection of bio-molecules and is encouraging the development of micro-fluidic platforms for bead-patterning after or

before interaction of bio-molecules conjugated to beads to other bio-molecules present in the sample [85]. The ability to pattern beads in a micro-array format has contributed to multiplexing of these assays and has enhanced the scope of molecular diagnostics [86]. The micro-patterning has also been investigated for cells. Usually, cell-patterning is the first and is an important step for doing research on cells using cell-based micro-devices. Cell-patterning can be classified as multiple-cell pattern or single-cell pattern based on number of cells on a particular area or spot of interest. In multiple-cell pattern, a group of cells are located at different locations on a substrate whereas in single-cell pattern, each cell is separated from other cells. In multiple-cell pattern, the cell study is based on the average data obtained across a large group of cells. A number of cells are put together and analyzed or are directed to grow or interact in a specified way. So, group effect of cells as well as interactions of a group of cells with another group of cells or effect of different reagents on a number of cells is studied at micro scale. Thus, it gives an insight of cumulative cellular behavior in micro-environment. Such micro-patterns have been used for tissue-engineering applications, for studying cell-to-cell and cell-to-surface interaction, for fundamental cell studies and for cell-based biosensors. Scientists have also shown interest in studying single-cell individually due to inherent heterogeneity in cell population. To take in to account of cellular heterogeneity, many scientists believe that such heterogeneity is inherent in cellular behavior and data collected from bulk of cells may not represent the true state of cellular phenomenon [164]. So, to peer into the molecular machinery of individual cells, single-cell pattern is required. Single-cell pattern is useful for investigating cellular level differences to understand a disease at the

molecular level. Other applications include biosensors, fundamental cell studies and drug screening.

Different techniques have been used for patterning of micro-entities. Herein, a brief discussion on this topic has been presented. These techniques have been divided into two broad categories for presentation: 1) Biomolecules modified surfaces for patterning and 2) Techniques for trapping micro-entities. The scope and limitations of these techniques have been discussed for each technique separately (together with their introduction).

2.4.1 BIOMOLECULES MODIFIED SURFACES FOR PATTERNING

Many techniques have been developed for patterning of micro-entities (especially cells) on different substrates by modifying surfaces with biomolecules. Biomolecules are imprinted on the surface to either enhance the surface properties for attachment of micro-entities to specific regions or to retard their attachment to undesired regions. Different techniques have been used for modifying surfaces with biomolecules for cell-patterning which is discussed below.

2.4.1.1 PHOTOLITHOGRAPHY

Photolithography has been used for generating patterns of biomolecules on which micro-entities can be attached on different types of surfaces [165]. In this technique, micropatterns are generated by transfer of a pattern from a photo-mask to a layer of photoresist using light as energy source. Then, materials of interest (e.g., cell-adhesion protein) are applied on the photoresist pattern, and the photoresist is lifted-off to obtain desired pattern of biomolecules. Then the surface is incubated with solution of micro-

entities and their desired pattern is obtained. Recently, single cell micro-array was created by patterning biomolecules on the surface using combination of photolithography and etching (Fig.2.8) [166]. The photolithographic technique is highly developed for producing accurate patterns; however, there are some disadvantages as it requires clean-room facilities and expensive equipment.

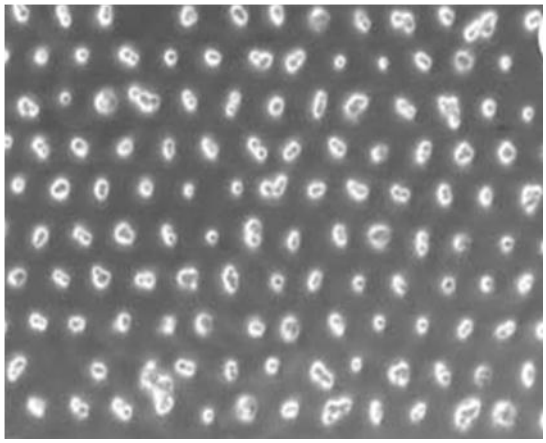

Fig. 2.8: Single-cell micro-array: Single-cell micro-array produced by patterning biomolecules using photolithography in combination with etching [166]. (Copyright permission obtained from publisher)

2.4.1.2 SOFT-LITHOGRAPHY

Whitesides and colleagues have developed a set of techniques called "soft lithography", which is suitable for patterning biomolecules on a substrate [167, 168]. The term soft lithography is used because a soft elastomeric material is used for pattern transfer by these techniques. In soft- lithographic techniques poly(dimethylsiloxane) (PDMS) is mostly used due to suitable properties of this material. It is biocompatible, optically transparent, permeable to gases, elastomeric, and durable. Cells can be cultivated on the surface of PDMS by modifying its surface. Different soft-lithographic techniques, like Microcontact printing [169], Microfluidic patterning Using microchannels [170], Stencil patterning [171] and Laminar flow patterning [172, 173], have been used for cell

patterning. This technique is simple and inexpensive; however it depends on other microfabrication techniques for development of the mold used for pattern transfer.

2.4.1.3 MICRO/NANO LITHOGRAPHY

Cell deposition and culture on flat substrate is a common procedure on the macro scale but it is difficult to analyze cells with single cell resolution. Ordered immobilization in a two-dimensional array format on micro patterned surfaces may enable simplified analysis at single-cell resolution, as a particular cell can be fixed and labeled by its position on the substrate. The surface micro patterning is used to pattern cell-adhesive molecules, like ECM proteins, to specific sites on the substrate for the cells to adhere and inhibit cell and protein attachment in the surrounding areas. Novel surface patterning technologies, like contact or non-contact printing technologies that can print an array of spots containing biomolecules with resolutions in nanometers is an emerging technology to create an array of single cells. Dip-pen lithography, focused-ion beam milling, inkjet and other droplet printing technologies have been used for this purpose [174]. Drawbacks of surface immobilization methods are that they are not applicable to non-adherent cells and deposition is usually irreversible. The choice of the surface coatings may also pose a problem. Surface immobilized cell-array platforms can be used as biosensors, drug screening and individual cell studies. Another important application is fundamental cell studies for understanding cell–surface interactions and cell responses to soluble stimuli. Cell-attachment sites can also be modified in topography or chemical composition to investigate the effect of such cues on cell behavior [175].

2.4.2 TECHNIQUES FOR TRAPPING MICRO-ENTITIES

The techniques mentioned in previous sub-section have been used for creating patterns of micro-entities by using modified surfaces. The main drawback of these techniques is large amount of time required before further experiments can be performed. Miniaturization technology provides facilities for rapid trapping of cells. Various methods have been applied to trap or immobilize cells. These techniques are based on the use of some force or field, like electromagnetic, acoustic, fluidic, or by using micro-structures. A brief discussion on trapping techniques follows. We have classified these techniques as electromagnetic and non-electromagnetic cell trapping techniques.

2.4.2.1 ELECTROMAGNETIC CELL TRAPPING

Electromagnetic forces or fields have been used for trapping single cells and an array of single cells can be obtained by such methods. These techniques use either intrinsic property of cell, like charge on cell surface for electrical trapping, or add some property to cell, like magnetic labeling for magnetic trapping, to trap a single cell. Some of these techniques are discussed here.

Electrical trapping: Trapping micro-entities with electrical means has emerged as a convenient tool due to ease of fabrication of electrical structures and generation of electrical potential at micro scale. Furthermore, electrically driven microchips are fast, flexible, controllable and easy to automate. Micro-entities trapping has mainly been achieved by using DEP. DEP has been discussed in section-2.3.2.1. Micro-entities are trapped based on differences between their permittivity and conductivity compared to their surrounding medium. Micro-entities are stably trapped when the DEP force balances

other forces such as fluidic force and electrophoretic force. The flow speed has to be adjusted to keep them immobilized or to balance these forces. Dielectrophoresis can be achieved by planar microelectrodes that can produce strong field gradient and DEP force. Micro-entities may be trapped in suspension for different applications such as biochemical assays, cell fusion, or electrical measurements of cell properties.

Optical trapping: Radiation from laser light can also be used for trapping micro-entities by exerting force for acceleration and trapping of micro-entities [176]. Axial force as well as a radial force is produced by laser beam. The axial force propels the particle along the axis of the beam and the radial force traps it on the beam axis. The optical forces depend on the optical (refractive index and absorption) and other properties (shape, composition, and surface charge) of micro-entities. This technique has been applied for trapping single cells using laser [177]. A major limitation for optical cell trapping is that the micro-entities should have refractive index different from that of the surrounding medium.

Magnetic trapping: Modulated magnetic field based on diamagnetic response of micro-entities has been developed for trapping micro-entities [178]. The advantage of this technique is that it is applicable to any diamagnetic micro-entity with different magnetic susceptibility from that of the medium. This method eliminates the need for magnetic labeling.

2.4.2.2 NON-ELECTROMAGNETIC CELL TRAPPING

The use of non-electromagnetic force to trap micro-entities has been used and is discussed here.

Mechanical trapping: This term encompasses methods which use mechanical force or physical structures for trapping micro-entities. One of the major mechanical trapping techniques is to create a hydrodynamic trap by modulating fluid flow to separate micro-entities from a flow and to immobilize them on certain sites. Mechanical obstacles or barriers are mostly used which sieve the object from a fluid by providing a passage for fluid only. The obstacle dimensions must be adjusted to capture particular type of micro-entity. Dam or wire structures have been developed to trap micro-entities like cells [179]. Once a cell is trapped, fluid flow is restricted and no other cell gets accumulated there. 'C' shaped microstructures with a small drain have been used for capturing single cells [93]. Though the efficiency and throughput for such trapping is high, but such a device needs to be optimized before cells of certain average size can be trapped efficiently. The problem with sieve based trapping is the high hydrostatic pressure experienced by cells during perfusion as trapped cell blocks the sieves and hinders fluid flow. The blockage also affects the flow of reagents in the cell trapping site. In another strategy, micro-wells have been used for trapping cells. The fluid flow in the well is low which prevents dislodging of trapped cells from these wells [180]. Although, such a strategy may create a cell pattern of high density single cell array, but docking of cells in micro wells is not an efficient process. Such pattern of cells can be used as a platform for drug screening, to

study effects of toxins or environmental pollutants, for single cell-based assays and many other applications.

Acoustic trapping: Standing acoustic wave field generated by one or more ultrasonic transducers can be used for acoustic trapping of micro-entities. The principle of acoustic force generation has been discussed in section-2.3.2.1. The micro-entities are trapped with balance acoustic forces.

Immobilization in gels: Micro-entities especially cells can be trapped and immobilized in hydrogels. Hydrogels have a high solvent content due to loose polymeric network. For example, agarose gels have high water content (more than 99%). Under such conditions cells are almost entirely surrounded by cell medium. Thus it helps in keeping cells alive. Moreover, cells can be released by dissolving the gel [181]. In one application, micro-fabricated cell-based biosensor has been developed by encapsulating cells using photolithography of poly(ethylene glycol) in hydrogel microstructures. An array of single or multiple encapsulated viable mammalian cells has been created for biological studies [182].

Chapter-3:

The 3D Microfabrication Technique

Chapter-3: The 3D Microfabrication Technique

3.1 INTRODUCTION:

To work in 3D micro-space can be a rewarding expedition with numerous applications at that scale. The simple way to define functional 3D micro-space is to fabricate 3D microstructures. However, the current techniques for fabrication of 3D micro-structures are complicated, expensive and slow besides being not easily available. Hence, a new technique overcoming these drawbacks of existing technology is clearly needed to receive wide acceptance from scientists with different technical expertise.

The above mentioned qualities desired for the new 3D microfabrication technique is commonly available in light based 2D microfabrication techniques. Energetic light-beams (like UV-light) are being widely used as a pattern transfer tool in these microfabrication techniques (like photolithography). Specially designed materials sensitive to energetic beams such as photoresists are used for recording the exposure pattern. Such an approach confers high efficiency and throughput in lateral pattern transfer, but it lacks control over the fabrication in vertical direction. Hence such approach is not used for 3D microfabrication. Instead highly localized exposure by using sophisticated equipment is used in the existing 3D microfabrication techniques. Most of these techniques focus on controlling the position or the distribution of light exposure on the material which allows controlled cross-linking in 3D micro-space. The exposure of material to energetic light-beam is either localized (e.g. two-photon photo-polymerization) or a gradient of exposure energy is generated (e.g. Gray-scale lithography). Thus, a cross-linking pattern is obtained which is developed as 3D microstructures. Fabrication of different types of 3D microstructures has been achieved by using this approach, but the requirement for highly

sophisticated equipment for controlling the exposure as well as low throughput due to 'point-to-point' exposure (like in Laser based exposure system) has limited their use. However, if the cross-linking can be controlled in the 3D micro-space without strict control over the exposure, a 3D microfabrication technique as simple and fast as 2D microfabrication techniques (as mentioned in the start of this paragraph) can be developed. This would retain the advantages of existing 2D microfabrication techniques, yet fabricate complex 3D microstructures.

Overall, the idea is to control the cross-linking of the material in 3D micro-space instead of controlling the exposure. The proposed approach can eliminate the need for any sophisticated equipment and reduce the related cost and time while retaining the advantage of light-based exposure system (patterned exposure and high throughput). However, controlling the cross-linking is challenging due to 'all-or-none' cross-linking pattern. Moreover, the exposed region is fully activated to cross-link isotropically. The cross-linking is energetically favorable and irreversible reaction which is difficult to be controlled. Hence, we hypothesized that partial activation (PA) may provide an opportunity to manipulate or control the cross-linking. In PA, the material would not cross-link instead some unstable bonding may occur which may favor anisotropic cross-linking into certain favorable configurations. In this work, we have studied this hypothesis and have proved anisotropic cross-linking due to partial activation of a photo-sensitive material. Based on this understanding, a new technique has been developed for the fabrication of 3D microstructures by simple methods. Technically, the technique developed here would require inexpensive and easily available resources, like plastic photo-mask, UV-light source (like Fluorescence-microscope with UV-light).

The idea used for developing this technique is new. A single photo-mask (inexpensive plastic mask) has been used for the fabrication of different 3D shapes in this study. The use of light and photo-mask in this technique is similar to the photolithography (a 2D microfabrication technique) which is used for transferring pattern from a 2D photo-mask to a layer of photo-sensitive material [183]. However, the use of PA for controlling cross-linking of exposed region is the core to this new technology. This technique has got high throughput like photolithography as arranged structures can be fabricated on a large area in a single process. Thus, it retains advantages of photolithography while fabricating 3D microstructures. Moreover, different 3D microstructures have been fabricated in this project using this technique, whereas only one type of 2D microstructure can be fabricated by a single photo-mask in photolithography. Hence, the concept and implication of this technique is very different from photolithography and it should not be considered just as an improvement of existing techniques. Overall, the technique is simple, efficient and inexpensive, the combination of traits which may ladder its acceptability by scientist and engineers of different research fields.

3.2 THE CHOICE OF MATERIAL

A light-sensitive material which cross-links after light exposure and which have multiple functional groups (for possible re-arrangement) would be required for testing this hypothesis. SU-8 has been selected as the suitable material for testing this hypothesis and for developing the technique for the fabrication of 3D microstructures in this project as it possesses above mentioned qualities. SU-8 is one of the commonly used negative photoresist for high-aspect ratio photolithography. SU-8 contains polymeric epoxy resin containing high density of epoxy functional-groups (around 8) within each molecule. These epoxy resins are dissolved in a solvent along with photo-initiator. The solvent is evaporated before exposing it to UV-light by soft-bake. When SU-8 is exposed to UV-light, the photo-initiators are converted into Lewis-acid which is referred to as photo-acid. The photo-acid initiates a cationic polymerization reaction which is very slow below glass-transition temperature of SU-8 (55°C) due to low molecular movements. The PEB at higher temperature is thus required for substantial cross-linking to take place. During PEB, polymerization reaction is initiated by photo-acids (H^+) via ring-opening reaction at epoxy bonds of SU-8 molecules [184]. Thus, the exposure by UV-light only activates SU-8, but the Post-exposure bake (PEB) at higher temperature completes the cross-linking [185]. During PEB, cross-linking species (i.e. photo-acids or activated cross-linking chains) in the exposed region may diffuse from exposed to unexposed region [186]. Such diffusion is undesirable for 2D pattern transfer techniques, like photolithography. However, partial activation (PA) can be generated by such diffusion which can help in the fabrication of 3D microstructures. The partial activation can also be generated by exposing SU-8 by the low dose of exposure energy.

3.3. MATERIALS AND METHODS:

3.3.1 REAGENTS, MATERIALS AND EQUIPMENTS

SU-8 2050 photoresist and SU-8 Developer were purchased from Microchem (Newton, MA). Sylgard-184 (PDMS) was purchased from Dow Corning (Midland, MI). Silicon-wafers were purchased from Teltec (Singapore). A photo-mask with a pattern of transparent circles (Scheme-S3.1a) was used for studying re-arrangement within the PA. The photo-mask with a pattern of opaque circles (Scheme-S3.1b) was used for the fabrication of 3D microstructures. Spin-coater (Cee, Brewer science) was used for coating a layer of SU-8 on the required substrate. UV-light exposure was done by using UV-light source in-built in the Mask aligner (Karl-SUSS Micro Tec.) or Fluorescence-microscope (transmitted light microscope, Axiostar plus, Carl-Zesis Inc.). The intensity of UV-light (365nm) was measured by a power-meter (Cole-parmer). Hot-plate (Sawatec.) was used for baking SU-8 at required temperature. Transmitted light microscope (Axiostar plus, Carl-Zesis Inc) or Scanning Electron Microscope (SEM, Jeol JSM5600) were used for visualization of samples. For FTIR analysis, a thin layer of gold was coated on the silicon-wafer by RF-sputtering system (Denton) before coating SU-8. The FTIR analysis was performed by the using Micro-FTIR (IR-microscope, AIM-8080, coupled with FTIR equipment, IR Prestige-21, Shimadzu Corp.).

3.3.2. STUDY OF ANISOTROPIC CROSS-LINKING DUE TO PARTIAL ACTIVATION

Single-layer sample: A layer of SU-8 was coated on a silicon-wafer at final rotational speed of 4000rpm (28µm thick layer, as measured by surface profiler, was obtained) and it was soft-baked for 2min at 65°C and 10min at 95°C to remove solvents. It was exposed

to the low dose of exposure-energy (according to Table-T3.1 as discussed in next section) without using any photo-mask (Scheme-S3.1c). This step was avoided for the control sample (Scheme-S3.1c). The second exposure was performed by the exposure energy of 280mJcm^{-2} through a photo-mask (Scheme-S3.1a) either immediately after first exposure or after performing PEB following the first exposure. The PEB was performed for 1min at 65°C and 5min at 95°C (after first and/or second exposure). It was developed for 5-7min in SU-8 developer solution. The result shown in Figure-3a and 3b was obtained by this experiment.

Double-layer sample: The double-layer samples were prepared for generation of PA at the interface of exposed and unexposed SU-8. These samples were prepared by coating and baking a layer of SU-8 as mentioned in previous paragraph. It was exposed by the required dose of exposure-energy (280mJcm^{-2}) without using any photo-mask. Another layer of SU-8 was then coated immediately, at same coating parameters as used for the first coating, without performing PEB of this layer (Scheme-S3.1d). For control samples, PEB was performed after the first exposure (1min at 65°C and 5min at 95°C) and before coating second layer of SU-8 (Scheme-S3.1d). It was soft-baked for 2min at 65°C and 10min at 95°C. It was then exposed through the photo-mask (Scheme-S3.1a) by the required dose of exposure-energy (280mJcm^{-2}). The final PEB was performed normally (1min at 65°C and 5min at 95°C) in one experiment (Fig.3.10a and b) whereas it was performed at high temperature (1min at 65°C and 5min at 105°C) in another experiment Fig.3.10c and d). It was developed as before.

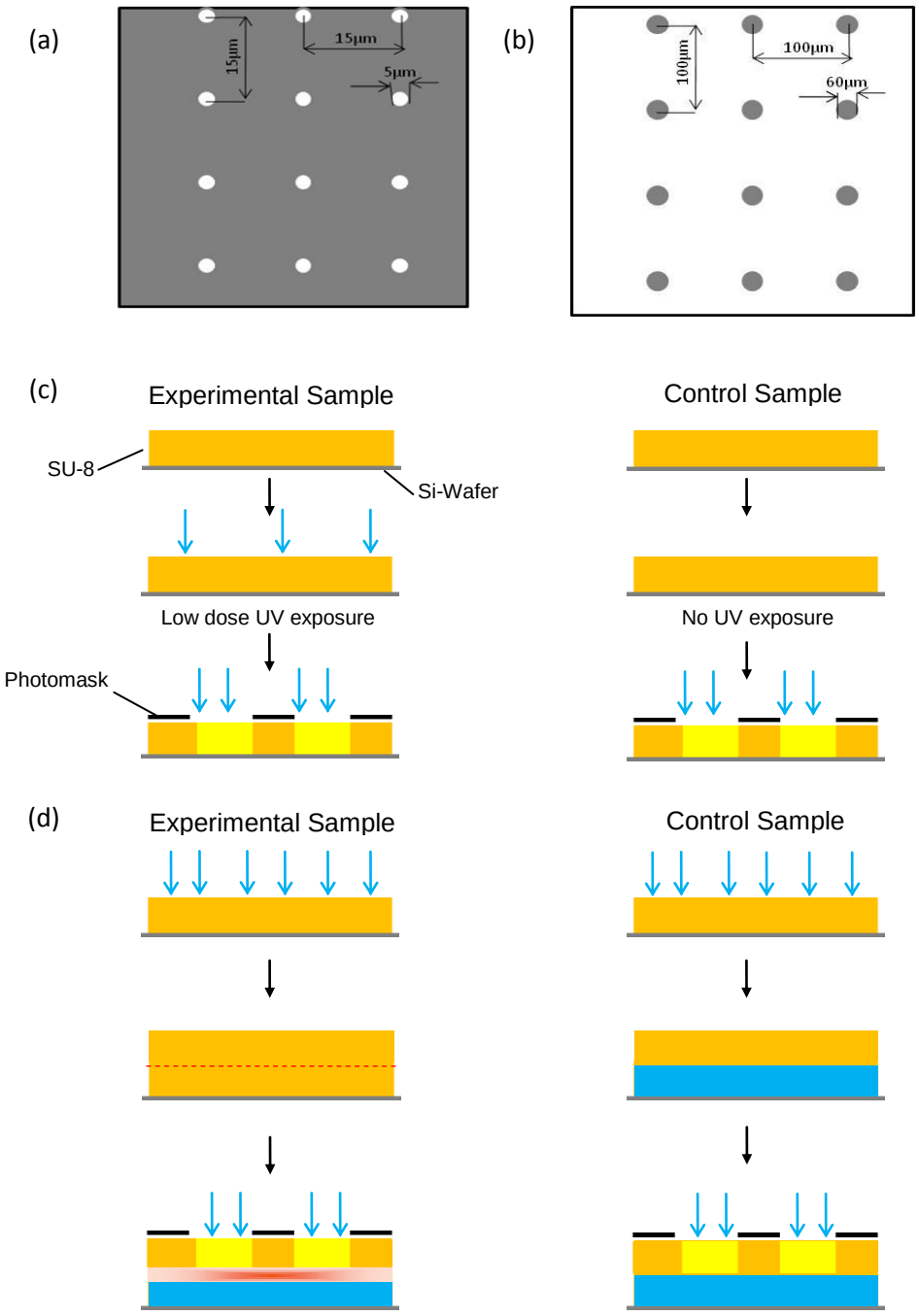

Scheme-S3.1: Photo-masks: (a) Photo-mask with a pattern of transparent circles, (b) Photo-mask with a pattern of opaque circles. (c) Single-layer sample preparation and experiments and (d) Double-layer sample preparation and experiments

FTIR analysis: All experiments for FTIR analysis were performed in the dark to avoid any effect of stray light on SU-8. The FTIR measurements were performed by using IR-microscope attached to the FTIR equipment. The sample was fixed on a glass-slide which could fit in the microscope stage. The sample position was fixed and was stored in the microscope software. The image of the sample was transferred to the aperture window and the required aperture was defined (right side in Fig.3.2a). The aperture position was also fixed and was stored in the software. Positional accuracy of the system was determined. To determine it, a small dirt-particle was enclosed in the aperture of 5µmX5µm. The glass-slide was removed and was placed back. The stored sample position and aperture position was restored. The position of dirt particle in the aperture was determined by maximizing the aperture window. The process was repeated to check the positional accuracy.

The FTIR measurements for SU-8 were taken in reflectance mode. About 80nm thick layer of gold (Au) was sputter-coated on the silicon-wafer at the power of 200W which acted as background for the IR-spectral measurements. A layer of SU-8 was coated on the gold-coated silicon-wafer at final rotational speed of 8000rpm (13µm thick layer was obtained) and it was baked for 1min at 65°C and 6min at 95°C to remove solvents. It was cooled for more than 30min before obtaining IR-spectra. The aperture-size was fixed in the software. Percent Transmittance was obtained which was converted to 'Absorbance' by the software attached to the equipment. Baseline corrections were performed before data-analysis. The spectral subtraction as well as determination of peak-intensity was performed using the same software. The steps detailed here were the basic step for all experiments done for the FTIR analysis.

FTIR study of Partially Activated SU-8: The IR-spectra of the soft-baked SU-8 was obtained by using the IR-microscope from an aperture of 40µmX40µm size. The sample position and the aperture-position were fixed and were stored in the software. It was then exposed to the low dose of exposure-energy (about 15mJcm^{-2}) without using any photo-mask. IR-spectra were obtained again from the same aperture area as stored in the software. Then, the PEB was performed for 1min at 65°C and 5min at 95°C. It was cooled for 30min and the IR-spectra were obtained from the same aperture area. This was target sample for studying the PA. Control sample for this experiment was prepared by performing the exposure by higher dose of exposure energy (about 100mJcm^{-2}) instead of low dose of exposure energy keeping all other steps same. The IR-spectra obtained from unexposed SU-8 was subtracted from the IR-spectra obtained after exposure to UV-light as well as from the one obtained after PEB. A comparison between two samples was made.

FTIR study of re-arrangement within the PA: The re-arrangement study was done by obtaining IR-spectra from different areas of interest. A layer of SU-8 was exposed to the low dose of exposure-energy (about 15mJcm^{-2}) without using any photo-mask. Then, a photo-mask (similar to one shown in scheme-S3.1a, but with different feature-dimensions, array 50µm circles with the pitch of 105µm) was used for the second exposure at the exposure energy of 100mJcm^{-2}. To take the IR-spectra after this step, the image of circles on the photo-mask was taken (the focus was done to image the circle area in contact with the SU-8 to avoid any mismatch due to thickness of the photo-mask). It was transferred to aperture window and apertures at different positions were defined. Then, the photo-mask was removed and the IR-spectra from different areas were

obtained. The PEB was then performed for the sample and IR-spectra were obtained again. After complete PEB, the exposed and unexposed areas can be visually distinguished (Fig.3.6a). The image was taken and was transferred to the aperture window where it was matched to the stored aperture position.

FTIR study of PA generation due to diffusion: For diffusion studies, the coating and soft-baking of SU-8 were performed as usual. After soft-bake, the substrate was exposed through a photo-mask containing an array of transparent squares (200µm side and 400µm pitch) by the exposure-energy of 100mJcm^{-2}. The PEB was performed either normally (1min at 65°C and 5min) or at high temperature (1min at 65°C and 5min at 105°C). FTIR measurements were obtained from different locations from the sample.

3.3.3 FABRICATION OF 3D MICROSTRUCTURES

The fabrication of 3D microstructures was done by using either a single-layer or double-layer of SU-8. The samples were prepared as discussed below.

Single-layer SU-8 sample preparation: SU-8 was spin-coated at a final rotational speed of 2000rpm for 40s on a clean silicon-wafer. It was soft-baked for 5min at 65°C and 20min at 95°C. It was cooled down for 10min and was exposed to UV-light by required dose of exposure-energy through the photo-mask (Scheme-S3.1b). For 'Single-layer Double-exposure' experiments, first exposure was performed with low dose of exposure-energy without a photo-mask immediately followed by second exposure through the photo-mask (similar to Scheme-S3.1c). Post-exposure bake (PEB) was performed for 1min at 65°C and 15min at certain temperature.

Double-layer SU-8 sample preparation: The first layer of SU-8 was coated at final rotational speed of 4000rpm and was soft-baked for 2min at 65°C and 10min at 95°C. It was cooled down for 8min and was exposed to the UV-light by an exposure-energy of 280mJcm^{-2}. The second layer was immediately coated without performing PEB of the first layer (similar to Scheme-S3.1c). The coating, baking and exposure of second layer were similar to the single layer mentioned in previous section.

Replica Molding: The Silicon-wafer containing SU-8 master mold was vapor-silanized by TRICHLORO(1H,1H,2H,2H-PERFLUOROOCTYL)-Silane in a vacuum chamber for 15min for easy release of PDMS replica. PDMS polymer base and cross-linking agent were mixed in ratio of 10:1 and stirred for uniform mixing. It was degassed in a vacuum desiccator. It was poured on SU-8 mold and baked for one hour at 70°C before peeling it out to obtain replica of structures in PDMS.

SEM imaging: A thin layer of gold was coated for 40s at 30mA in a gold sputter-coater (Jeol) on PDMS or SU-8 samples and they were visualized through the SEM (Jeol).

Data Analysis: The SEM images were used for measurement of different features of structures. The dimensions were measured using a soft-ware ImageJ (downloaded from www.rsbweb.nih.gov). The values were normalized with respect to maximum expected values. The base-width and the top-width were normalized by dividing the measured value by the known dimension of circular aperture on the photo-mask (60µm). The height was normalized by dividing the measured height by the SU-8 thickness obtained at the given spin-speed (here 60µm). The angle was normalized by maximum expected value of

90°. The Mean and Standard Deviation of measurements were calculated and were plotted by using Origin software.

3.4. RESULTS AND DISCUSSION

3.4.1 STUDY OF PARTIAL ACTIVATION

3.4.1.1 STUDY OF ANISOTROPIC CROSS-LINKING DUE TO PARTIAL ACTIVATION

As hypothesized earlier, the partially activated polymer may favor anisotropic cross-linking. To study this hypothesis, a simple experiment has been performed here. A layer of SU-8 is coated on a silicon-wafer and is soft-baked. It is uniformly exposed to the low dose of exposure energy and is baked again. The low dose of exposure energy in this step would initiate partial activation during baking step. Then, it is exposed again through a photo-mask (an array of transparent circles of diameter 5µm with the pitch of 15µm, Scheme-S3.1a) by required (as specified by the manufacturer) dose of exposure energy for complete cross-linking. PEB and development are performed normally. The first exposure (with low dose of exposure energy) is not performed while keeping rest of steps the same in the control sample of this experiment. Usually, exposure through the given photo-mask would produce an array of pillars as seen in the control sample (Fig.3.1b), but unexpected connecting structures between pillars are observed in target sample (Fig.3.1a). Since all other conditions are kept same for both of these samples, the connecting structures can only be attributed to the PA initiated by the first exposure with low dose of exposure energy. Though, the low dose of exposure energy used here is not enough to produce any cross-linked structures (it has been tested separately), yet,

connecting structures are formed. Also, the first exposure has been performed uniformly on the sample but connecting structures are observed in certain configuration only (between adjacent pillars). The result supports the hypothesis and indicates that the PA may favor anisotropic cross-linking. A range of exposure energy for the first exposure has been tested here (Table-T3.1). The result in the Table-T3.1 suggests that connecting structures are formed within a short-range of exposure energy only.

To further confirm the finding and to make sure that the observed effect is not limited to a particular size of pillars or pitch of the array, different pillar size with varying pitch has been tested and the same result has been obtained (data is shown for pillar size of 50µm with pitch of 105µm in Fig-3.1c and d). It elicits an interest to know more about behavior of the PA and their possible anisotropic cross-linking. To study the partial activation at molecular level, Micro-FTIR has been used in this work. The sample can be viewed using the Microscope attached to Micro-FTIR and IR-spectrum can be obtained from the exact area of interest. Thus, it gives a glimpse of changes taking place at molecular level at a particular area of interest. The next sub-section has discussed it in detail.

1st Exposure Energy	**No PEB after 1st exposure**	**PEB after 1st exposure**
7 $mJcm^{-2}$	No connecting structures	Connecting structures
14 $mJcm^{-2}$	Connecting structures	Connecting structures
21 $mJcm^{-2}$	Connecting structures	No connecting structures
28 $mJcm^{-2}$	No connecting structures	No connecting structures

Tabel-T3.1: Range of low dose of exposure energy for the formation of connecting structures: Different low dose of exposure energy with or without baking after the exposure is used. The same Photo-mask and SU-8 coating and baking condition, which are used for obtaining Fig.3a, have been used for this experiment.

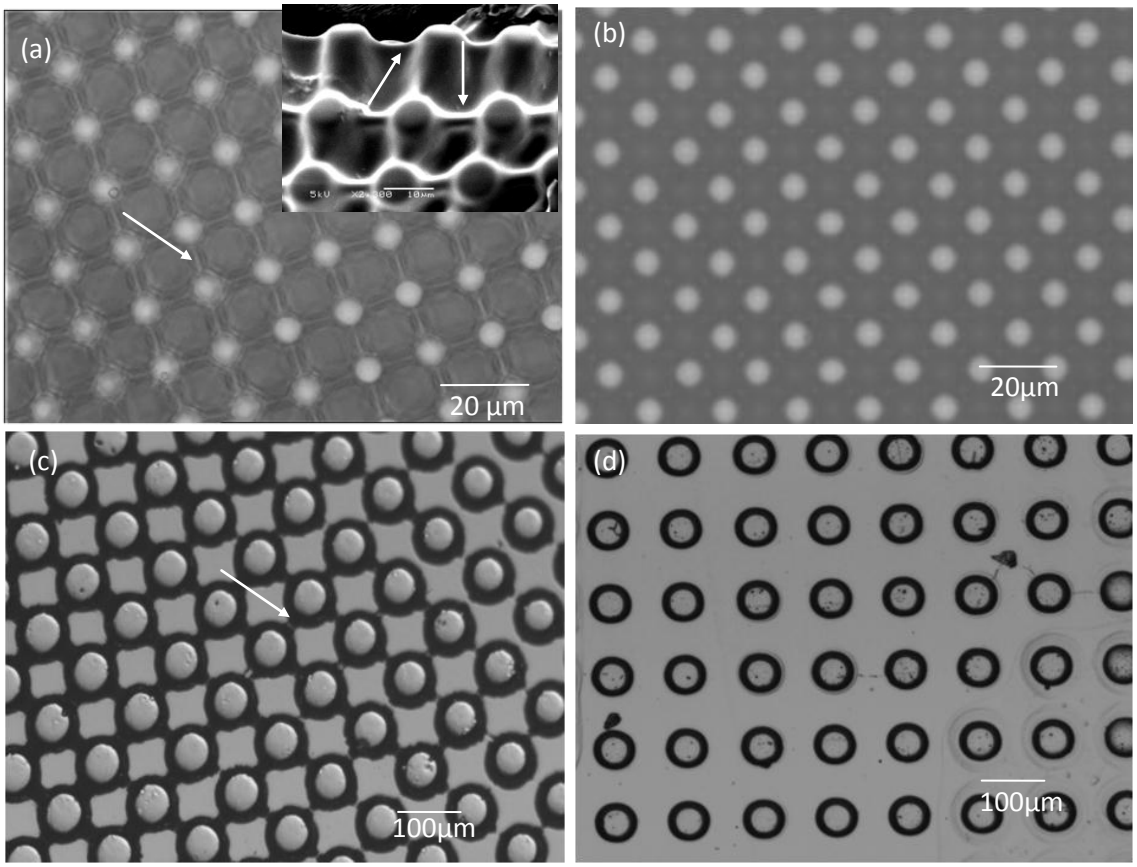

Fig. 3.1: Formation of connecting structures by the PA: (a) optical image of connecting structures between pillars (5µm pillars separated by 15µm) is obtained by the PA initiated by low dose of exposure energy, (b) is optical image of pillars without any connecting structures for the sample with no PA. Inset in (a) is the SEM image showing the connecting structure. (c) optical image of 50µm pillars separated by 105µm showing connecting structures which is obtained by partial exposure while (d) is obtained by using same mask as (c) without any partial exposure. Arrows point to the connecting structures.

3.4.1.2 Molecular study of Partial activation using Micro-FTIR

Positional Test for FTIR microscope: Micro-FTIR is a useful tool for obtaining IR-spectrum from a small area of interest. The position of the sample can be fixed and co-ordinates of the position can be stored in the attached software which allows retrieval of the same position. Thus, IR-spectrum from the same area of interest can be obtained after each experimental step. The positional accuracy of the equipment has been tested and it has been found that it is quite accurate in the error-margin of 5µm (Fig.3.2 and 3.3). To

test the positional accuracy, an aperture of 5μmX5μm is located around a small dirt particle (Fig.3.2a). The sample is removed and is replaced and the position is noted each time. It has been found that the dirt-particle remains in the defined aperture of 5μmX5μm (Fig.3.2b). In the same way, the spectral accuracy has been tested by obtaining IR-spectra from a particular position each time after replacement. The difference between any two spectra obtained from the same position is negligible (Fig.3.3).

FTIR peak allocation: The IR-spectrum for a particular experiment has been obtained from a single position; hence peak normalization with respect to any standard is not required for comparing spectra obtained after each experimental step. To compare the spectra obtained from two different positions/samples, spectral subtraction between spectrum with particular treatment and spectrum without any treatment is performed for both samples separately which are then compared. The IR-spectrum has been obtained in reflectance mode using the IR-microscope. For the FTIR study done in this work, the SU-8 has been coated on a gold-coated silicon-wafer as gold is an excellent reflector of IR. The IR-spectra of SU-8 without any light exposure (i.e. after soft-bake) has been obtained (Fig.-3.4b). Different absorbance peaks in the IR-spectra obtained here can be assigned to different bonds and their mode of vibrations [187]. The cross-linking in SU-8 proceeds with conversion of epoxy bonds to aliphatic ether bonds via cationic polymerization reaction. Hence, monitoring changes in the peaks related to ether bonds and epoxy bonds can give a glimpse of the cross-linking process. Saturated branched ether bond shows two or more peaks in wave-number range of 1070-1210cm^{-1}[188]. Two peaks, the peak at 1126±4cm^{-1} and 1111±4cm^{-1}, have been chosen here for reliable monitoring of changes

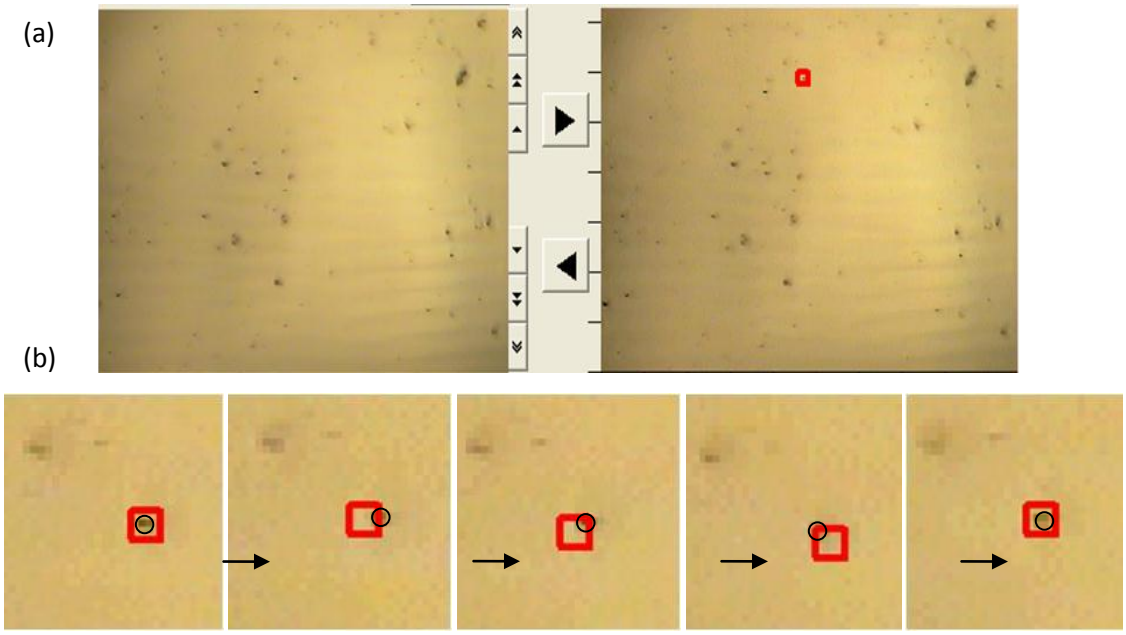

Fig. 3.2: Test for positional accuracy of the IR-microscope system: The positional accuracy of microscope stage is tested here. The coordinates of the sample position can be stored in the software. A sample with dirt particles is taken for this experiment. (a) shows the picture of sample (view mode, left-side) which is transferred to the aperture window (right-side) to define the aperture. The position of aperture is also stored. The aperture size of 5µmX5µm is fixed around a small dirt-particle in this study. The sample is taken out of the stage and is put back again and the aperture position is restored. The same particle is located by the relative position of other surrounding particles. The aperture-window is maximized and particle position in the aperture is located. (b) shows maximized image (cropped from original image). The dirt-particle is encircled here to show its location. The position of the particular particle is tracked after each time it is removed and is replaced. The series of images shows that the particle remains within the aperture area. So, the microscope can be used accurately at least with the aperture size greater than 5µmX5µm or with an error margin of 5µm.

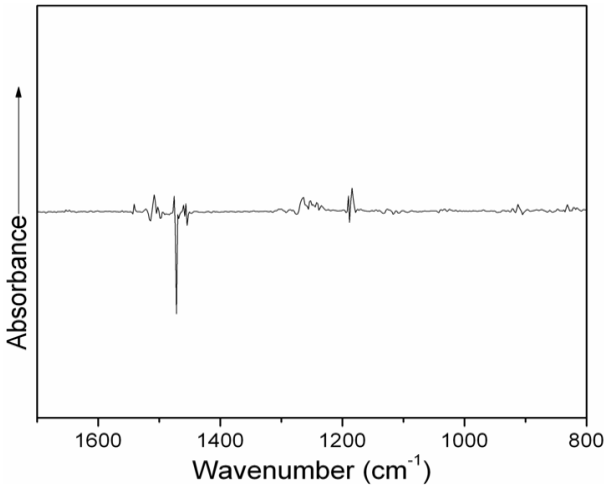

Fig. 3.3: Test of spectral accuracy with the FTIR-microscope system: The spectral accuracy is tested for the microscope by taking spectra from an untreated SU-8 with the aperture size of 40µmX40µm. The IR-spectrum from a particular position is obtained. Then sample is removed from the stage and is placed back and the same position is restored by the software. IR-spectrum is obtained again from that position. The difference of the two spectra is calculated as shown here. It can be seen here that two spectra nearly matched. The peaks of interest are zero.

in ether-bonds (has been observed to show expected variation and have also been used in literature, Ref-187). With certain treatments the peak positions change to slightly nearer wavenumbers, hence the peaks closet to the assigned peak, in the defined range, is chosen during analysis. The peaks at 914±4cm^{-1} and 862±4cm^{-1} are assigned for epoxy ring modes and have been chosen here for monitoring changes in epoxy bonds. Apart from these peaks corresponding to the functional groups participating in the cross-linking reaction, another peak corresponding to the bond that does not participate in the cross-linking reaction has been monitored to determine if the base molecule is affected in the PA. The change in peak intensity of a cross-linking bond would be due to disintegration or formation of that bond, but such change in non-cross-linking bond would be due to change in dipole-moment of that bond which can be due to change in charge distribution in the molecule [188]. Thus, monitoring changes in non-participating bonds would indicate the change in charge distribution within molecules in PA state. Each molecule of SU-8 contains about eight aromatic rings which do not participate in the cross-linking reaction. The peak at 1608cm^{-1} is assigned to aromatic ring C-C stretch mode. Normally, the peak intensity at 1608cm^{-1} should not change and that is reason for selecting it as reliable internal standard in previously published works [187]. Since this peak corresponds to bonds that do not participate in the cross-linking reaction, any changes in peak-intensity of the peak may suggest change in charge distribution around aromatic rings. Hence, change in peak-intensity of this peak has also been monitored in this work to understand if partial activation state affects the charge distribution in molecule.

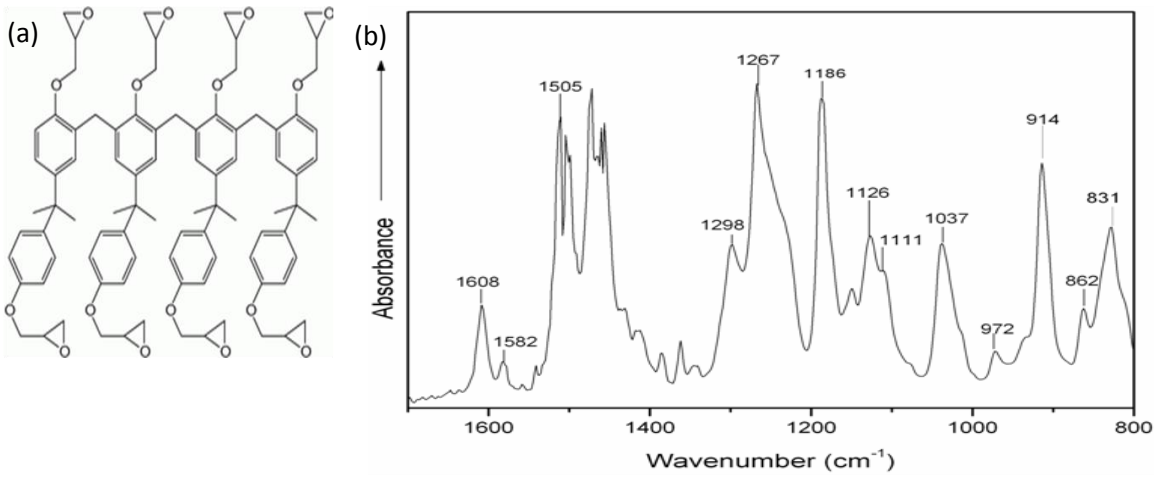

Fig. 3.4: SU-8 and its IR-spectra: (a) Molecular structure of SU-8, (b) IR-spectra of un-exposed SU-8.

FTIR study of partially activated SU-8: To start with, a sample with complete cross-linking has been studied as the control. A layer of SU-8 is exposed to the required dose of exposure energy (which is enough to cross-link SU-8 to from stable structures, about 100mJcm^{-2}) and PEB is performed normally. FTIR-spectra are obtained after each treatment from the same area. Spectral subtraction is performed for determining the corresponding changes due to each treatment. No significant change has been observed by the exposure to UV-light in any peak of interest which confirms that cross-linking does not occur with UV exposure until PEB is performed. After PEB, significant changes have been observed. The peaks corresponding to ether bonds increase while epoxy related peaks decrease (Fig.3.5a). The finding is reasonable and indicates the formation

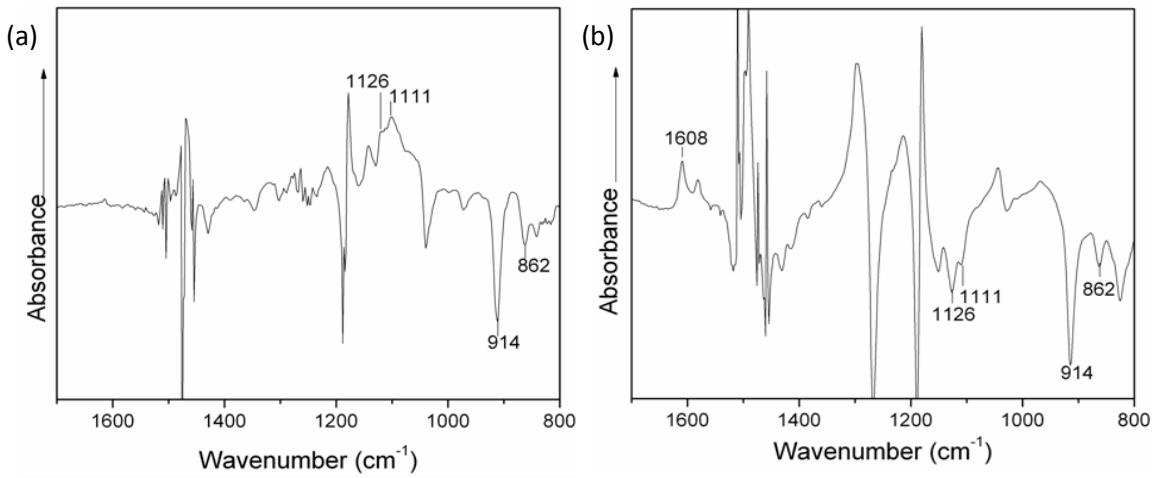

Fig. 3.5: IR-spectral study of cross-linking: Spectral changes due to complete and partial activation: The plots are obtained here by subtracting IR-spectra of unexposed SU-8 from (a) fully exposed and baked SU-8 (complete cross-linking), and (b) partially exposed and baked SU-8 (partial activation). The range of scale is same for (a) and (b).

of ether bonds with disintegration of epoxy bonds. The peak at 1608cm^{-1} has not changed during this experiment. Next, the target sample with induced PA is studied. A layer of SU-8 is exposed to the low dose of exposure energy (about 15mJcm^{-2}) and is baked as usual (PEB). FTIR spectra are obtained after each step. No significant change has been observed by UV-exposure (as before) but significant changes have been observed in the peaks of interest after baking step. Interestingly, the peaks related to both ether bonds and epoxy bonds have decreased significantly in their intensity after PEB (Fig.3.5b) while the peak at 1608cm^{-1} had increased in its intensity. The finding for this experiment is contrasting to the control experiment and indicates that the behavior of PA is quite different from their fully cross-linked counterpart. Although the exposure energy for PA is very low, the decrease in epoxy bonds is similar to that of complete cross-linking. Moreover, ether bonds also have decreased instead of increased. Thus, such decrease in epoxy bond should not be due to its disintegration as the decrease is unreasonably high and no new ether bonds have formed. The cross-linking reaction can only cause increase

in ether bond. Thus, the decrease in ether bond observed here means existing ether bond in the molecule has been affected in the PA state. An ether bond connected to the epoxy group and the aromatic ring does exist in SU-8 (Fig.3.4a). Also, the non-participating chemical bonds from aromatic rings have been affected. More than 25% increase in the corresponding peak intensity has been observed. As noted from the control experiment, this peak remains unaffected by the UV-exposure (which generates active/charged species) and PEB (which induces cross-linking). Thus, it can be inferred that such effects are unlikely due to activation or cross-linking reaction. Thus, the observed changes in the peaks of interest are due to change in dipole-moment of the bonds. However, it is difficult to predict the exact charge distribution in the SU-8 molecule pertaining to the observed changes. This might happen due to partial bonding of oxygen atom in epoxy bond with H^+ ions produced by the exposure. Since the amount of exposure energy is less, the amount of H^+ ions produced would also be less. Different oxygen atoms surrounding H^+ ions may interact with it but new bonds may not from. Such interaction may cause change in the partial charge on different atoms in SU-8 molecule, thus changing the overall charge distribution.

Anisotropic cross-linking in the PA: In section-3.4.1.2, the formation of unexpected connecting structures between pillars due to PA, as shown in figure-3.1a and 3.1c, has been studied. Herein, this phenomenon has been further studied by using Micro-FTIR. The conditions used for obtaining pillars with connecting structures in target sample shown in Fig.3.1c and pillars without connecting structures in the respective control sample shown in Fig.3.1d have been used for this study. Three areas of interest have been

selected by defining an aperture of 40µmX40µm (inset in Fig.3.7a). The aperture size has been chosen to be smaller than feature size to take into account the error margin in the positional accuracy. Area-1 is defined between two adjacent pillars, area-2 is defined at the center of four adjacent pillars and area-3 is defined on the top of a pillar. A layer of SU-8 is exposed to the low dose of exposure energy (about 15mJcm^{-2}). The IR-spectra from all three regions are obtained and are copmpared. No significant change among spectras is oserved. Then, it is exposed again through the photo-mask (an array of transparent circles of 50µm with pitch of 105µm) and the PEB is performed as usual. For the control experiment, the first exposure (by low dose of exposure-energy) is not performed, but rest of steps is kept same as the target experiment. IR-spectra are obtained from the defined areas of interest and are compared (Fig.3.6a, b). Area-3 and area-1 show increased peak-intensity for ether bonds and decreased peak-intensity for epoxy bonds whereas area-2 shows decrease in peak-intensities for both of these peaks (Fig.3.6b). The peak-intensity for the peak at 1608cm^{-1} is significantly increased for area-2 while it is slightly increased for area-1 and area-3. This indicates complete cross-linking at area-3 and area-1, while partial activation at area-2. Although area-1 and area-2 have been subjected to same treatments, area-1 has shown complete cross-linking behavior while area-2 has shown PA behavior.

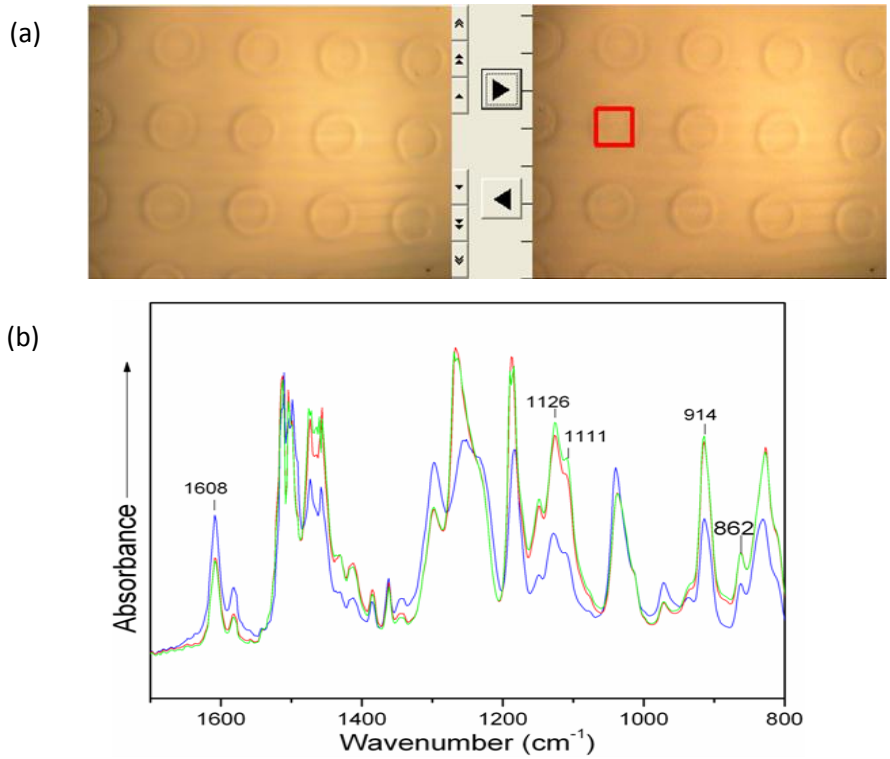

Fig. 3.6: IR-spectra from different areas: (a) Image taken from the software attached to micro-FTIR to shows how an area of interest is marked in the software and spectra is obtained from different areas. Area-3 is marked in this picture (discussed in main text). The IR-spectra from different position have been obtained. (b) The combined IR-spectra from Area-1 (red), Area-2 (blue) and Area-3 (green) after completing exposure through photo-mask and PEB are obtained for studying re-arrangement within the PA. The peak-intensities from Area-1 and Area-3 are similar while they differ from Area-2.

To further analyze the result, the spectral difference between different regions has been obtained. Untreated or UV-exposed SU-8 from all three regions does not show any significant difference. After PEB, for the control sample, the difference between IR-spectra obtained from area-1 and area-2 are negligible (Fig.3.7a). The area-3 shows higher peak intensity for ether peaks and lower peak intensity for epoxy peaks compared to area-1 (Fig.3.7b) which indicates higher degree of cross-linking at the exposed region (area-3). The peak at 1608cm^{-1} remains unchanged for the control experiment. The target experiment, however, has shown differences between IR-spectra obtained from all three

areas of interest (Fig.3.6b). The difference between IR-spectra obtained from area-1 and area-2 is significant (Fig.3.7c). Both ether and epoxy peaks from area-1 are much higher than area-2, but the peak-intensity of the peak at 1608cm^{-1} is lower. The increased peak-intensity at 1608cm^{-1} and decreased peak-intensity for ether and epoxy bonds from area-2 compared to area-1 indicates more PA at area-2 compared to area-1. The difference between IR-spectra obtained from area-3 and area-1 is less (Fig.3.7d). The ether peaks from area-3 are slightly higher than ether peaks from area-1 while difference between epoxy-peaks and aromatic C-C peak (at1608cm^{-1}) is negligible. The similarity in spectra between area-3 and area-1 indicates that cross-linking of polymers at area-3 and area-1 is similar. This supports the previous finding about the formation of connecting structures which is caused due to increased cross-linking at area-1. This finding suggests that the cross-linking at area-1 is affected by cross-linking at area-3. Another important thing to note here is the degree of cross-linking at area-3 and area-1. Although, the area-3 is exposed to exposure energy much higher than area-1, the degree of cross-linking at area-3 and area-1 is similar. The area-1 is only exposed partially, like area-2, but it shows much higher cross-linking than area-2. Hence, findings here suggest that cross-linking proceeds in an anisotropic manner in the PA regions under influence of rapid cross-linking at fully activated regions.

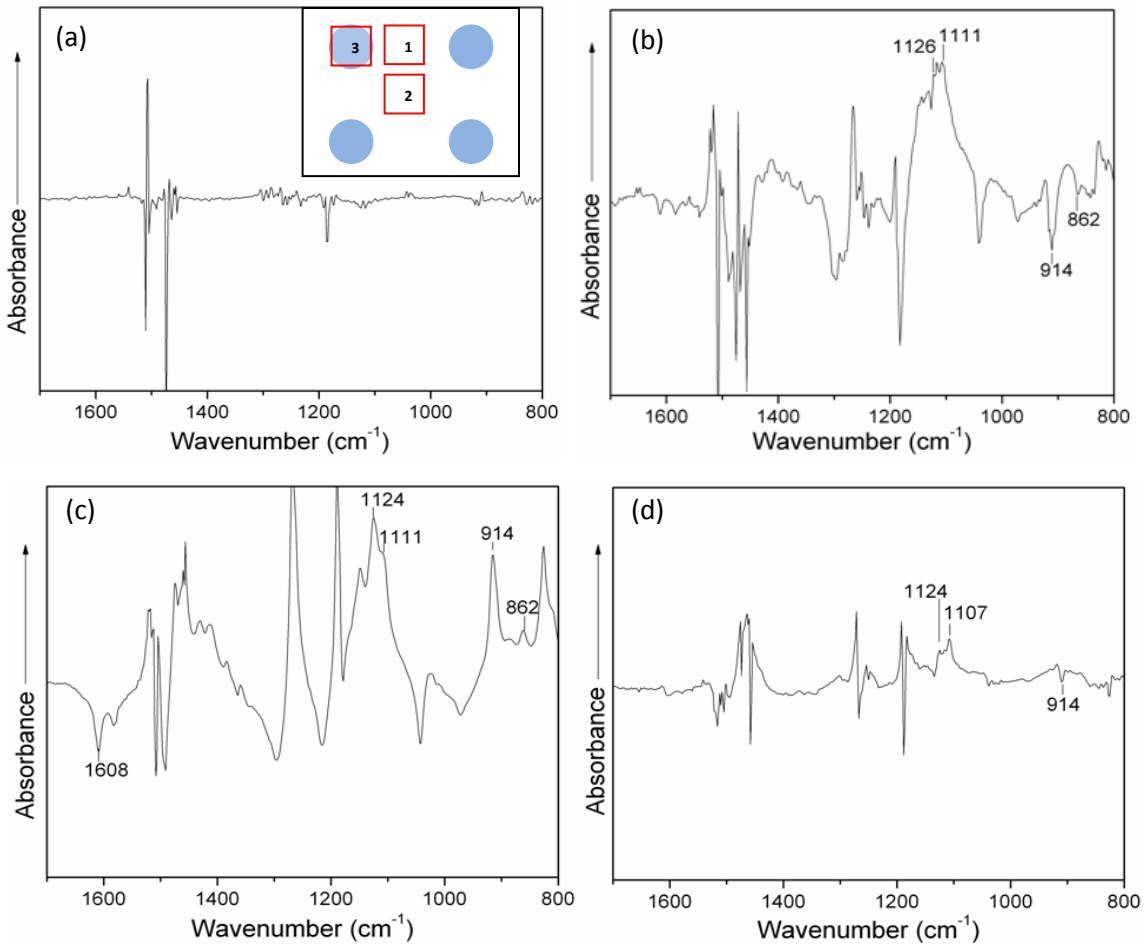

Fig. 3.7: Studying cross-linking at different areas under partial cross-linking: Inset in (a) shows the areas of interest for spectral measurements. (a-d) are spectral differences between different areas of interest. (a and b) are obtained from control sample without partial exposure, (a) is obtained by subtracting IR-spectrum of area-2 from area-1, and (b) is obtained by subtracting IR-spectrum of area-1 from area-3. (c and d) are obtained from target sample with partial exposure, (c) is obtained by subtracting IR-spectrum of area-2 from area-1, and (d is obtained by subtracting IR-spectrum of area-1 from area-3. The range of scale is same for (a-d).

To further investigate deeper on how the cross-linking occurs at different areas; an experiment has been performed to track the cross-linking process in the target sample. After exposure through the photo-mask, the PEB is performed by gradually increasing the PEB temperature while monitoring the spectral changes between all three areas as PEB occurs during cross-linking. It has been performed for 2min at 65°C, then 2min at 80°C and then another 2min at 95°C. The change in peak-intensities of the three peaks,

ether related peak at 1126cm^{-1}, epoxy related peak at 914 cm^{-1}, and peak for aromatic ring mode at 1608cm^{-1}, with respect to untreated SU-8 have been plotted here (Fig.3.8). The change in the peak-intensity of each peak of interest is plotted for all three areas of interest at four conditions, namely, the peak-intensity after UV-exposure through photo-mask, and after PEB at 65°C, 80°C and 95°C (Fig. 3.8). Plot shown in Fig-3.8a, 3.8b and 3.8c represents changes in peak-intensity of epoxy bonds, ether bonds and aromatic ring modes, respectively. Fig-3.8a and the Fig. 3.8b show that curve obtained from area-1 is between area-3 and area-2. The area-2 is expected to have PA and area-3 is expected to have complete cross-linking. Hence, the area-1 would possess characteristics of both partial as well as complete cross-linking. The plot for tracking changes in epoxy bonds (Fig. 3.8a) shows that the peak-intensity from area-3 decreases as PEB temperature is increased to 80°C and then it increases just slightly as PEB-temperature is increased to 95°C. For the same area, the plot for ether bonds shows an increasing trend (Fig. 3.8b). This indicates increase in the degree of cross-linking at this area with increase in PEB temperature (as expected). The peak at 1608cm^{-1} does not show significant change (Fig. 3.8c). The plot for area-2 shows different characteristics than area-3. For both ether peak and epoxy peak, the peak-intensity remains unchanged when PEB is performed at 65°C, and then a sharp decrease in peak-intensity is noted as PEB temperature is increased to 95°C (Fig. 3.8a and b). The peak at 1608cm^{-1} shows opposite characteristics for the same range of temperature from the same area (Fig. 3.8c). The sharp decrease in the plot from area-2 for epoxy bonds as well as ether bonds and concomitant increase in the peak at 1608cm^{-1} indicates increase in partial activation at area-2. The plot from area-1 shows

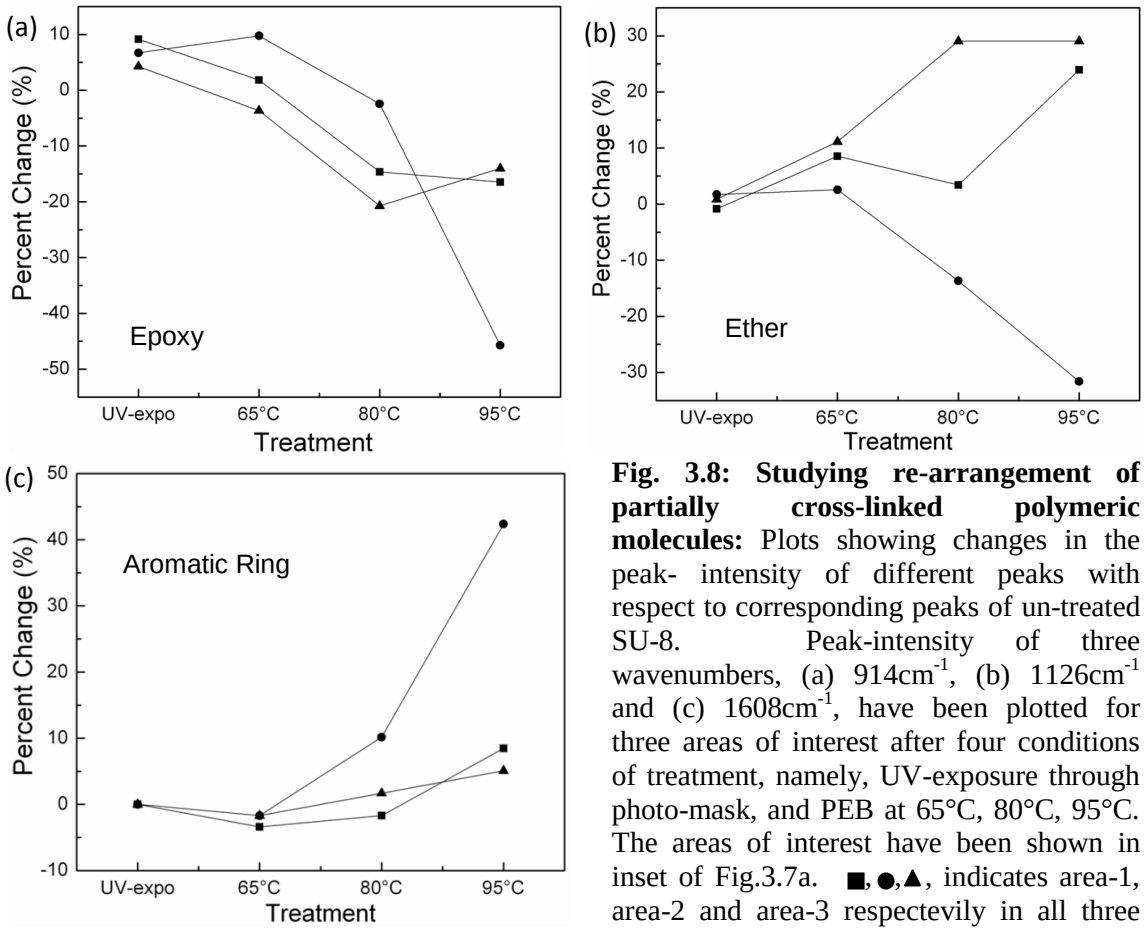

Fig. 3.8: Studying re-arrangement of partially cross-linked polymeric molecules: Plots showing changes in the peak- intensity of different peaks with respect to corresponding peaks of un-treated SU-8. Peak-intensity of three wavenumbers, (a) 914cm^{-1}, (b) 1126cm^{-1} and (c) 1608cm^{-1}, have been plotted for three areas of interest after four conditions of treatment, namely, UV-exposure through photo-mask, and PEB at 65°C, 80°C, 95°C. The areas of interest have been shown in inset of Fig.3.7a. ■, ●,▲, indicates area-1, area-2 and area-3 respectevily in all three plots.

a trend different from both area-3 and area-2. For the area-1, the plot related to epoxy bonds (fig. 3.8a) is similar to the area-3, but the corresponding plot for the ether bonds is different (Fig. 3.8b). The similarity in changes in epoxy bonds (almost through-out the experiment) suggests that the cross-linking at area-1 is influenced by area-3, as these two areas have been treated differently. Although, area-1 and area-2 have received same exposure treatment, yet, cross-linking at area-1 is similar to area-3. The peak at 1126±4 cm^{-1} (ether) from area-3 increases continuously which indicates formation of new ether bonds. The same peak from area-1 increases then slightly decreases and then increases again. This shows that cross-linking begins in area-1 as ether peak increases. Slight

decrease in ether peak suggests that there is generation of PA molecules along with complete cross-linking, as ether peak in PA shows decrease in intensity. Finally, it cross-links completely similar to area-3. This further suggests that cross-linking at the area-1 is influenced by cross-linking at area-3. This conclusion is supported by results from area-2 which shows sharp decrease for epoxy and ether peaks besides sharp increase in aromatic-ring peak. Although area-2 and area-1 have received same exposure treatment, their cross-linking pattern is very different. This proves the anisotropic cross-linking within PA material under the influence of rapid cross-linking at area-3.

3.4.1.3 STUDY OF PARTIAL ACTIVATION DUE TO DIFFUSION

FTIR study of partial activation due to diffusion: As discussed in the previous sub-section, the PA can be generated by low dose of exposure energy. PA can also be generated by diffusion of activated molecules from exposed region to unexposed region. The exposure to UV-light activates SU-8, but the cross-linking takes place during PEB, which may allow diffusion of active species from exposed region to unexposed region. If the amount of diffusion is high, the unexposed region will cross-link completely, but if it is low PA may be generated in the unexposed region due to low amount of diffused cross-linking initiators. Micro-FTIR has again been used to study the generation of PA due to diffusion. A layer of SU-8 is exposed to UV-light through a photo-mask (opaque Square area of 200µmX200µm). Two such samples are prepared. PEB for one of them is performed as usual at 95°C while for other it is performed at 105°C. Diffusion is expected to be higher at higher temperature. The IR-spectra is obtained from a fixed aperture size of 50µmX50µm and from three positions of interest as shown in inset of

Fig.3.9a (also refer to Fig.3.9e). The position-1 is located in the exposed region while position-2 and position-3 are in the unexposed region. All conditions for both samples remain same except for the temperature of PEB. A comparison between these two samples can indicate the differences due to diffusion at different temperatures. The IR-spectra from these three regions does not show any significant difference before any treatment, but after PEB at 95°C, the difference between IR-spectra obtained from position-1 and position-2 shows no change for aromatic C-C stretch peak, positive change for ether peaks and negative change for epoxy peaks (Fig.3.9a). This indicates that cross-linking at position-1 is higher than position-2, which is reasonable as position-1 is exposed while position-2 is not. Though, position-3 is also not exposed, but it shows slight increase in aromatic C-C stretch peak and decrease in both ether and epoxy peaks compared to position-2 (Fig.3.9b). This indicates PA at position-3 which could be due to diffusion as it is adjacent to position-1. The result obtained here differs from the one obtained from another sample with PEB at 105°C. In this sample, the peak-intensity of aromatic C-C stretch peak has increased at position-2 compared to position-1 as it is negative (Fig.3.9c). This indicates the some PA characteristics at position-2. However, the ether peak is not increased as expected (considering it should be negative for PA at position-2). Thus, at position-2, characteristics of both PA and complete cross-linking exist. This can happen due to high diffusion at increased temperature as other parameters are kept same for these two samples. The difference between position-2 and position-3 is negligible which supports that the diffusion is high enough to allow diffused species to reach the position-2. This is confirmed by developing these two samples. The sample with PEB at 105°C has much reduced feature size compared to the sample with PEB at

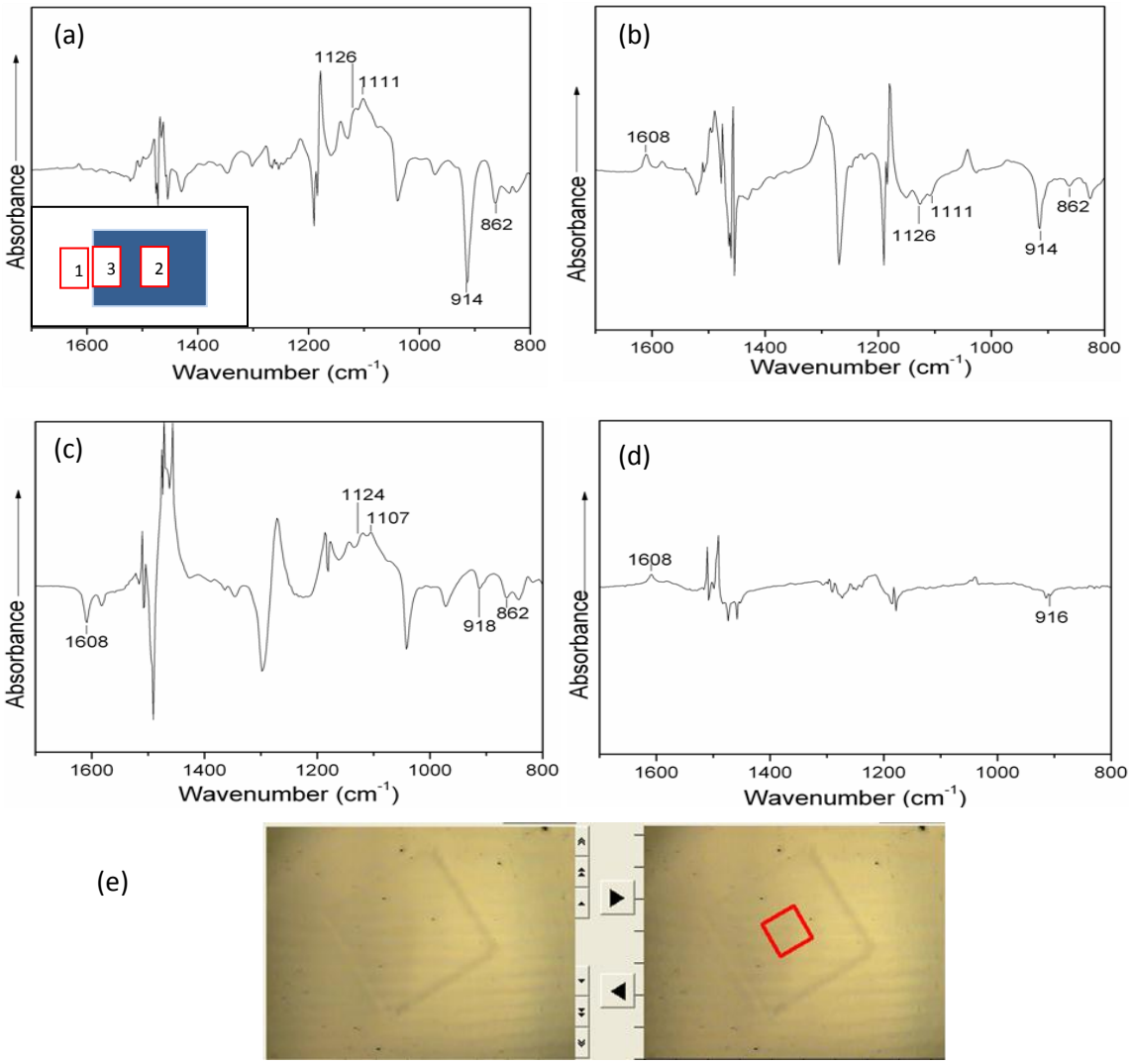

Fig. 3.9: Partial cross-linking due to diffusion: (a-d) are obtained by subtracting IR-spectra from one position to another position (different positions are shown in inset in (a)). For the PEB performed at 95°C, (a) is obtained by subtracting IR-spectrum of position-2 from position-1, (b) is obtained by subtracting IR-spectrum of position-2 from position-3. For the PEB performed at 105°C, (c) is obtained by subtracting IR-spectrum of position-2 from position-1, (d) is obtained by subtracting IR-spectrum of position-2 from position-3h. (e) is the image taken from the microscope-software showing feature in view-window (left hand side) and feature with aperture in the aperture window (right hand side). The range of scale is same for (a-d).

95°C. Thus, the two samples show different trends due to difference in PEB temperature which suggest that diffusion of activated species can take place during PEB and PA can be generated due to diffusion.

Formation of structures due to the PA obtained by diffusion: Next, the formation of structures due to re-arrangement of PA caused by diffusion has been studied here. To study this, another sample consisting two layers of SU-8 has been prepared. A layer of SU-8 is exposed to UV-light and then another layer is coated without performing PEB of first layer. As cross-linking of the first layer would not be completed without PEB, diffusion of activated cross-linking species from exposed layer to unexposed layer would take place. The second layer contains solvent which would enhance this process. A gradient of partial activation is expected at the interface of two layers. To prepare a control sample, the PEB is performed after exposure of first layer to complete the cross-linking and to avoid any interaction between two layers. The second layer is exposed to normal dose of UV-light through the photo-mask (an array of transparent circles of 5µm with pitch of 15µm) and the PEB is performed normally at 95°C. Similar type of connecting structures is observed at the bottom of pillars in the target sample (Fig.3.10a), whereas no such connecting structures are observed in control sample (Fig. 3.10b). Since the PA is expected at the interface between first and second layer, connecting structures are only formed at bottom of pillars (Fig.3.10a and e). The replica mold in PDMS obtained from the target sample (Fig.3.10a) shows dome-shaped microstructures formed due to space enclosed between connected structures at bottom of pillars (inset in Fig.3.10e). This confirms the anisotropic cross-linking due to PA generated by diffusion.

The next question to answer is whether the PA can dynamically affect the cross-linking in the adjacent regions. To study this, samples have been prepared in the same way as the previous experiment (above paragraph). All conditions for both of these experiments are kept the same except for the temperature of final PEB. The final PEB is performed at 105°C instead of 95°C. The idea is to allow diffusion of cross-linking species from pillars at higher temperature. In this set-up it can be observed if PA at interface affects the cross-linking of diffusing molecules. At increased PEB temperature (105°C), the results are interesting. Diffusion is expected to be high within second layer at this temperature which can be interpreted from the control sample. For control sample, no distinct pillars are formed and all structures are nearly merged together due to increased diffusion (Fig.3.10d). Same conditions for diffusion exist for target sample also, but connecting structures, through-out the height of pillars, are formed by diffusing species in this sample (Fig.3.10c and f). The PDMS replica mold obtained from target-sample (Fig.3.10c) shows large micro-structures formed due to space enclosed between pillars due to connecting structures through-out the length of pillars (inset in Fig.3.10f). Since, the only difference between the target and the control sample is the PA at interface; it indicates that the diffusing species in adjacent layer are dynamically influenced by the PA at the interface. This provides an opportunity to control such cross-linking which can help in 3D microfabrication.

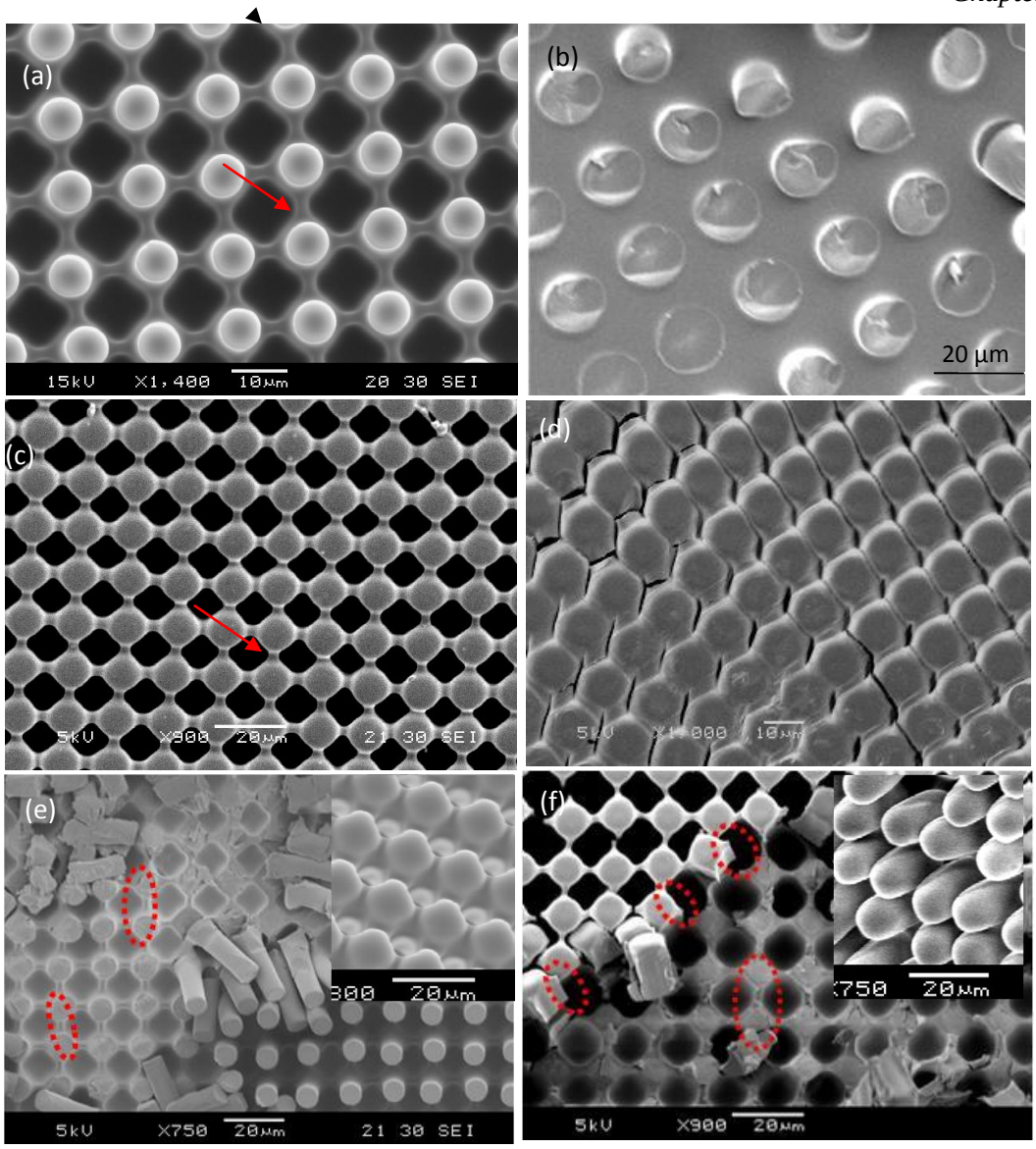

Fig. 3.10: Re-arrangement of Partially activated polymer obtained by diffusionof activated species: (a-f) are SEM images of SU-8 samples for the experiment with double-layers of SU-8. The insets in (e) and (f) are PDMS replica of respective samples. (a) and (c) are experimental sample obtained by coating second layer without performing PEB of the first layer. For control sample (c and d), PEB of first layer is performed normally. Second exposure is carried-out through photo-mask (array of transparent circles). Final PEB for sample (a and b) is performed at 95°C and for sample (c and d) is performed at 105°C. Connecting structures at pillar's bottom are seen in SEM image (a) but not in (b) (pillars are broken to show the bottom in (b)). Connecting structures between pillars are seen in SEM image of SU-8 mold (c) and no distinct pillars or connecting structures can be seen in (d). (e) and (f) are obtained by deliberately breaking pillars (to see the bottom) in sample (a) and (c) respectively. Red-elipses show connecting structures at bottom of pillars in (e), but in (f) they show connecting structures at the bottom as well as through-out the pillar. Inset in (e) shows small PDMS structures while inset in (f) shows larger PDMS structures (similar in size to SU-8 pillars in main-figure shown in f).

3.4.2 THE 3D MICROFABRICATION TECHNIQUE

3.4.2.1. EFFECT OF EXPOSURE ENERGY AND PEB TEMPERATURE

The anisotropic cross-linking due to partially activated SU-8 has been studied in the previous section. In this section, several methods would be demonstrated for fabrication of 3D microstructures based on this principle. These methods are based on generating the PA and allowing it to cross-link anisotropically to fabricate unique 3D microstructures. The two important experimental parameters, exposure energy and PEB temperature, can affect the structure formation and hence the section starts with the study of their effects on the cross-linking of SU-8.

It has been demonstrated in the previous section that partial activation can be generated by diffusion of the activated cross-linking species from exposed to unexposed region. The temperature of PEB and energy of exposure are two important parameters that can affect the diffusion and hence structure formation. The PEB temperature controls the amount of diffusing species while exposure energy would determine the amount of activated species in the exposed region which can initiate diffusion (due to concentration gradient). Thus, the effect of exposure energy and PEB temperature on the structure formation has been studied in this project (Fig.3.11). The general scheme for this experiment has been presented in Fig-3.11(a). The design of photo-mask used for these experiments have been shown in Scheme-S3.1b. It is normal photolithography, in which the sample is exposed through the photo-mask by using different amount of exposure energy and PEB is also performed at different temperatures.

After development, the structures are replicated in PDMS. The base-width/diameter of a

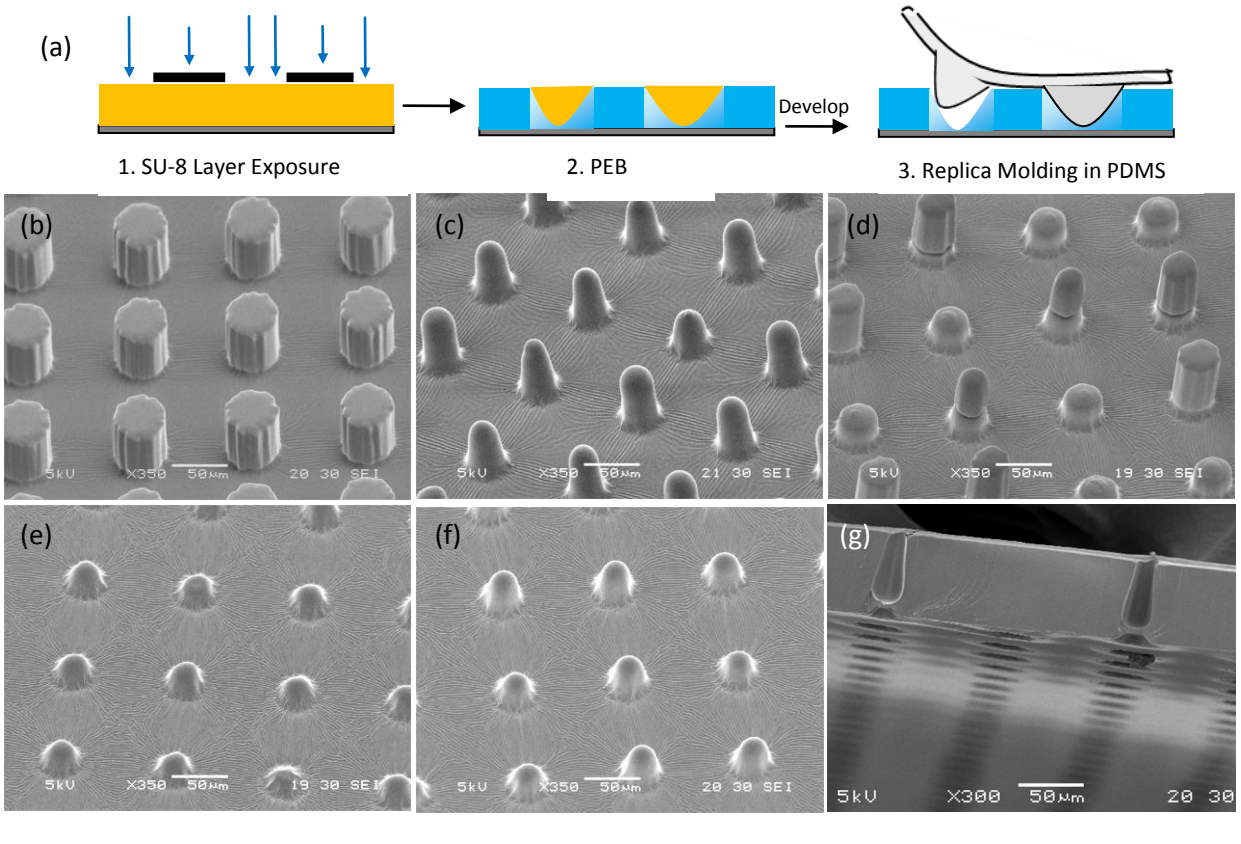

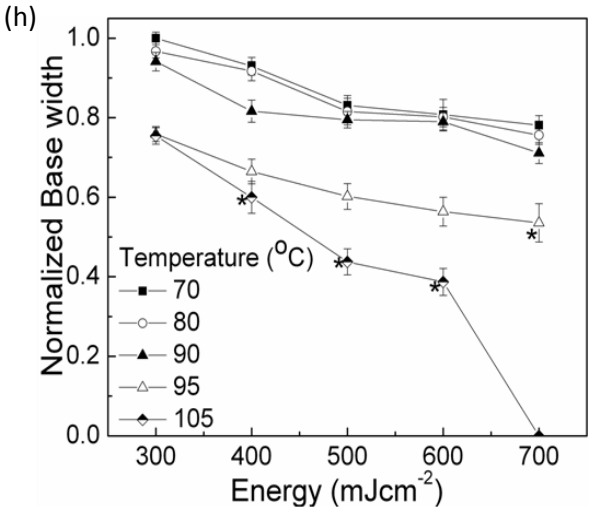

Fig. 3.11: **Effect of the exposure-energy and the PEB- temperature:** a general schematic for experiments (a). SEM micrographs (b-f) are PDMS replica mold and (g) is SU-8-mold structure. (h) is the graph obtained by varying exposure energy dose at different PEB temperature. (b) is the normal 2D structure and (c-f) are 3D conical structures obtained at conditions indicated by (*) in plot-h. (c) is obtained by exposure-energy of 700mJcm^{-2} at 95°C and (d-f) are obtained by 400-600 mJcm^{-2} (in ascending order) of expoosure-energy at 105°C respectively. (g) is the SU-8 mold for the replicated structures shown in (d).

replicated structure is measured and it is normalized by the width/diameter of a feature on the photo-mask. The decrease in this ratio gives an idea of diffusion of activated species from exposed region to unexposed region. A plot between different exposure energies and normalized base width has been obtained for different PEB temperatures (Fig-3.11h). The plot indicates that the size of structures decreases with increase in exposure energy as well as PEB temperature and this effect is more prominent at the higher values of these parameters. During PEB, the photo-acids (H^+) can diffuse to the unexposed region initiating cross-linking reactions [189]. The diffracted or refracted UV-light during exposure may also contribute to this effect. 2D cylindrical pillars (without any curve or inclined line in vertical dimension) have been obtained (Fig.3.11b) at many of these conditions, but at few conditions (indicated by (*) in the plot), 3D conical microstructures (Fig.3.11c-f) and 3D microstructures with 'kink' (Fig.3.11d and g) have been obtained. The 3D microstructures have been obtained at higher values of exposure energy and PEB temperature. At higher values of these parameters the diffusion is higher (prominent decrease in base-width). The 3D conical microstructures might have been caused due to non-uniform diffusion, but formation of 'kink' indicates the anisotropic cross-linking within PA caused due to diffusion. Overall, this experiment shows that exposure energy and PEB temperature can affect the extent of diffusion as well as the structures formation.

3.4.2.2 Fabrication of 3D microstructures by low dose of exposure energy

In the previous section on partial activation (Section: 3.4.1), it has been shown that the PA induced by low dose of exposure energy can from unexpected structures (like

connecting structures between pillars). This section deals with the fabrication of 3D micro-structures by the PA induced by low dose of exposure energy.

Simply, a single layer of SU-8 is exposed by UV-light to the low dose of exposure energy without any photo-mask and then it is exposed again through the photo-mask (Scheme-S3.1b). A range of exposure energy (400-800 $mJcm^{-2}$) is used for the exposure. Two different exposure energies have been studied here as the first exposure ($7mJcm^{-2}$ and $14mJcm^{-2}$). The PEB temperature used for this study is 80°C. The formation of 3D structures has not been noticed at this temperature without any partial exposure (Fig.3.11). Hence, the 3D microstructures fabricated by this method can be attributed to the PA induced by the low dose of exposure energy. Prominent 'Hour-glass' shaped micro-structures and conical structures with high angle of cone have been obtained by this method (Fig.3.12a-d). Plots have been drawn between normalized values of different defining features of 3D microstructures and exposure energy (Fig.3.12e and f). In these plots, (*) indicate the formation of microstructures with double-level architecture ('Hour-glass' shaped) as shown in Fig.3.12a-c. Also, with increase in energy of exposure for the first exposure (low dose), the kinked structure is formed at lower value of exposure energy (1^{st} point in plot in Fig.3.12f) and with further increase in exposure energy more conical-like structures are formed (Fig.3.12d). As no such structure forms at same values of exposure energies and PEB conditions without uniform exposure to low dose of energy (Fig.3.11), so the PA generated by the first exposure should be the cause of formation of double-level structures. Since the first exposure is uniform through-out the layer of SU-8 (exposure without any mask), the 'kink' formation should be caused by

anisotropic cross-linking within the PA. The result indicates that the PA can cause the formation of double-level 3D microstructures with 'kink'.

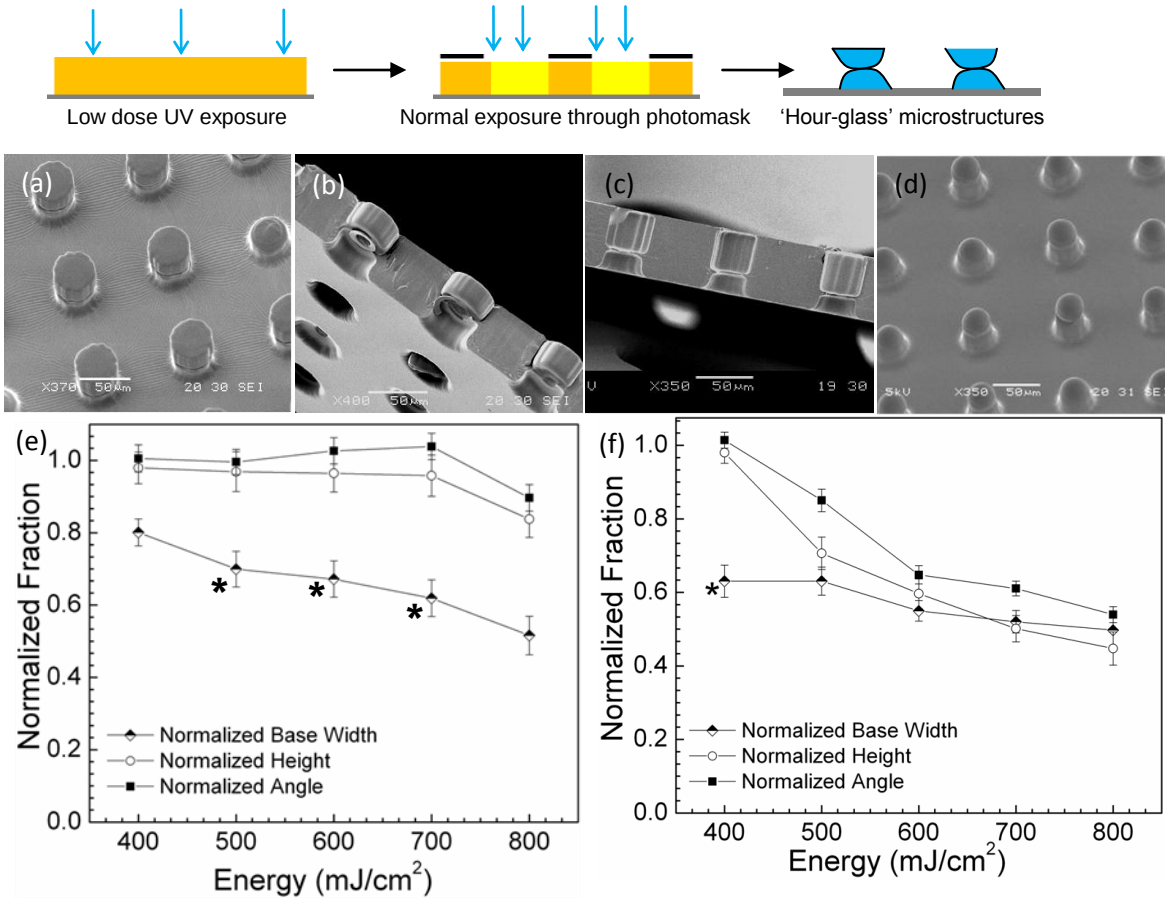

Fig. 3.12: Partial activation by low dose of exposure energy: schematic shows the low dose exposure method. (b and c) are the SEM-images of the SU-8 mold while (a and d) are the SEM-images of the PDMS replica. The Plot (e and f) represents the change in normalized value of different defining features against exposure energy. (*) in the plot indicates the formation of 'Kink'. A layer of SU-8 is exposed by the low dose of exposure energy (7mJcm^{-2} for obtaining (e) and 14mJcm^{-2} for obtaining (f)). It is then exposed through a photo-mask and PEB is performed at 80°C. (a) is obtained at 2nd point while (b) is obtained at the 4th point in the plot shown in (e). (c) appears at the 1st point while (d) appears at the 2nd point in the plot shown in (f).

3.4.2.3 FABRICATION OF 3D MICROSTRUCTURES BY RAMPING-UP PEB TEMPERATURE:

The preceding sub-section has shown the possibility of fabrication of 3D micro-structures by the PA generated by low dose of exposure energy. In this section formation of 3D microstructures by the PA generated by diffusion would be explored. Herein, it is hypothesized that if PA is non-uniformly distributed, then their re-arrangement may produce different 3D microstructures. To cause such non-uniformity, PEB has been performed by ramping-up temperature in this study. Captivatingly, different types of 3D microstructures, with double-level architecture like 'Hour-glass shaped', 'Popsicle-shaped' and 'Doll-like', have been obtained from these experiments (Fig.3.13a-f). Assuming these structures to be conical, plots between exposure-energy and normalized values of different defining features have been drawn (Fig.3.13g-i). The (*) indicates the condition at which double-level structures (by appearance of a kink) have been obtained. Conical structure has been obtained at rest of conditions. Based on the previous experiment on the effect of exposure energy and PEB temperature on cross-linking, the temperature range 85°C-90°C, 90°C-95°C and 95°C-100°C have been empirically classified as less, moderate and highly sensitive diffusion zone. Ramping-up temperature in low diffusion range does not show any prominent formation of 3D microstructures (data not shown). Hence, the first temperature ramp-up range has been chosen as 85°C-95°C as a combination of low and moderate diffusion range. It is hypothesized that in this range, some degree of cross-linking would take place (between 85°C-90°C) before diffusion supersedes (between 90°C-95°C). So, this would restrict the diffusion of cross-linking species and would allow the PA in unexposed region. The second ramp-up temperature has been chosen in moderate (90°C-95°C) diffusion range of PEB-

temperature. Interestingly, the distinct kink formation has been observed for the first temperature range for ramp-up (85°C-95°C) which becomes prominent with increase in exposure energy (Fig.3.13a-c). At first two energy points in the plot (Fig.3.13g), kink is smaller as shown in Fig.8a, but it becomes prominent and distinguished as the exposure-energy is increased to towards 4^{th} point (Fig.3.13b and c). The further increase in exposure energy suppresses the formation of kink and results in formation of single-level conical structures as obtained at 5^{th} point in Fig.3.13g. The formation of conical structures indicates the increase in diffusion which is reasonable here as the exposure energy is increased. In the second temperature range of ramp-up (90°C-95°C), the structures are more conical indicating more diffusion than the first one (Fig.3.13h). Unique 'Doll-like structures' have been obtained in this range. 'Kink' (between neck and body of the 'Doll-like structures') can be observed for this range also. The kink formation observed here should have been caused due to re-arrangement within the PA. The explanation is further supported by the experiment done in the temperature range 95°C-100°C (diffusion is expected to be high in this range), where no kink is observed in the exposure energy range used for earlier experiments (2^{nd} point onwards in fig.3.13i). The kink only occurs at reduced exposure energy (1^{st} point in fig. 3.13i) and with increase in diffusion 'Kink' is not prominent. Hence, the kink formation is due to PA caused due to low amount of diffusion.

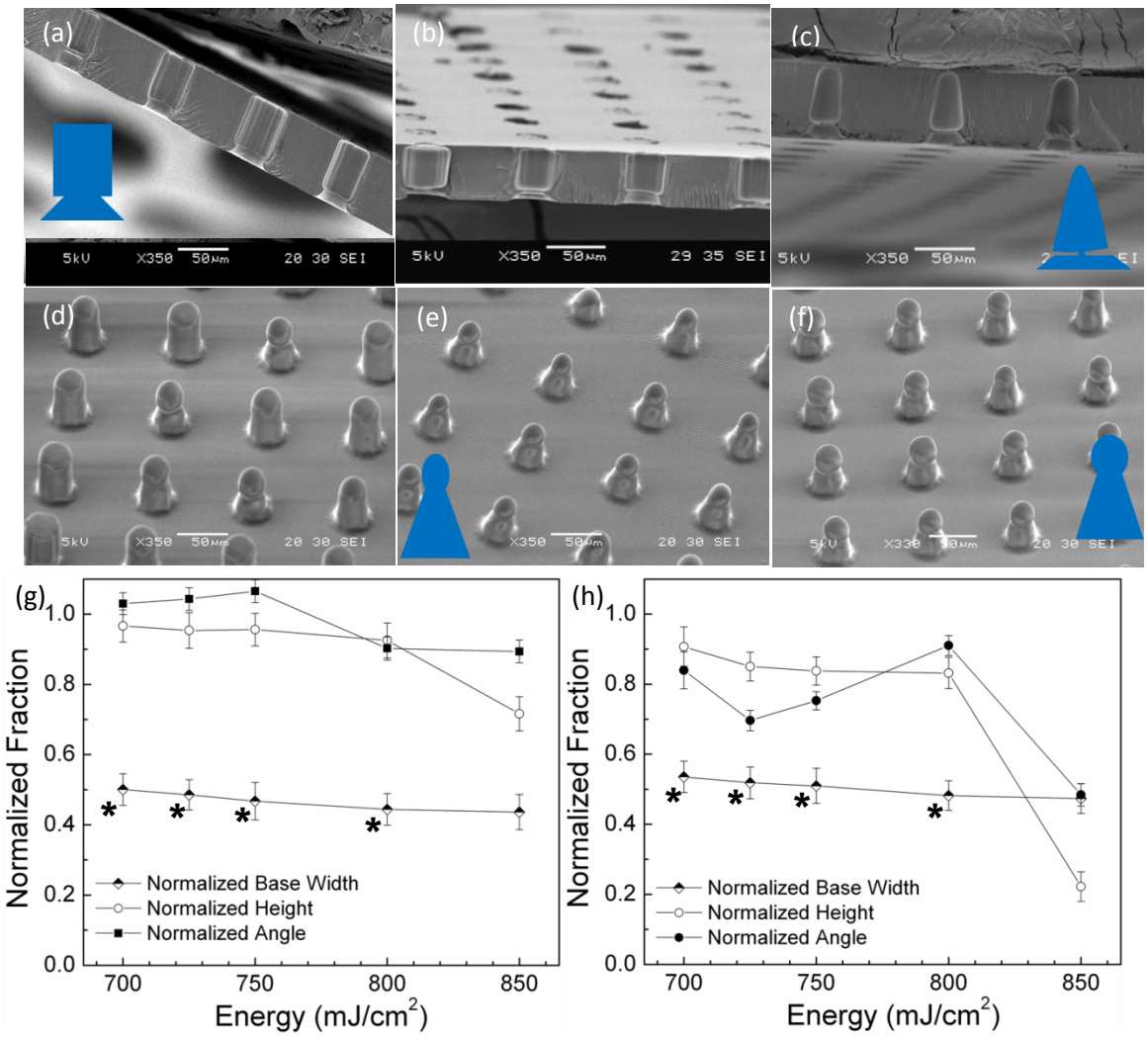

Fig. 3.13: Ramp-up temperature PEB: The cartoons in some figures shows the shape of some special structure formed by this method. SEM images of SU-8 mold (a and b) showing 'Hour-glass' structures and (c) showing 'Pop-sickle' structure and (d-f) are SEM-images of 'doll-like' structures replicated in PDMS. (g-i) are plots showing variation of different defining-features of structures with variation of exposure energy at a ramp-up PEB temperature range of 85-95°C, 90-95°C and 95-100°C respectively. (*) indicate 3D microstructures with 'Kink'. (a-c) are obtained from 1st, 3rd and 4th energy point in plot-g respectively and (d-f) are obtained from 1-3rd energy points in plot (h) respectively. Structures are assumed to be conical for defining different features.

3.4.2.4 FABRICATION OF 3D MICROSTRUCTURES BY INTERFACIAL PARTIAL ACTIVATION

As discussed before, the PA can be generated at the interface of exposed and unexposed material by the diffusion of activated cross-linking species from exposed region to the unexposed region (section-3.4.1.3). The PA at interface can help in fabrication of 3D microstructures different from other methods as only limited part of the structure (top-part in this case) would be affected, unlike other methods demonstrated here. In this method, a layer of SU-8 is exposed to UV-light by the required dose of exposure energy without using any photo-mask and then another layer is coated on it without performing PEB for the first layer. Soft-bake is performed after coating the second layer to allow diffusion of cross-linking species from exposed layer to the unexposed layer. Finally, it is exposed through the photo-mask (Scheme-S3.1b). PEB-temperature is kept at 80°C for this experiment also for the same reason as 3D microstructures are not formed at this temperature due to diffusion (Fig.3.11h). Unique ‘dome-like’ microstructures have been fabricated here by this method (Fig.3.14a-c). A plot showing normalized values of defining features against exposure-energy has also been obtained (fig.3.14d). The 3D microstructures fabricated here are dome-like and not conical as only top-portion of structures is affected by the re-arrangement of partially activated interface.

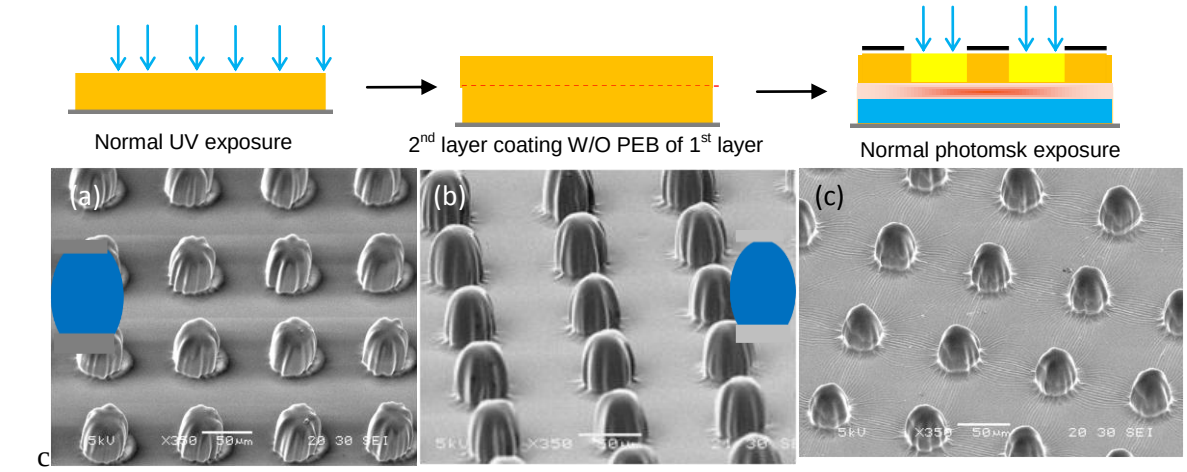

Fig. 3.14: 3D microfabrication by 'Double-layer' of SU-8: The scheme shows the steps in this method and cartoon in figures show the shape of special microstructures. A layer of SU-8 is coated and is exposed with sufficient energy (without any mask) and then second layer is coated without PEB of the first layer. Second exposure is carried out with the photo-mask as before. (a-c) are representative SEM-images of 'dome-like' structures replicated in PDMS and (d) is the plot showing variation of different features with change in dose of the exposure energy at PEB temperature of 80°C. (a-c) are obtained at 1st, 2nd and 4th point in plot (d) respectively.

3.4.2.5 3D MICROSTRUCTURES BY COMBINATION OF METHODS

Combination of 'Double-layer' with 'Low dose of exposure': The two methods for generating the PA, i.e. exposure to low dose of exposure energy and PA at the interface of exposed and unexposed layer of SU-8 has been demonstrated. Now, these two methods can be combined for the fabrication of some more types of 3D microstructures. Although, there can be different ways for combining these two principles, two different

ways have been explored here for this purpose. In the first way, the double-layer sample is prepared as discussed before in the previous sub-section. This sample is then exposed to UV-light to low dose of exposure energy (7mJcm^{-2}) without any photo-mask. Then it is exposed again through the photo-mask (Scheme-S3.1b). The idea here is to generate a non-uniform distribution of partially activated SU-8, higher at interface and lower at rest of the part. Finally, it is baked at 80°C. Uniform 'dome-shaped' microstructures have been obtained (Fig.3.15a-c), the shape of which can be controlled by changing the exposure energy (final exposure through photo-mask) as shown in the plot (Fig.3.15d).

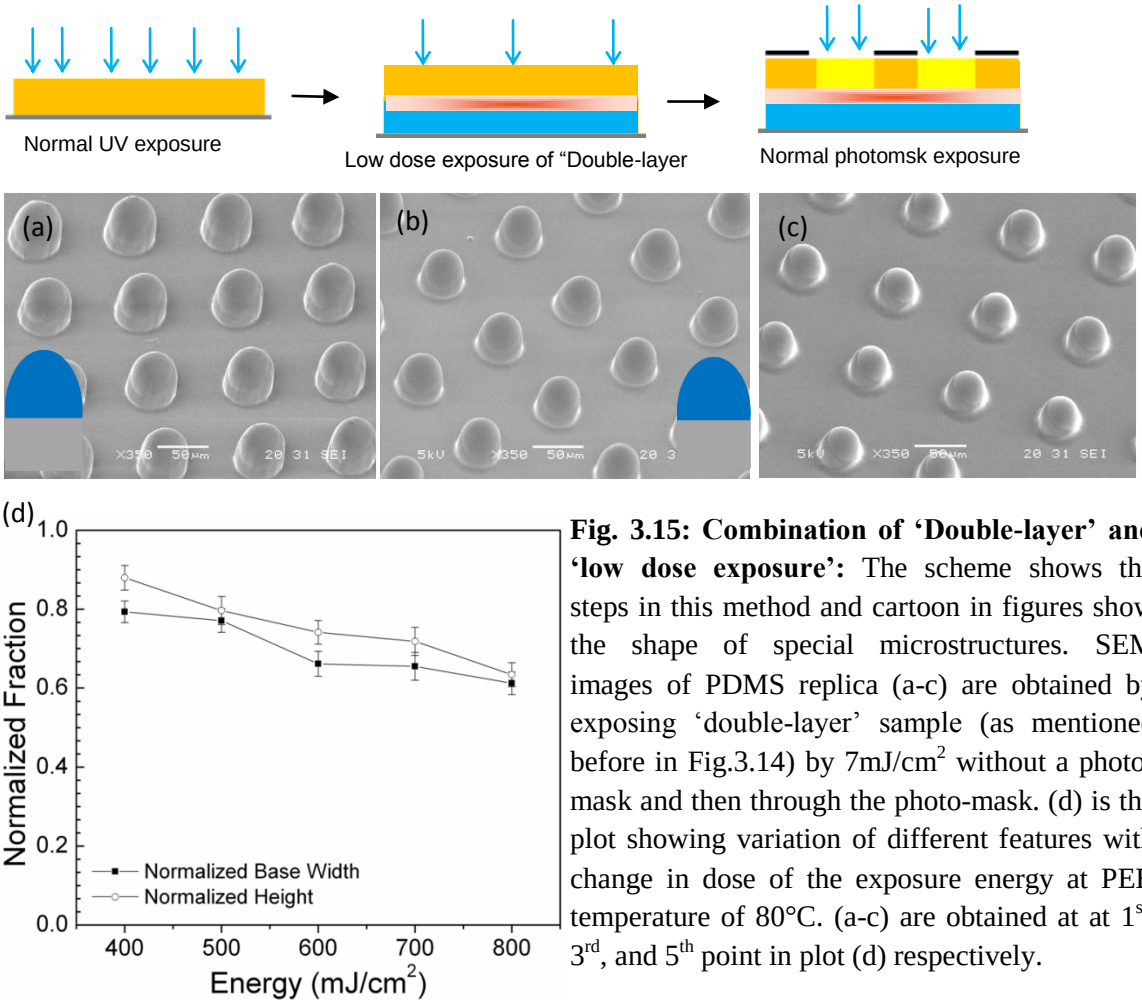

Fig. 3.15: Combination of 'Double-layer' and 'low dose exposure': The scheme shows the steps in this method and cartoon in figures show the shape of special microstructures. SEM images of PDMS replica (a-c) are obtained by exposing 'double-layer' sample (as mentioned before in Fig.3.14) by 7mJ/cm^2 without a photo-mask and then through the photo-mask. (d) is the plot showing variation of different features with change in dose of the exposure energy at PEB temperature of 80°C. (a-c) are obtained at at 1st, 3rd, and 5th point in plot (d) respectively.

Combination of 'Low dose of exposure with Double-layer: In the second way, a layer of SU-8 is first exposed to a low dose of exposure energy ($14mJcm^{-2}$) and then the second layer is coated over it. The idea is to generate a gradient of the PA in the first layer and at the interface without affecting the second layer. The first layer and the interface would have the PA but second layer would not have it. Thus, better control over dimensions may be achieved by this method compared to other methods. This method has been developed to modify the top or upper part of structures without losing dimensions at rest of part. The second exposure is done normally and it is baked at low PEB temperature (80°C). Since the partial activation is generated at the first layer which is further reduced at the interface, a non-uniform distribution of partially activated species is expected here. Unique shape of 3D microstructures has been fabricated (Fig.3.16a) and their shaped can be modulated to fabricate pyramidal shaped 3D microstructures (Fig.3.16b, c) by changing exposure energy (Fig.3.16d).The plot in Fig.3.16d shows that the change in base-width is more restricted than change in top-width with increase in exposure energy. This experiment here is a conceptual representative of the idea and further exploration may be useful for modulating the shape and size of such structures.

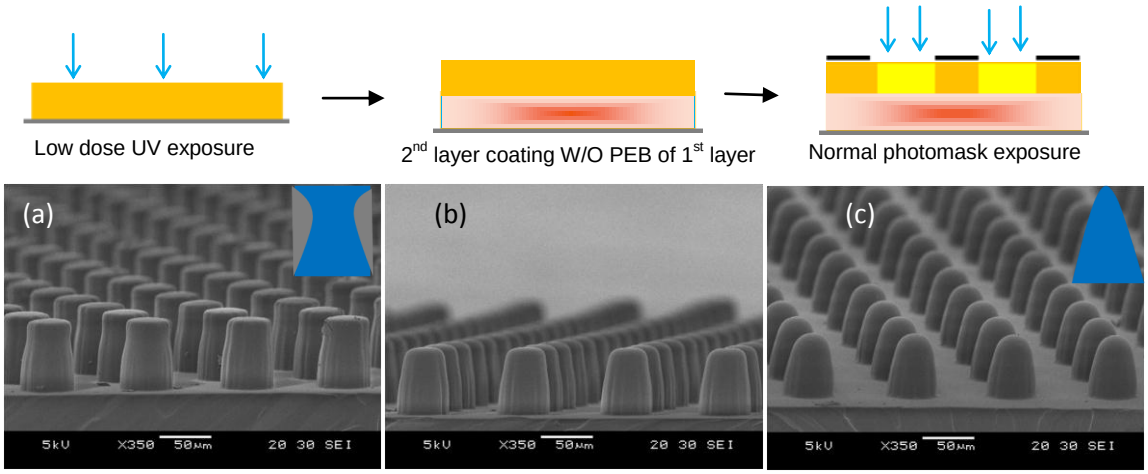

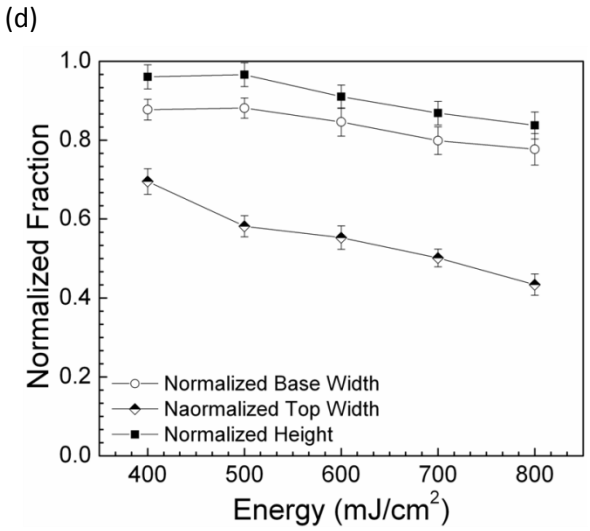

Fig. 3.16: Combination of 'low dose exposure' and 'Double-layer': The scheme shows the steps in this method and cartoon in figures show the shape of special microstructures. SEM images of PDMS replica (a-c) are obtained by exposing a layer of SU-8 by low dose of the exposure energy (14mJ/cm^2) without a photo-mask and then another layer is coated and is baked. It is then exposed through a photo-mask by different amount of exposure energy. (d) is the plot showing variation of different features with change in exposure energy dose at PEB temperature of 80°C. (a-c) are obtained at at 1st, 3rd, and 5th point in plot (d) respectively.

3.4.2.6 SCOPE OF THE 3D MICROFABRICATION TECHNIQUE

The 3D microfabrication technique developed in this project has been demonstrated to fabricate 3D microstructures with circular cross-section and for particular aspect ratio. However, the technique is not limited to such cross-section or aspect ratio. The 3D microstructures with other cross-section can be fabricated by this technique but it is difficult to obtain sharp edges. Due to anisotropic cross-linking the edges tend to lose

sharpness and are rounded off. The 3D microstructure with different aspect ratio can also be fabricated by this technique. However, it would not be suitable for very high or very low aspect ratio as the method depends on the diffusion of cross-linking initiators. At high aspect ratio, the chances of diffusion are higher which may cause difficulty in making high aspect ratio microstructures. At low aspect ratio, diffusion may not be enough to cause any significant change.

3.5. CONCLUSIONS

A novel, simple, inexpensive, and high throughput technique has been developed for the fabrication of 3D microstructures. The technique is based on the study of the cross-linking behavior of the PA of a photosensitive material. A anisotropic cross-linking within PA has been demonstrated. This property has been harnessed for developing the new technique for 3D microfabrication. Different types of 3D microstructures including conical, dome-shaped, pyramidal microstructures have been fabricated in this project. Moreover, 3D microstructures with double-level architecture such as ‘doll-like’, ‘hour-glass’ have also been fabricated. All 3D microstructures demonstrated in this work have been fabricated by a single inexpensive plastic photo-mask. The technique is simple as it does not require special equipment and laboratory and hence, can be adopted by scientist working in different fields for using 3D microstructures in various applications.

Chapter-4: The 3D pyramidal porous membrane

Chapter-4: The 3D pyramidal porous membrane

4.1 INTRODUCTION

Emerging technologies have presented various micro-devices for biomedical applications. Many such devices have been used for sorting of biological micro-entities (cells or functionalized beads). Cell-sorting is an important step in cell-based screening for diagnostic and therapeutic purposes. For instance, broad attention has been placed on sorting circulating tumor or cancer cells from the blood [105, 190], separation of rare epithelial or endothelial cells from the blood [90, 191], sorting blood cells or blood-cell subtypes from the plasma [92, 156, 192] and isolation of stem cells from amniotic fluids [91]. Bead-sorting is an emerging platform for immunoassays [85]. The sorting of micro-entities has been achieved in various types of micro-devices either by using external forces or by using micro-filters. The use of external forces, like dielectrophoretic [193], magnetic [194] and optical [195] however, is complicated, expensive and may require tagging of micro-entities. On the other hand the use of micro-filters, like pillar-type, wire-type, cross-flow and porous membrane, is rather simple. Nonetheless, micro-filters suffer from either low through-put or unclean separation [146]. Compared to other types of micro-filters, porous membrane is the simplest one and can perform micro-filtration with higher efficiency and throughput [196].

Porous membranes have been widely used for various industrial processes, like filtration/separation of substances from fluids, wastewater treatment [197], reaction catalysis [198], and sterilization. They are also an essential component for many research and biomedical applications, like stem-cell culture [199], micro-particle or cell sorting [200, 201], detection of biomolecules [202], diagnosis, prognosis and treatment of

diseases [141, 203, 204]. However, filtration through porous membranes suffers due to clogging of pores. Such pore clogging greatly affects their performance by decreasing filtration efficiency and by increasing the operational and maintenance cost [3-5]. Flow of fluid is reduced due to pore clogging which causes increase in the fluidic pressure over the membrane. The high fluidic pressure may have deleterious effect on biological entities, like cells or blood. Thus, pore clogging is a serious limitation in using porous membranes. To overcome this problem, cross-flow filtration has been applied [205], but filtration efficiency is reduced in this case. Another strategy to overcome this problem is frequent washing of clogged micro-entities [201], but this strategy is not suitable for continuous operation and it would reduce the throughput of the process. Hence, the need to develop new anti-clogging strategies for porous membrane is significant.

Herein, we present a unique anti-clogging porous membrane integrating three-dimensional (3D) pyramidal microstructures which we have termed as '3D Pyramidal porous membrane' (3DPPM). The idea is to create a micro-trap above each pore, so that micro-entities can be trapped above the pore leaving an interstitial-gap. This gap would allow fluid or smaller micro-entities to pass through as shown in Scheme-S4.1. However, fabrication of such a porous membrane is challenging due to fabrication and integration of complex 3D microstructures together. Although a new method of 3D microfabrication has been developed in this project (Chapter-3), the integration of such microstructures to develop an anti-clogging membrane is difficult. The problem related to such fabrication and integration and their solutions is the focus of this chapter. Two methods for such integration have been developed in this study and would be discussed here.

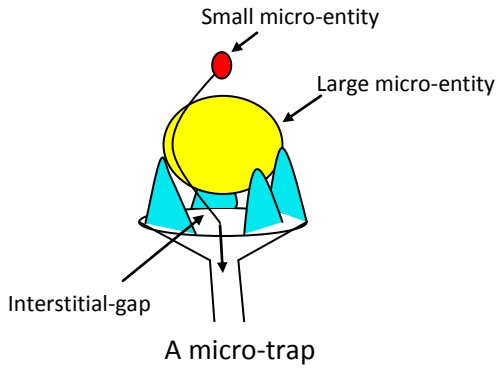

Scheme-S4.1: The idea- the scheme represents the idea of using three-dimensional pyramidal microstructures surrounding each hole in a porous film for development of an anti-clogging porous membrane. Trapped micro-entities (Large one, yellow color) do not obstruct the fluid-flow and smaller micro-entities (small one, red color) can pass through the 'interstitial-gap' between trapped micro-entity and the pore.

4.2 Design of the 3D Pyramidal Porous Membrane:

The 3DPPM consists of an array of well-arranged funnel-like pores (through-holes), wherein each pore is surrounded by four 3D pyramidal microstructures. This design helps in sorting and trapping of micro-entities without blocking pores. The trapped particles are being held by these structures, leaving behind interstitial-gaps between the trapped particles and the pores, thus preventing these pores from being fully clogged (Scheme-S4.1). The funnel-like pores consists of a 3D conical region (top to middle part) and a 2D cylindrical region (middle to end part, through holes). The pyramidal structures would help in trapping particles and would also help in generating interstitial-gap between a trapped particle and the pore. The funnel structure would help in non-blocking of pores by the trapped particles due to its curvature. Moreover, the pyramidal shape would help in trapping micro-entities of different sizes. It would provide largest angular structure compared to other types of 3D microstructures. Now, the next question which arises is 'How to achieve it?' i.e. how to integrate the 3D micro-structures together to achieve this goal. This question would be answered in this chapter.

4.3 MATERIALS AND METHODS

4.3.1 REAGENTS AND MATERIALS: SU-8 2050 photoresist and developer were purchased from MicroChem (Newton, MA). Sylgard-184 was purchased from Dow Corning (Midland, MI). (Tridecafluoro-1,1,2,2-tetrahydrooctyl)-1-trichlorosilane was purchased from Sigma–Aldrich (Singapore), Isopropyl Alcohol (IPA) was obtained from Fisher Scientific, UK.

4.3.2 MASTER-MOLD FABRICATION

4.3.2.1 'Low dose exposure energy' method: The process flow is shown in Scheme-S4.2a. A SU-8 layer was spin-coated (spin-coater, Cee 100, Brewer science, MO, USA) at 4500rpm on an oxygen-plasma (PX-250 plasma chamber from March Instruments, Concord, Massachusetts, USA) treated silicon-wafer and was soft-baked for 2min at 65°C and for 10min at 95°C on a hot-plate (Sawatec, Germany). It was exposed to UV-light for 40s at a power of 7mW/cm^2 through a photo-mask (design for the channels) by a mask-aligner (Karl-SUSS Micro Tec., Waterbury Centre, VT, USA). A second layer of SU-8 was coated after exposure at 6000rpm. It was soft-baked for 3min at 65°C and for 15min at 95°C. It was then exposed to UV-light for 1.2s without any photo-mask. A post-exposure bake (PEB) was then performed for 1min at 65°C and for 1min at 95°C. Third layer was then coated at 5000rpm. It was soft-baked for 1min at 65°C and for 15min at 92°C. It was exposed again through the same photo-mask aligned to the same position for 50s. PEB was performed for 3min at65°C and then a drop of SU-8 (soft-baked) was put over the region containing microstructures. The temperature was then ramped to 96°C within 2min and was baked at this temperature for 15min. It was cooled down before developing it for 8min.

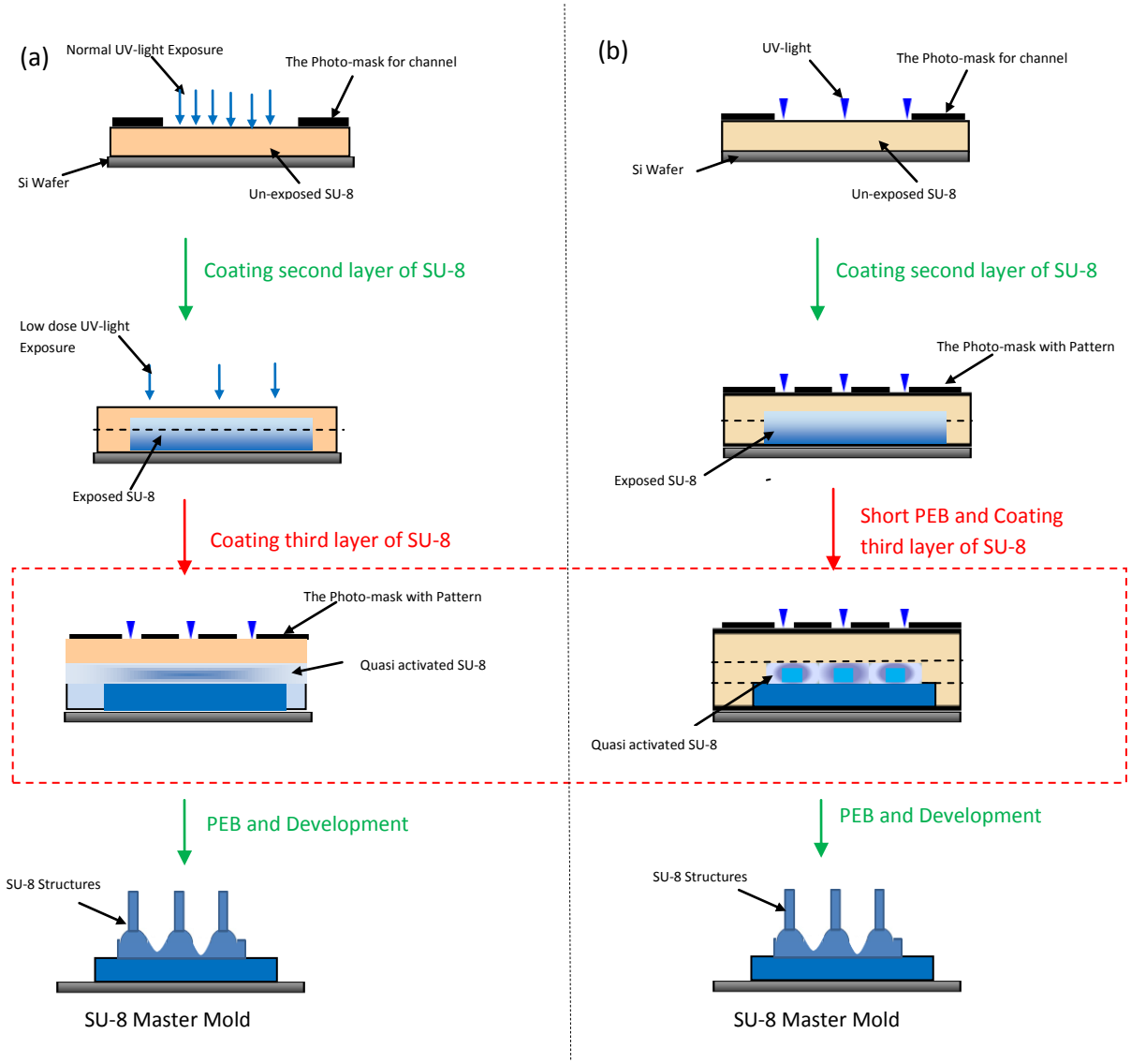

Scheme-S4.2: Methods of Integration: (a) 'Low Dose Exposure Energy Method' and (b) 'Diffusion Method' to integrate 3D microstructures for the fabrication of the required master-mold. Red things show the difference between these two approaches.

4.3.2.2 'Diffusion' method: The process flow is shown in Scheme-S4.2b. A SU-8 layer was spin-coated at 4500rpm on an oxygen-plasma treated silicon-wafer and was soft-baked for 2min at 65°C and for 10min at 95°C on a hot-plate. It was exposed to UV-light for 40s at a power of 7mW/cm^2 through a photo-mask (design for the channels) by the mask-aligner. A second layer of SU-8 was coated after exposure at 5000rpm. It was soft-

baked for 3min at 65°C and for 15min at 95°C. It was then exposed to UV-light for 30s through another photo-mask (with rectangular array of circular open window of 5µm diameter separated by 15µm) aligned with first exposure. A post-exposure bake (PEB) was then performed. The PEB was performed for 30s at temperature ramping from 78°C to 86°C. A third layer was then coated at 5000rpm. It was soft-baked for 1min at 65°C and for 15min at 92°C. It was exposed again through the same photo-mask aligned to the same position for 50s. PEB was performed for 3min at 65°C and then a drop of SU-8 (soft-baked) was put over the region containing microstructures. The temperature was then ramped to 96°C within 2min and was baked at this temperature for 15min. It was cooled and developed for 8min.

4.3.2.3 Master-mold for the sink: The master-mold for sink was fabricated by spin-coating a layer of SU-8 on a silicon wafer at 2000rpm. It was soft-baked normally and was exposed through a photo-mask (with an array of transparent circles of 40µm diameter and center-to-center distance of 100µm between nearest circles, located in the sink channel) for 100s at a power of 7mW/cm^2. The PEB was performed by baking it for 1min at 65°C and it was transferred to the hot-plate (Sawatec., used before) at ramping temperature of 90-96°C and then for 15min at 96°C. It was cooled and developed normally.

4.3.3 FABRICATION OF SINK LAYER: The master-mold of sink was treated with silane as described before. The sink was fabricated by pouring PDMS on the master-mold for sink

according to the required thickness and was de-gassed before baking it for 60min at 70°C. It was peeled-off and cut in shape before pasting it to the film.

4.3.4 DEVICE FABRICATION: A layer of (Tridecafluoro-1,1,2,2-tetrahydrooctyl)-1-trichlorosilane was coated on the master-mold by vacuum depositon in a vacuum desiccator for 10min for easy release of PDMS film. PDMS-base solution was mixed to the curing agent in a ratio of 10:1 by manual stirring. It was degassed in vacuum desiccators for 30-45min. A small drop of PDMS solution was put on the arrayed structures to cap them and was baked for 15min at 70°C. PDMS was then spin-coated (spin-coater, P6700, Specialty Coating Systems, INC. Indianapolis, Indiana, USA) at 1400rpm on the master-mold to cover channels and baked for 10min at 60°C on a hot-plate (Fisher scientific). The cap was then removed and another layer of PDMS was coated at 4000rpm. A small piece of silicon-wafer was used as weight to remove excess PDMS and it was baked for 5min at 60°C. The weight was removed and it was wiped by another small piece of silicon wafer over arrayed pillars in the master-mold. It was allowed to stand for 15min and was baked again for 60min at 70°C in an oven (Venticell, MMM-group). A PDMS piece containing sink (which contains an array of unique 3D microstructures) was aligned to micro-filter region and was pasted by oxygen-plasma treatment. It was then submerged in IPA and was incubated for 30min at 70°C. The porous membrane along with sink-layer was gently peeled-off from the master-mold and was dried in air flow in a Laminar-flow chamber. Holes were punched for inlets and outlets in appropriate layers which were pasted appropriately by oxygen-plasma treatment for 30s at the power of 200W. The device was again treated with oxygen-plasma before use.

4.4 RESULTS AND DISCUSSIONS

4.4.1 INTEGRATION OF 3D MICROSTRUCTURES

This section deals with two integration challenges: 1) Integration of 3D microstructures together to fabricate 3DPPM consisting an array of the micro-traps and 2) Integration of 3DPPM in a functional micro-device.

Although, a simple method has been developed for the 3D microfabrication in this project, fabrication of complex 3D microstructures such as one containing positive as well as negative relief features is difficult. Moreover, if more components (like micro-pillars over 3D microstructures) are required to be integrated, this may become complicated. Such integration may require use of more than one layer of materials and alignment of exposures during fabrication process which may be tedious. In this study, efforts have been made to reduce the number of steps or number of layers for such integration. Anti-shapes of required 3D microstructures are fabricated in a 'master-mold' that is used for replication of the required 3D microstructures by replica-molding. Thus, the fabrication process is done once to fabricate the master-mold, which is used many times for the fabrication of 3DPPM which simplifies the overall process.

There can be two different ways for the integration of 3DPPM in a functional micro-device. One of ways can be to fabricate 3DPPM separately and then integrate it with other components of the micro-device. This method may be simple in some cases but may need high precision of alignment in other cases and may not always be possible to do so. Other way for such integration can be to fabricate 3DPPM together with other components of the micro-device. For example, a mold can be fabricated with replica for

micro-channels over which the fabrication of 3DPPM can be carried out. Although, such integration would need some specialized equipment, like mask-aligner, and one extra layer of material, but such integration would reduce the hassle afterwards. This method is preferred as the alignment has to be carried out only once i.e. during fabrication of the mold. Once the mold is fabricated, it can be used for replication of structures without any need for alignment. Hence, it would avoid alignment step each time the micro-device is fabricated, unlike the first method where each time structures have to be aligned, the second method has been chosen in this project. However, this method too is not free of problems. In this section, the problems of such integration would be discussed. It would follow by the discussion on the solution to this problem and how has it been achieved for the fabrication of the 3DPPM.

4.4.1.1 Challenges in integration of 3D microstructures:

As discussed before, the master-mold can be fabricated with anti-shape of the required 3D microstructures that can be used for replicating these structures in another polymer. As per the design (shown in scheme-S4.1), the master-mold would consist of three parts, pyramidal pits (for the fabrication of pyramids), dome-like structures (for the fabrication of funnels) and micro-pillars (for the fabrication of cylindrical through-holes as pores). However, fabrication of such master-mold would pose three major problems. 1) It has been found that 2D micro-pillars cannot stand firmly on the completely cross-linked SU-8 (Fig.4.1). 2) Although ‘dome-like’ 3D microstructures have been fabricated in PDMS in Chapter-3, the fabrication of these microstructures in SU-8 may be difficult and has

not been demonstrated. 3) More than one photo-mask and strict alignments may be required. Thus, this approach of integration is not suitable and there is a need for finding a better strategy, which is the focus of this study.

To fabricate this master-mold, three layers of SU-8 would be required; each layer contributing to one type of structure which would increase the overall complexity of the procedure. Therefore, if 3D microstructures can be fabricated by using a single layer then minimum number of layers required for such integration would be two. One layer is essentially required for fabrication of 2D micro-pillars as 2D and 3D microstructures cannot be fabricated simultaneously. A new approach has been developed in this project to fabricate two types of 3D microstructures simultaneously, with positive and negative feature contour, just from a single layer. The solution to this problem has come from the partial activation (PA) and the unique re-arrangement within it. The required 3D pits are fabricated by the re-arrangement of the PA, thus avoiding the need for a separate layer. This also obviates the need for more than one photo-mask. In fact, all three problems listed above have been solved by the PA generation and its possible re-arrangement.

As mentioned in section-4.4.1, the 3D microstructures need to be integrated in a functional micro-device. It is also discussed there that the master-mold should be fabricated to contain replica of 3D microstructures as well as components of the micro-device. Thus, such integration should be done during the fabrication of the master-mold. Hence, at least one layer of SU-8 would be required for fabrication of components (here

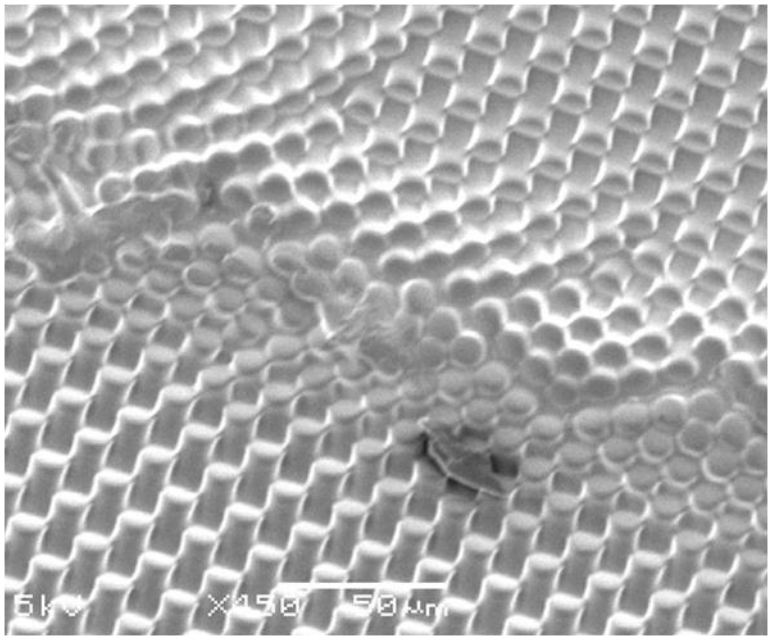

Fig. 4.1: Agglomeration of pillars: SU-8 pillars fail to stand on a completely cross-linked layer of SU-8 due to lack of interaction between pillars with substrate.

microchannels) on which 3D microstructures can be fabricated. Hence, at least three layers of SU-8 would be required for the fabrication of the required master-mold. Although three layers may sound tedious, it would save lot of time and energy during subsequent replication of microstructures for the fabrication of 3DPPM integrated in a micro-channel.

4.4.1.2 STRATEGIES FOR INTEGRATION OF 3D MICROSTRUCTURES

Before discussing the strategies for the integration of 3D microstructures, it is important to solve the first problem presented in section-4.4.1.1, i.e. micro-pillars cannot stand on the completely cross-linked SU-8. This can be attributed to lack of interaction of completely cross-linked SU-8 with another layer of fresh SU-8, as it may not have

functional group left for any interaction. Reducing the pillar size would not solve the problem as it would affect the pore (through-hole) formation and overall thickness of the porous membrane. This problem can be solved by increasing the interaction between SU-8 layers. This can be achieved by coating second layer of SU-8 (the one that would be used for the fabrication of pillars) on a layer of SU-8 which is not completely cross-linked. As noted in the previous chapter, doing so would create partially activated interfacial layer. This interfacial layer would link the two layers which may help micro-pillars to stand stably. To study this hypothesis, a layer of SU-8 is coated on a silicon-wafer and is exposed without any photo-mask to the required dose of exposure energy for complete cross-linking. Then, another layer is immediately coated over it without performing PEB for this layer. It is baked for enhancing the interaction at the interface. Finally, it is exposed through a photo-mask (an array of transparent circles). Subsequent PEB and development is performed normally. The result of this experiment has been shown in Fig.4.2. It has been found that pillars can stably stand (Fig.4.2a). This finding can be attributed to the enhanced interaction between SU-8 layers as the second layer is coated without completion of cross-linking in the first layer, unlike the sample shown in Fig.4.1. The solvent in the second layer would enhance inter-diffusion due to increased thermal motion of SU-8 molecules in solvent. This fact has been confirmed from the analysis of width of two layers. Although the spin-coating speed has been kept same for both layers, the width of both layers has been found to be different. The width of the first layer is greater than the width of second layer. The inter-diffusion would allow dispersion of photo-acid from first layer to second layer which may produce a gradient of photo-acid in the interfacial layer. During soft-bake of second layer, the cross-linking in

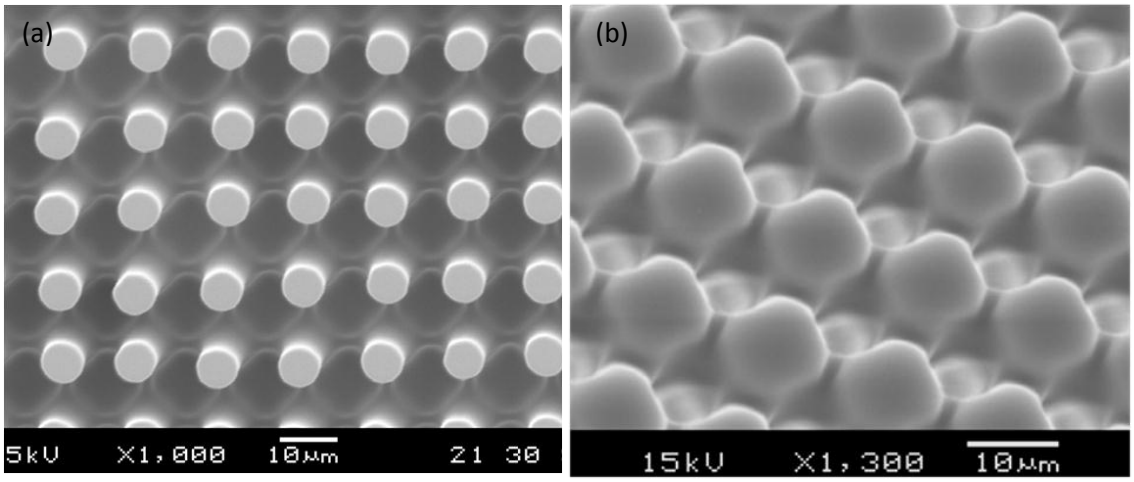

Fig. 4.2: Standing SU-8 pillars due to enhanced interfacial interaction: A layer of SU-8 is exposed and another layer is coated without performing PEB of first layer to enhance interaction of layers at the interface. The Second layer is exposed through a photo-mask. (a) SEM-image of SU-8 mold with standing pillars. (b) SEM-image of PDMS-replica obtained from SU-8 mold. The connecting structures at bottom in (a) provides enough strength for pillars to stand.

interfacial layer would start. A portion of the interfacial layer with relatively higher concentration of photo-acid within this gradient, i.e. the layer near the exposed layer, cross-linking would be complete causing increase in width of the first layer. The rest of the portion within the interfacial layer would have PA. The PA in the interfacial layer re-arranges after second exposure and PEB to from connecting structures at the bottom of micro-pillars. These connecting structures act as support for micro-pillars and help these structures to stand firmly. The space enclosed between pillars is replicated as dome-shaped structures which supports the analysis made above about the interfacial layer and the possible re-arrangement (Fig.4.2b). It also shows that the micro-pillars remain stable during replication.

All three challenges for the integration of 3D microstructures as mentioned in section-4.4.1.1 have been solved in this project by generation of the PA and its re-arrangement.

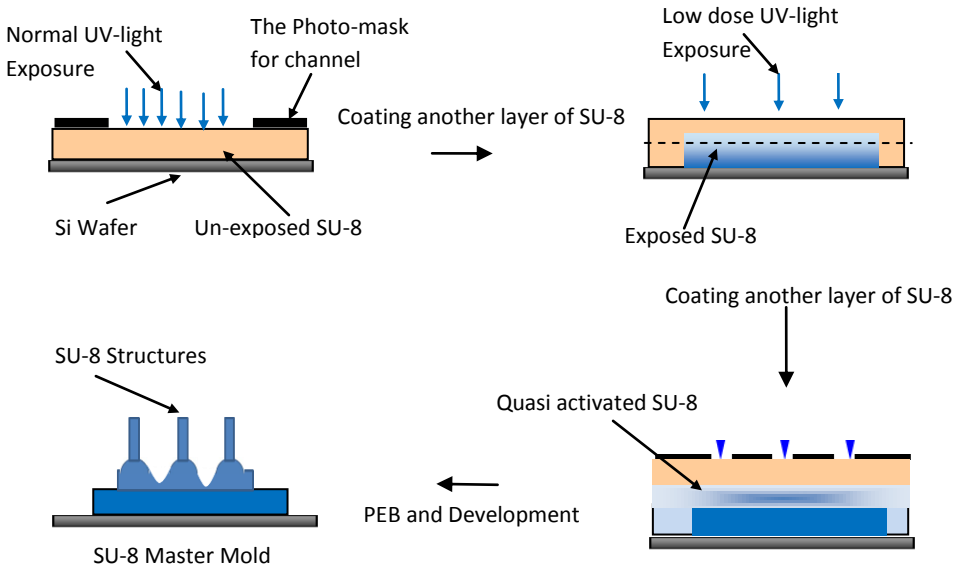

Scheme-S4.3: Integration of 3D microstructures by 'low dose exposure energy' method: A layer of SU-8 is exposed through a photo-mask with micro-channel design. Another thin layer of SU-8 is coated over it and is baked to allow inter-mixing of interfacial layers. It is exposed to low dose of exposure energy before coating third layer. It is baked and is exposed through the photo-mask. PEB and development is performed normally to obtain the required master-mold in SU-8.

This approach has allowed linking and solving all three problems together. Two methods have been demonstrated in Chapter-3 for the generation of PA: 1) exposure by low dose of energy and 2) diffusion. Hence, two separate methods have been developed in this project for the fabrication of the required master-mold based on these principles. The discussion on these methods is as follows.

4.4.1.2.1 'Low dose exposure energy' method: In this method the PA is generated by the low dose of exposure energy. The method has been presented schematically in Scheme-S4.3. As mentioned before, a minimum of three layers are required for the integration of 3D microstructures together and with the components of the micro-device. This method requires three layers only. The first layer is coated on a silicon wafer and is exposed

through a photo-mask containing design of a micro-channel. Then, the second layer is coated and is baked to allow intermixing of layer to generate PA at the interface. This layer is exposed to the low dose of exposure energy to create a gradient of PA, higher at the interface and lower in the second layer. This method is similar to the one demonstrated in Section-3.4.2.5. It is baked for a short time before the third layer is coated over it. The combined layers are baked together to further increase the non-uniformity in the PA distribution. Finally, it is exposed through the photo-mask for the fabrication of micro-pillars. After exposure, PEB is performed. During PEB, molecular re-arrangement within the PA would take place. This re-arrangement would determine the shape of 3D microstructures. As a gradient of the PA exist at the interface of first and second layer, its re-arrangement produces 3D pyramidal pits enclosed between four dome-like microstructures in the second layer (Fig.4.3a). The third layer produces micro-pillars. Overall, two types of 3D microstructures are fabricated along with micro-pillars. After PEB, it is developed to obtain the required SU-8 master-mold, which can be used for the fabrication of the 3DPPM (Fig.4.3b-d).

The ‘Low dose exposure energy’ method is simple and does not require multiple photo-masks or alignment steps. Only one alignment step is involved. The alignment also does not require strict control as it has to be done over micro-channel rather than microstructures. Though, the fabrication of microstructures requires three layers by this method, but the first layer acts as a layer for micro-channel fabrication as well as for generating PA at interface. Hence, there is no need for an extra layer. The size of pyramidal microstructures can be easily changed by changing the thickness of the second layer (Fig.4.4a). However, it is difficult to change the shape or size of ‘dome-like’

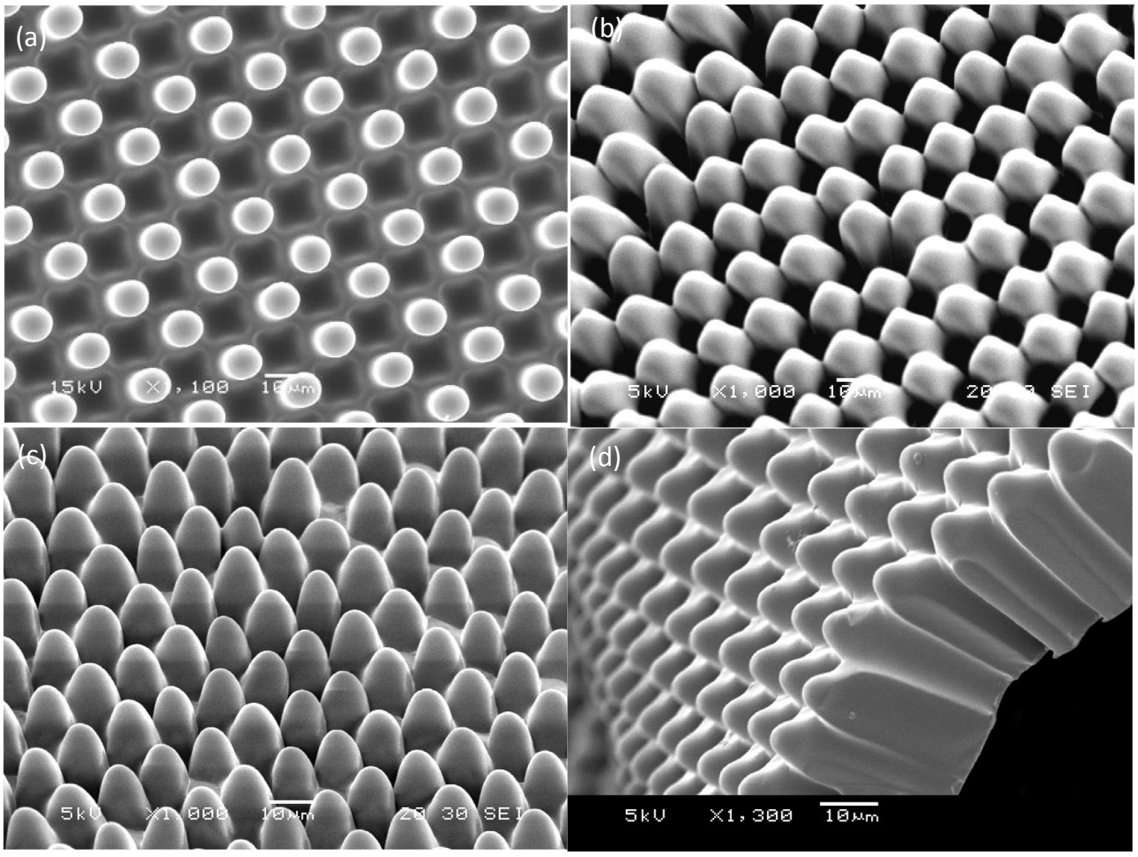

Fig. 4.3: The integration of 3D microstructures by 'Low dose exposure energy': SEM images showing different aspects of 3D microstructures developed by this method. (a) the SU-8 master mold. (b-d) top, tilted and side view of the PDMS replica obtained from the master-mold. (d) is the 3D porous membrane finally fabricated by this method.

structure in this method. This is because the shape of dome-like structure is entirely dependent on the re-arrangement of the PA in the second layer which occurs around the exposed region (for pillars through photo-mask) and it is difficult to increase its width based on re-arranging molecule. Any change in PA to control it, affects the pyramidal shape and height of pyramidal pillars (like the one shown in Fig.4.4a). Moreover, the 'dome-like' 3D microstructures formed by this method have short width and low curvature (Fig.4.4). These structures are more 'cone-like' rather than 'dome-like' (red dots in Fig.4.4). Although, this does not limit its use for the fabrication of the desired

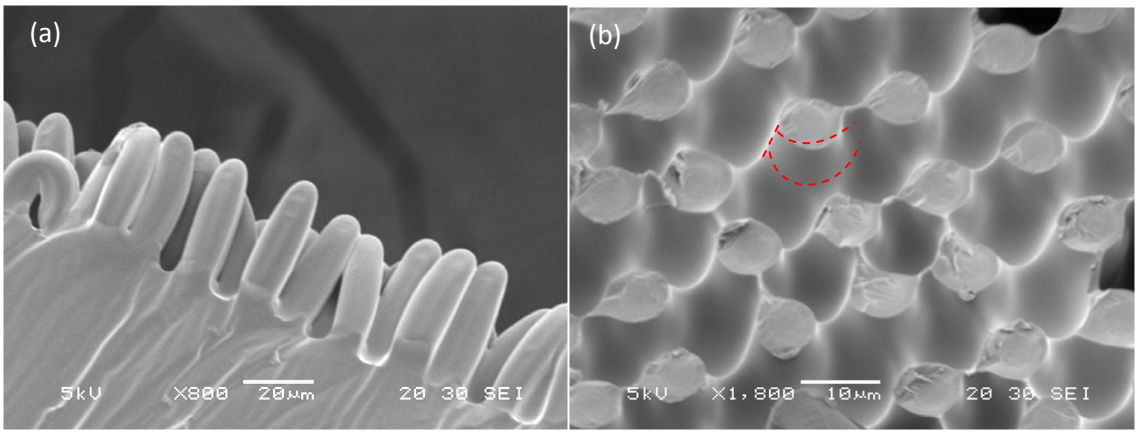

Fig. 4.4: Characteristics of the 'Low dose exposure energy' method: (a) SEM image of a PDMS replica showing pillar-like microstructures obtained by increasing the size of Pyramidal microstructures by this method. The size of pyramids can be increased simply by increasing thickness of the second layer. (b) SEM image of SU-8 master-mold fabricated by this method showing enclosed 3D pits between 'cone-like' 3D microstructures. The micro-pillars have been broken to show the microstructures in detail. Red dotted curves indicate cone-like structures. It is difficult to change the shape and size of 'cone-like' microstructures by this method.

anti-clogging 3DPPM, but the other method developed in this project (to be discussed next) can been used for developing better 'dome-like' structures. Hence, the second method has been used here to develop funnel-shape in the 3DPPM for cell/bead sorting and patterning (to be discussed in chapter-5).

4.4.1.2.2 Diffusion method: This method has been developed here as another approach for the integration of 3D microstructures. In this method, generation of the PA depends on the diffusion of activated cross-linking species from exposed region to unexposed region. The advantage of this method is that gradient of PA can be created in vertical as well as horizontal directions, thus generating more non-uniformly distributed PA. The scheme for the integration of 3D microstructures has been provided in Scheme-S4.4. A layer of SU-8 is coated on a silicon-wafer and is exposed through a photo-mask designed for the micro-channel. Another layer is then

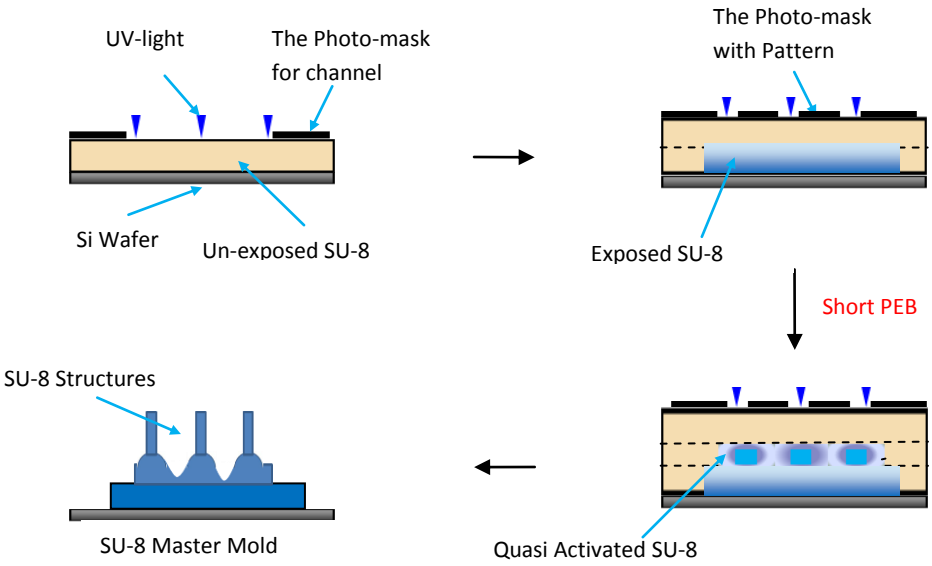

Scheme-S4.4: Integration of 3D microstructures by 'Diffusion' method: A layer of SU-8 is exposed through a photo-mask with micro-channel design. Another layer of SU-8 is coated over it and is baked to allow inter-mixing of interfacial layers. It is exposed through a photo-mask with sufficient dose of exposure energy. PEB is performed for short time and another layer is coated. It is soft-baked and exposed again through the same photo-mask aligned to the same position. PEB and development are performed normally.

coated and is soft-baked which is then exposed to the UV-light through a photo-mask and the PEB is performed for a short time at lower temperature (lower than recommended by manufacturer) to generate only partial activation during PEB (Scheme-S4.4). Then, third layer is quickly coated over it and is baked. This would allow intermixing of layers during baking step due to incomplete cross-linking of the second layer. Also, the third layer contains solvent that would enhance the intermixing of layers. During this step, activated SU-8 from exposed region can diffuse to unexposed region. This would cause non-uniformly distributed Partially activated polymeric chains around the exposed SU-8 in the second layer (Scheme-S4.4, third picture). As the exposure of the second layer is performed through a

photo-mask, the diffusion would create the PA non-uniformly distributed in the micro-space. Then the third layer is exposed through the photo-mask aligned to the same position and the PEB is performed. This step allows formation of 2D micro-pillars as well as molecular re-arrangement within the PA. The re-arrangement allows formation of two types of 3D microstructures due to non-uniform distribution of the PA. 'Dome-like' microstructures surrounded by anti-pyramidal pits are formed from the first layer while micro-pillars standing on the dome-like structures are formed from the second layer (Scheme-4.4, Fourth picture). It is interesting to note that two different 3D microstructures with different profiles (up and down) have been formed from a single layer by this technique. Finally, it is developed to obtain the required master-mold.

The 'Diffusion' method may not essentially require three layers for the fabrication of 3D microstructures, but three layers have been included here to integrate microstructures to micro-channel. Now, it is important to justify the steps included in this scheme and how can fabrication be controlled. The simplest from of this scheme would be to perform the exposure of the second layer without any photo-mask and coat third layer without perorming PEB (i.e. keep the time for short PEB to zero). This would allow gereation of the PA at the interface of the second and the third layer. This experiment produces result similar to the one shown in Fig.4.2. Although, it shows the fabrication of 3D microstructures (dome-shaped in PDMS, Fig.4.2b), the shape of such microstructures cannot be changed. Different parameters such as temperature, exposure energy have been adjusted, but change in shape has not been

observed. The reason is lack of non-uniformity in the interfacial layer as diffusion should be uniform between two layers. Moreover, these microstructures are not angular as well as no funnel-like microstructures are fabricated as required for 'the idea' presented in the scheme-S4.1. Thus, to fabricate the integrated funnel-like and pyramidal microstructures, the exposure through photo-mask has been introduced. This would help in generating gradient of the PA in vertical as well as in horizontal direction.

Next, inclusion of PEB for short time after exposure of the second layer should be studied. As mentioned before (in Chapter-3, Section-3.4.1.3), the diffusion of activated species from exposed layer to unexposed layer causes complete as well as partial activation depending on the gradient of activated species. Therefore, it is important to study the effect of diffusion in this scheme of fabrication. So, an experiment has been performed here according to this scheme (Scheme-S4.4). The time for the short PEB is kept zero in this experiment. Other values of parameters such as exposure energy and PEB temperature have been set according to recommendation from manufacturer of SU-8. The result of this experiment is shown in Fig.4.5. It can be seen from the figure that the dome-like structure have been formed (Fig.4.5). Although, the photo-mask used in this experiment has transparent circles of size 5μm and other parameters have been kept to the recommended values, microstructures formed here are of size 10μm. Moreover, dome-like structures have been formed instead of distinct pillars. This clearly suggests the cause of this result is diffusion of activated species from the second layer. Since the PEB is not performed after exposure of the second layer; the activated species from the exposed region can diffuse to the unexposed layer causing increased cross-linking around pillars

in the third layer. Slight re-arrangement can also be noticed as small pillar can be seen in the replica mold around the dome-shaped pits (Fig.4.5b). This experiment justifies the inclusion of short PEB after second exposure in the Scheme-S4.4 which would allow some amount of cross-linking before diffusion can take place and would contribute in controlling the formation of 3D microstructures. This experiment also proves the hypothesis made in the scheme that diffusion in the second layer can take place and dome-like structures can be fabricated by such diffusion. Although the result presented in Fig.4.5 is for the third layer, exposure pattern of the second and third layer is same. Thus, these findings can be extrapolated to the second layer also.

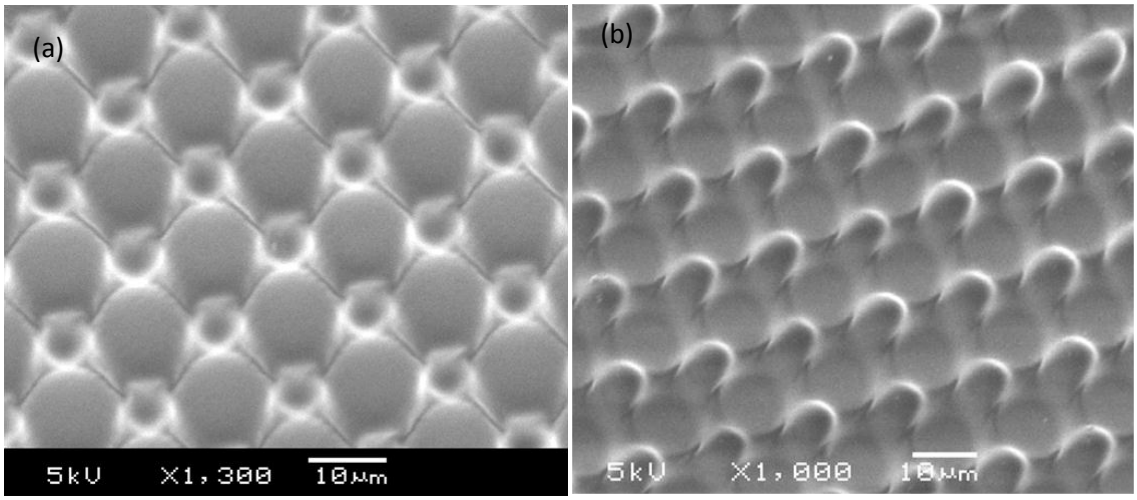

Fig. 4.5: Cross-linking due to un-controlled diffusion: the samples have been prepared here by following the scheme-S4.4, with time for short-bake equal to zero. (a) SEM image of SU-8 mold and (b) SEM image of PDMS-replica obtained from SU-8 mold.

Now, to fabricate the desired mold, a brief study has been done to evaluate the effect of short-PEB after second exposure in Scheme-S4.4. The short PEB (Scheme-4.4) after the second exposure has been used as a parameter for controlling structure formation. The short PEB has been performed at ramping-up temperature (at a rate of 15°C/min) to

enhance the non-uniform distribution of the PA. Few temperature ranges with the average temperature of 70°C, 80°C and 90°C have been tested for this purpose keeping other parameters the same. Different 3D microstructures are obtained in PDMS replica. When the short PEB is performed at the temperature ramping from 67°C to 73°C, pillars with curved top have been obtained as 3D microstructures (Fig.4.6c). This may be due to low rate of diffusion in this range. When the short PEB is performed at the temperature ramping from 77°C to 83°C, the pyramidal structures have been obtained as 3D microstructures (Fig.4.6d). When it is performed at the temperature ramping from 87°C to 93°C, frustum-like 3D microstructures are obtained while funnel-like microstructures shows increase in size compared to the previous result (Fig.4.6e). This can be explained by the increased diffusion at higher temperature range. The desired 3D microstructures are somewhere between the 3D microstructures shown in Fig.4.6d and Fig.4.6e. Hence, the desired 3D microstructures with pyramidal microstructures surrounding funnel-like microstructures are obtained in temperature range of 78°C to 86°C (Fig.4.6f). The fabrication of the desired master-mold has been achieved (Fig.4.6a). 3D microstructures (marked by red dots) can be seen in Fig.4.6b (pillars are deliberately broken to show structures). The ‘dome-like’ microstructures surrounded by 3D pits can be seen in Fig.4.6b.

The diffusion method can be used for the fabrication of different types of 3D microstructures. The ‘Diffusion’ method has been found to be more versatile in terms of changing the shape and size of 3D microstructures. Since diffusion can allow cross-linking in the unexposed region, the shape of dome-like 3D microstructures in the master-mold can be changed, unlike the ‘Low dose exposure energy’ method. This method does

not essentially require three layers for the fabrication of 3D microstructure and hence is more flexible in terms of integration to any other type of micro-device as it is not essential to fabricate them on components of the micro-device. However, this method does require good control over alignment step as alignment has to be done over microstructures.

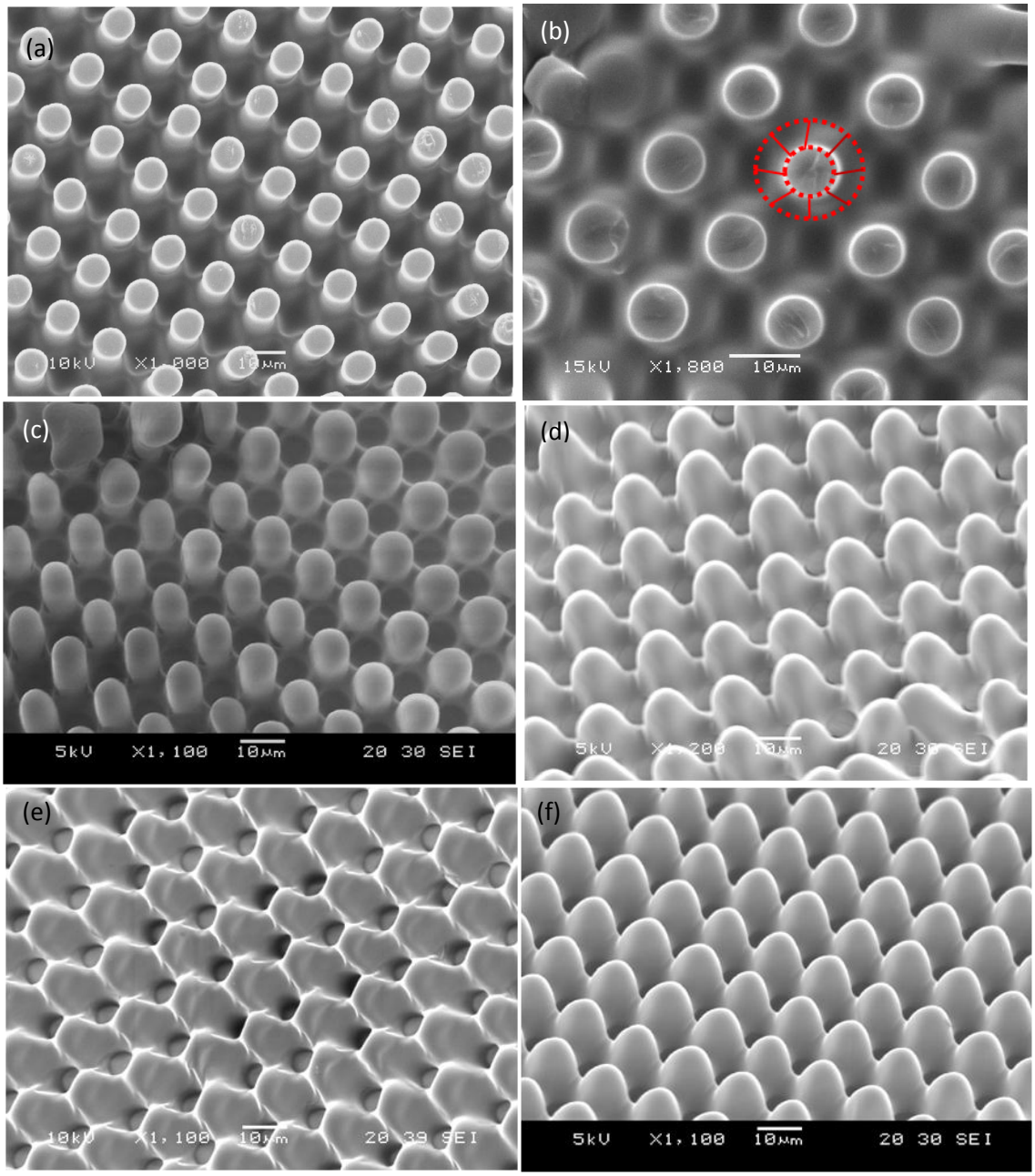

Fig. 4.6: Integration of 3D microstructures: SEM images (a) and (b) are SU-8 mold while (c-f) are PDMS replicas. (a) SU-8 mold obtained from the scheme of fabrication shown in Scheme-S4.4 and (b) detailed view of 3D microstructures at the bottom of this mold (pillars are broken to show the bottom). Red dots and lines highlight 'dome-like' microstructure at the bottom. (c-e) are obtained by performing the short PEB at ramping temperature (15°C/min) from 67°C to 73°C, 77°C to 83°C and 87°C to 93°C respectively. (f) is obtained by performing short-bake from 78°C to 86°C.

4.4.2 FABRICATION OF 3D PYRAMIDAL POROUS MEMBRANE

4.4.2.1 CHALLENGES IN THE FABRICATION OF THROUGH-HOLES (PORES)

The fabrication of the master-mold with integrated 3D microstructures has been explained in the previous section. The 'master-mold' is used for carrying out fabrication of the 3DPPM. One such master-mold can be used for many times for such fabrication. The 3D micro-structures are replicated in PDMS while micro-pillars are used for making through-holes to obtain pores in the 3DPPM. A thin film of PDMS is coated over the master-mold to obtain an array of through-holes in the membrane. However, the fabrication of through-holes with integrated 3D microstructures has been found to be challenging due to accumulation of PDMS over microstructures (Fig.4.7a). It has been noted that the PDMS forms a hump over the region containing microstructures. The PDMS thickness near the edge has been found to be lesser than that near center of the array. The accumulation of the PDMS may take place due to dense array of microstructures which might induce capillary force and surface tension over PDMS to accumulate it. The increase in coating speed is not helpful either. Even at high coating speed (6000rpm), through-holes have been observed only at sides of the membrane (Fig.4.7b). So, a weight extrusion approach has been used here to overcome this problem, which is the topic of discussion of the next sub-section.

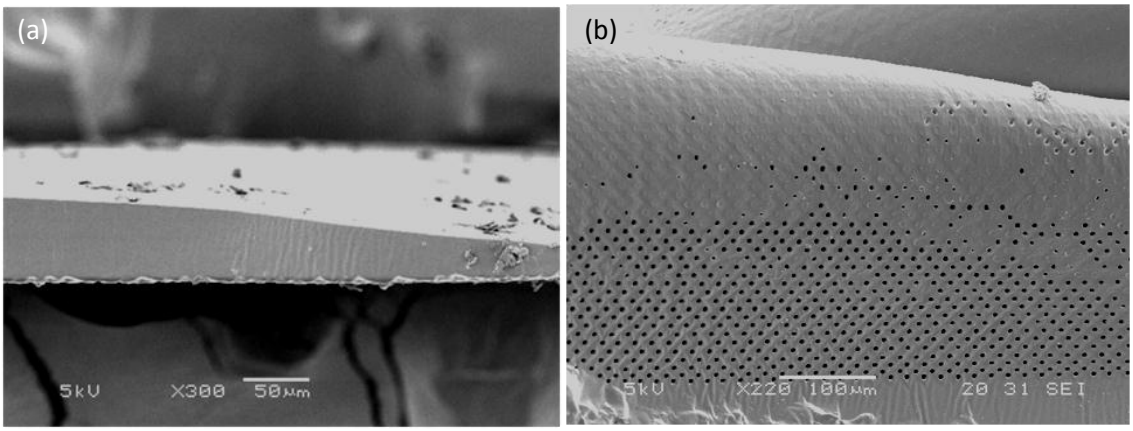

Fig. 4.7: Accumulation of PDMS over structures: The PDMS is coated on the master-mold. (a) SEM-image of PDMS film in cross-sectional view. It tends to accumulate over microstructures. The thickness of PDMS film can be seen to increase towards the center of the arrayed structures (left hand side). (b) the SEM image of the film obtained by increasing the coating speed. Only sides have got through-holes.

4.4.2.2: FABRICATION OF THROUGH-HOLES

To solve this problem, a small weight is applied to push-out the accumulated PDMS. It is then baked for short time to make PDMS stickier and then excess PDMS is removed by tapping a small piece of silicon-wafer on it. It is spun again to make the layer of SU-8 uniform. It is allowed to settle down at room temperature before baking it to cross-link PDMS. This method helped in fabrication of an array of through-holes as pores. The overall method for the fabrication of the 3DPPM has been shown in Scheme-S4.5.

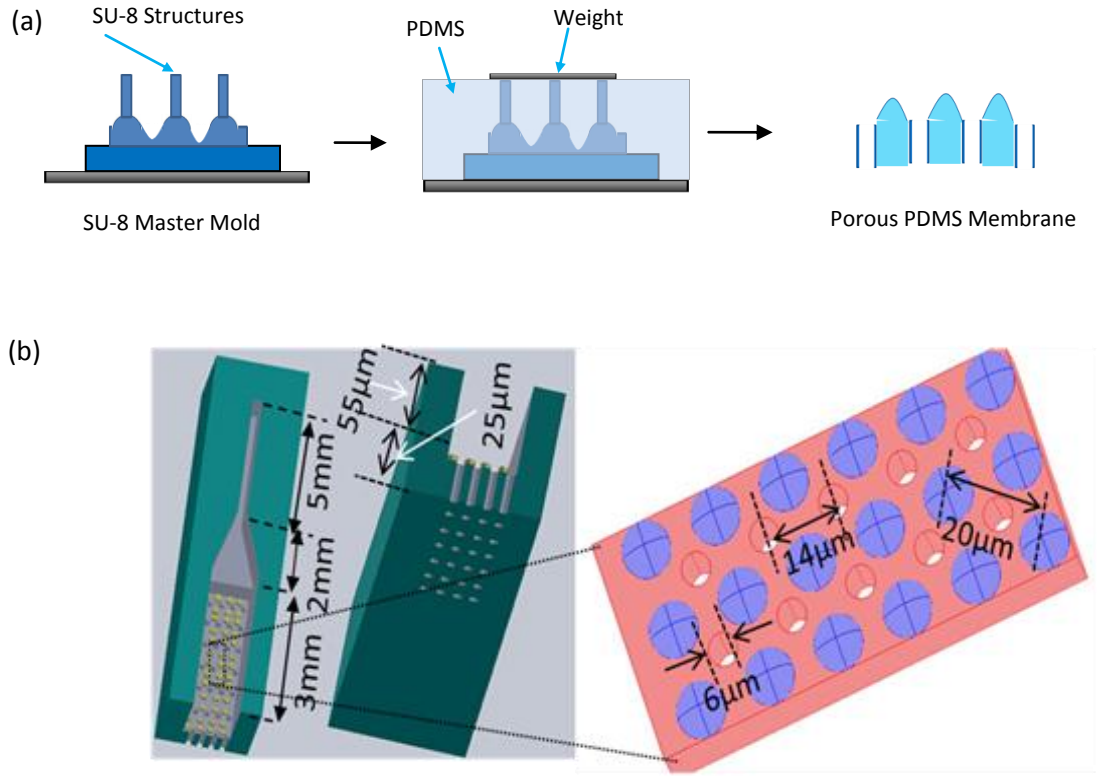

Scheme-S4.5: The fabrication of 3D pyramidal porous membrane: (a) PDMS is spin-coated on the master-mold. Excess PDMS over microstructures is removed by weight and is then baked. The porous PDMS film is then released from the master-mold by using 2-propanol at 70°C. (b) The top and the tilted view of the 3D pyramidal porous membrane integrated in a micro-channel. The expanded view of the integrated micro-filter illustrates pyramidal shaped microstructures (blue) surrounding each pore.

4.4.2.3 PEELING-OFF THE MEMBRANE:

It has been found here that peeling the membrane off the master-mold can damage it. Also, handling thin membrane is difficult. Hence, a PDMS piece containing sink is pasted on it by aligning the sink to the region containing microstructures before peeling it off. As the membrane is pasted to the sink layer (relatively thicker), it is convenient to handle it, but even with sink layer the membrane cannot be peeled-off without any damage. To avoid the damage, a solvent-based approach has been demonstrated here to facilitate an easy release. The mold is immersed in Isopropyl Alcohol (IPA) and is incubated in an oven at 70°C for about 30min. It is interesting to note that heating in IPA helps in easy release of the membrane (Fig.4.8). It may be hypothesized here that swelling of PDMS might be the cause for such release. So, sizes of pillars and pores have been measured to verify this hypothesis. The size of pore and the pillar has been found to be almost similar. So, swelling of PDMS is not the cause. We believe that heating allows better penetration of IPA between SU-8 and PDMS microstructures which helps its release as without heating it is not released properly. Finally, the successful fabrication of the desired 3DPPM has been achieved in this project (Fig.4.9).

Fig. 4.8: Peeling-off the membrane: The picture shows how membrane is peeled-off from the master-mold using IPA. The film is automatically released from the mold if it is kept at 70°C for about 30min.

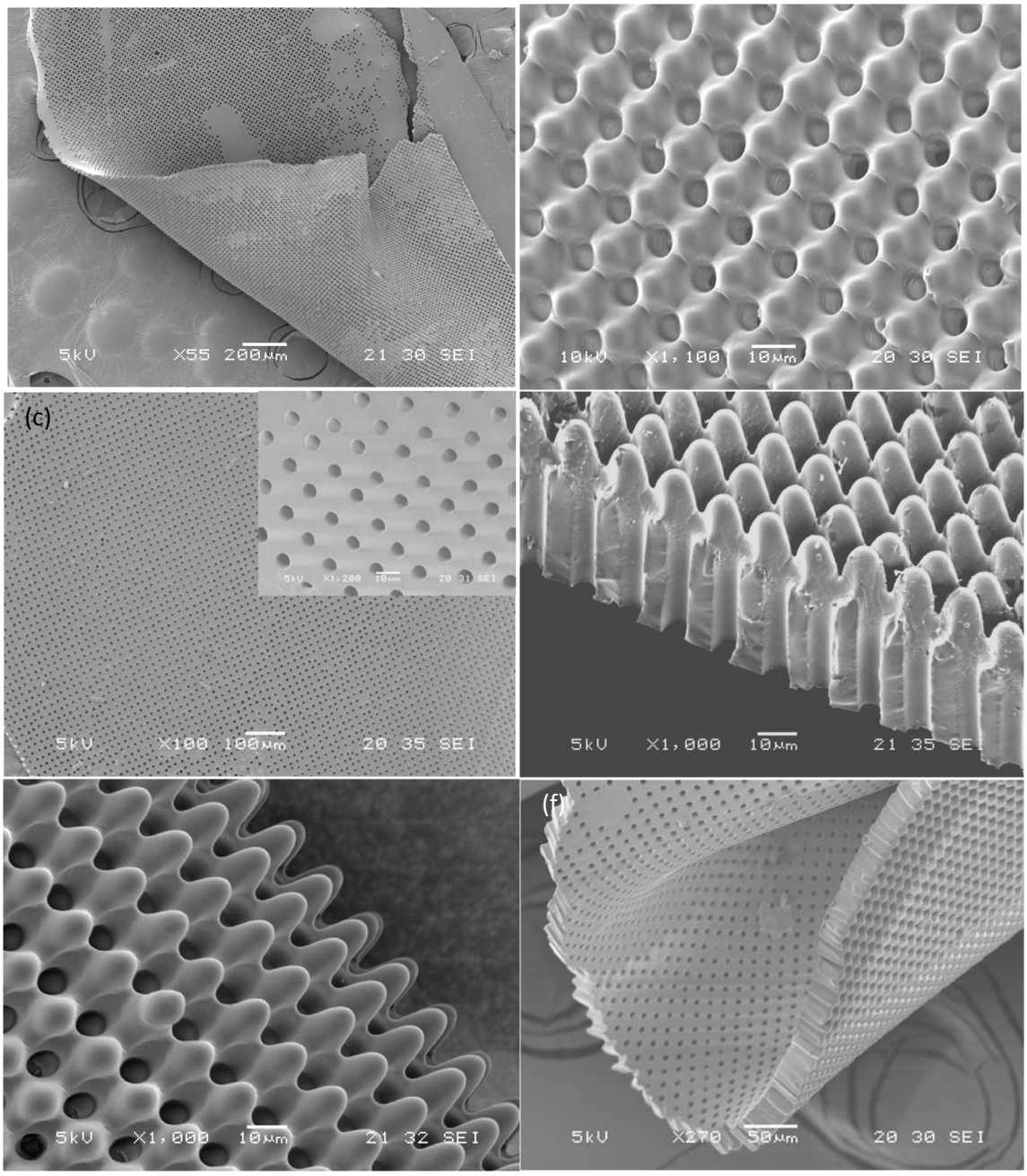

Fig. 4.9: 3D Pyramidal Porous Membrane: SEM images of 3D pyramidal porous membrane fabricated by the method developed in this project. (a) the porous membrane, (b-e) are top, bottom, cross-sectional and tilted view of the 3D pyramidal porous membrane respectively. Inset in (c) presents the magnified view of bottom of the membrane showing holes. (f) the membrane is folded to show all three views together.

4.4.3 FABRICATION OF THE MICRO-FLUIDIC DEVICE

The 3DPPM is obtained from the master-mold as integrated in the sink layer. This can be developed as a micro-device. However, the porous membrane in the device may sag in the sink which may affect its performance and it can also prevent imaging of the membrane. To overcome this problem, an array of 'doll-like' 3D microstructures has been fabricated in the sink by using 3D microfabrication technique developed in this project (Chapter-3). These microstructures have truncated cone-like base with a short pillar (with curved top) standing over it. The structure is slightly hinged at the point of connection which makes it flexible (Fig.4.10). The flexible pillars help adjusting with fluidic pressure variations during filtration process besides keeping the membrane flat. The curved top and smaller diameter at top of these pillars allow minimum blockage of pores. The broad base provides stability to the structure which can withstand high fluidic pressure-drop. Also, the height of these structures (50µm) is slightly lesser than the sink depth (60µm) which ensures that pillars are not pasted on the film. This allows taking the film out of the device whenever it is required (e.g. SEM analysis).

The device fabrication has been carried out by assembling different components together. As mentioned before, the porous membrane integrated with the sink is obtained from the above mentioned method. The channels are then sealed by another layer of PDMS containing appropriate inlets and outlets (Fig.4.11). The final device contains one inlet and two outlets (one from the sink and another from the main channel).

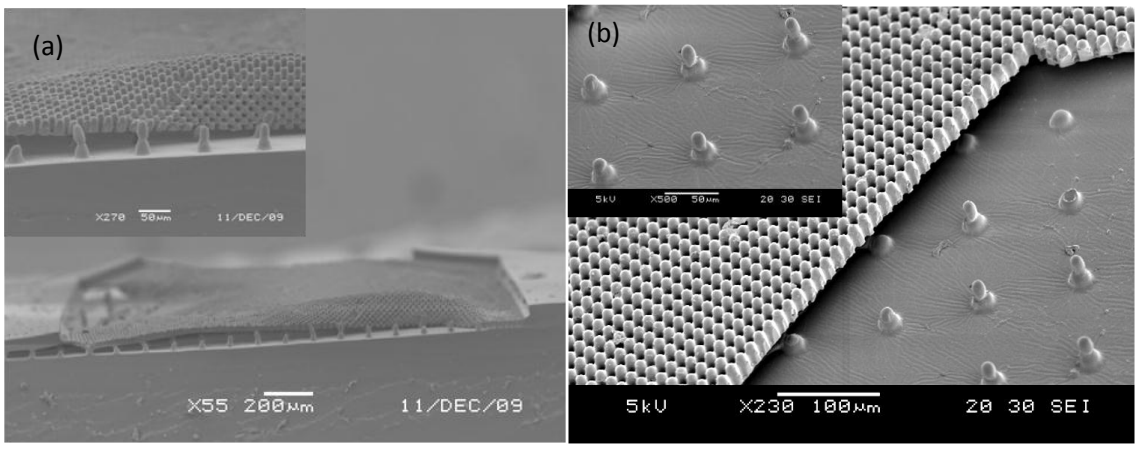

Fig. 4.10: 'Doll-like' 3D microstructures for supporting the membrane: (a) and (b) front-view and the side-view of the membrane resting on doll-like 3D micro-structures. Insets show the enlarged view of the 'Doll-like' 3D microstructures.

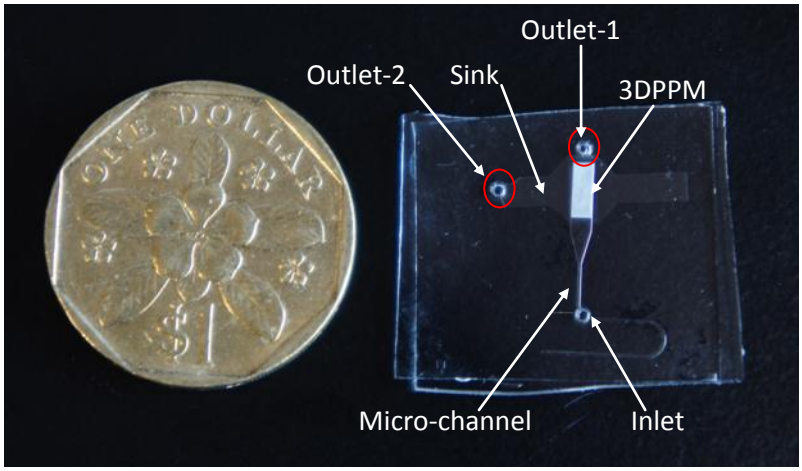

Fig. 4.11: The micro-device: The picture here shows the micro-fluidic device containing 3D pyramidal porous membrane. The red circles show the two outlets; one in the main channel and other in the sink. The S$1 coin is kept for size comparison.

4.4.4 TEST OF THE DEVICE

The micro-fluidic device fabricated here has been tested by flowing fluid at different flow rates to check its stability. The fluid can pass through the pores (through-holes) and can be collected at the outlet of the sink when the outlet in the main channel is closed and outlet in the sink is opened. After opening the outlet in the main channel, fluid can be collected from both outlets. The fluid (1X PBS) has been flowed in the device at different flow rates ranging from 10-1000μl/min. The device has been found to be stable after the flow. The porous membrane has been observed during flow by using the microscope. During flow at high flow-rates (more than 200μl/min), the membrane has been observed to defrom but it recovers back to its original position after flow is stopped. This shows that the 'Doll-like' 3D microstructures used as support for the membrane works well i.e. they adjust themselves accordingly and help in keeping the membrane flat.

4.5 CONCLUSIONS

The integration of 3D microstructures has been achieved in this project to fabricate the 3DPPM. Two methods have been developed for this purpose: 'Low dose exposure energy' and 'Diffusion' method. 'Low dose exposure energy' method is simpler than 'Diffusion' method. However, 'Diffusion' method is more versatile than 'Low dose exposure energy' method. The 3D microstructures have been integrated to a micro-channel during fabrication of the master-mold. Different types of integrated 3D microstructures have been fabricated. The master-mold has been used for fabrication of the desired 3DPPM. The fabrication of through-hole in the porous membrane has been achieved by weight extrusion method. The solvent based approach has been found in this project for peeling-off such membrane from the master-mold. Unique 'Doll-like' 3D microstructures have been developed here for supporting the membrane in the sink.

Chapter-5: Sorting and Patterning by the Anti-clogging 3DPPM

Chapter-5: Sorting and Patterning by the Anti-clogging 3DPPM

5.1. INTRODUCTION

The recent developments in technology have presented a variety of micro-devices for handling micro-entities such as cells or micro-beads, to satisfy biological and medical needs. These devices are in demand for sorting/separation and patterning/trapping of micro-entities. For instance, micro-devices are being developed for various applications such as separation of circulating tumor or epithelial cells from blood [90, 190], separation of white-blood cells or blood-cell subtypes from whole blood [92, 192] and isolation of stem cells from amniotic fluids [91]. Devices for cell-patterning are useful for basic cell-biology studies including single-cells studies [206], whereas separation and patterning of micro-beads act as a new tool for immunoassays [85]. Nevertheless, these devices are normally intended for performing either sorting or patterning of micro-entities and a single approach for achieving both simultaneously, with high performance efficiency, is still challenging. The development of a novel micro-device to achieve this underlined goal with added functionality is thus encouraging and useful.

Different techniques that have been used for the sorting and the patterning of micro-entities are presented in Chapter-2. One of the popular techniques for sorting of micro-entities is the filtration through porous membrane, but pore clogging is a drawback in using the porous membrane which adversely affects their performance. Here, we demonstrate an anti-clogging 3D pyramidal porous membrane (3DPPM) integrated in a micro-fluidic device for simultaneous separation and patterning of micro-entities. The membrane consists of an array of funnel-like pores where each pore is surrounded by four 3D pyramidal microstructures. The 3DPPM presented here has four interesting features

that are unique to it as a micro-filter. 1) It is characteristically anti-clogging as pores are not blocked by the filtered micro-entities. This anti-clogging characteristic would allow uninterrupted sorting of micro-entities continuously, such as that of cancer cells from the blood. 2) Micro-entities of different sizes can be trapped (Scheme-S5.1a). This feature is potentially useful for single-cell studies by trapping cells from an inhomogeneous cell population of different sizes. 3) Simultaneous sorting and patterning of micro-entities can be performed by using 3DPPM (Scheme-S5.1b). This feature would be useful for sorting cells from actual samples (e.g. blood) as well as patterning them in an array of single-cells for further studies. 4.) Bi-directional sorting can be achieved by using 3DPPM (Scheme-S5.1b). The sorting of micro-entities can take place in the direction of the fluid flow in micro-channel (sorting in the micro-channel) as well as that perpendicular to it (sorting through pores). The sorting through pore is similar to traditional 2D porous membrane, wherein smaller micro-entities (red particles in Scheme-S5.1b) pass through the pores while bigger particles (yellow particles in Scheme-S5.1b) are retained on the membrane. High sorting efficiency can be achieved if smaller micro-entities can also pass through the interstitial-gaps, which is an additional feature of the 3DPPM. However, the sorting efficiency would remain low in case smaller micro-entities are unable to pass through these interstitial-gaps. In this case, many smaller micro-entities would also be retained on the membrane along with bigger micro-entities. Unlike 2D porous membrane, bigger micro-entities are trapped in 3DPPM and thus unsorted smaller particles can be washed-off through outlet in the main micro-channel (outlet-1 in Scheme-S5.1b). The bigger micro-entities are retained on the 3DPPM and hence get separated from smaller micro-entities (bi-directional sorting). Thus, high sorting efficiency or purity can be

achieved even if smaller particles do not pass through interstitial gaps. Indeed, the bi-directional sorting is unique to the 3DPPM. Overall, these features help in achieving high efficiency of the sorting and the patterning, which is a clear advantage over 2D membranes or other micro-filtration techniques. Other than direct applications of the 3DPPM in the sorting and the patterning related applications, it can also be used in applications that require enhanced interaction of fluid with micro-entities, such as capture of analyte from fluid on functionalized-beads [207]. As the flow of fluid is maintained through interstitial-gaps, analytes from sample can interact well with the functionalized-beads patterned on the 3DPPM while passing through these interstitial-gaps. Such interaction may increase chances of analyte being captured on beads. Thus, the idea of 3DPPM would be interesting to scientists working in different fields.

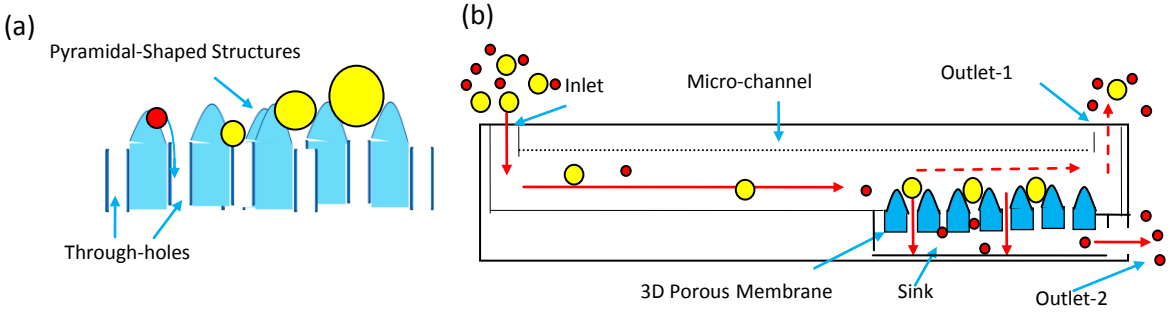

Scheme-S5.1: Characteristics of the 3DPPM: (a) the 3DPPM allows smaller micro-entities (Red ball) to pass through pores while larger micro-entities (Yellow ball) are trapped. Simultaneous sorting and patterning is achieved by this method. Micro-entities of different size can be singly patterned (Yellow balls). (b) The schematic for flow, sorting and patterning of micro-entities in the micro-fluidic device. Outlet-1 is kept closed and solution containing different micro-entities is flowed in the device to sort them through pores. Then outlet-2 is closed and outlet-1 is opened and unsorted micro-entities are washed-off. Bi-directional separation is achieved in this way.

5.2 MATERIALS AND METHODS

5.2.1 REAGENTS AND MATERIALS

Materials used for the device fabrication have been mentioned in the previous chapter. Parafromaldehyde, hexamethyldisilazane (HMDS), Calcein-AM and Propidium Iodide (PI) were purchased from Sigma–Aldrich, Singapore. Micro-beads were purchased from Polysciences (Warrington, PA) and Cancer cells (MDA-MB-231) were purchased from ATCC (Manassas, VA). Basal DMEM cell-culture media, fetal-bovine serum (FBS), and CMPTX live-cell labelling dye were purchased from Invitrogen, Singapore. Yeast cells were a kind gift from Department of Microbiology, National University of Singapore, Singapore.

5.2.2 BEAD SEPARATION AND PATTERNING

Beads were counted using a Hemocytometer. 10µL of bead solution was pipetted in the Hemocytometer. The beads were counted and their concentration was estimated by standard procedure. The bead solution was then diluted to the desired concentration (10^5 beads/mL) using DI-water. For patterning beads, 100µL of bead solution was flowed in the device at a flow-rate of 50µLmin^{-1} using a syringe pump (Kd Scientific, Holliston, MA). For separation and patterning studies, the bead mixture was prepared according to the desired concentration. 100µL of bead solution was flowed in the device at a flow-rate of 50µLmin^{-1}. Particles passing through pores were collected from the sink and were counted using the Hemocytometer. The un-patterned or unsorted particles were washed away from the device and were collected back and were flowed again in the device. The process was repeated. Finally, the micro-filter membrane was carefully cut and was taken

out of the device and was sonicated for 1-2hrs in 100µL of IPA to remove most of the beads. IPA was dried and it was reconstituted in 100 µL of DI-water. The number of beads was then estimated by using the Hemocytometer. The 3DPPM was observed again to count any left-over beads. The percentage was calculated accordingly. Separation and patterning efficiencies were calculated as per the formulae discussed given in next section. Scanning electron microscopy (SEM) images were obtained for trapped beads by sputter-coating the dried sample with gold and imaging using SEM (JSM-5600, Jeol). For studying the patterning efficiency of particles with different sizes, concentration of each type of beads was adjusted to 10^5beads/mL. For studying the separation and patterning efficiency of mixture, the concentration of bigger bead (10µm) was fixed to 10^5beads/mL and concentration of smaller beads was varied according to the desired ratio.

5.2.3 CELL SEPARATION AND PATTERNING

Cancer cell-line MDA-MB-231 was cultured in a DMEM cell culture-medium supplemented by 10% FBS in a cell-culture flask. Cells were trypsinized and were counted using a hemocytometer. Cell solution was diluted in complete culture medium to the concentration of 10^5cells/mL. Yeast cells were taken from agar plate and were mixed in cell-culture medium. The concentration was adjusted by dilution. Cell mixture was obtained in different ratios keeping concentration of cancerous cells to 10^5cells/mL in the mixture. 100µL of the cell mixture was flowed in the device at a flow rate 50µLmin^{-1}. The process was repeated. Patterned cells were removed from the device by back-flow of fluid. The cells collected in fluid were centrifuged and were diluted in 100µL of media before counting by using Hemocytometer. Separation and patterning efficiencies were calculated according to formulae mentioned earlier.

SEM of cells: For trapped cells, cells were fixed by using 4% parafromaldehyde (in PBS) for one hour in the device. It was then dehydrated by using gradient of ethanol solution varying from 10% to 100% of ethanol with an increment of 10% for 5min incubation at each point. It was dried on the device by using different ratio of ethanol and HMDS with increasing concentration of HMDS (3:1, 2:1, 1:1, 1:2, 1:3,) and left for overnight drying for overnight. The sample was sputter-coated (Jeol Sputter-coater) for 30-40s at 30mA before obtaining Scanning Electron Microscopy (SEM) image.

5.2.4 FLUID FLOW THROUGH INTERSTITIAL-GAPS

A 2D porous membrane, without any micro-structures, was obtained by reversing the 3D porous-membrane. Beads were patterned on the device as before. 100µL of DI-water was flowed in the device at different flow-rates. Beads that were pushed through pores were collected and were counted using the Hemocytometer.

For experiments to show that smaller beads can pass through interstitial-gaps, smaller beads (1µm, 3µm or 5µm) were diluted to the concentration of $3x10^5$beads/ml and 100µL of bead solution was flowed in the device with either beads (12µm) or cells (labeled with CMPTX live-cell labeling dye) patterned on the 3DPPM at a flow-rate of $50\mu L min^{-1}$. The movie for showing particle's flow through interstitial-gap was captured by using a High-speed camera (Photron Fastcam SA3) at frame-rate of 125frames/S.

The bead solution was normally diluted in DI-water, but when cells were involved, the dilution was done in 1XPBS.

5.2.5 CELL VIABILITY

For cell-viability studies, the device was sterilized by UV-light for 15min and by flowing 70% ethanol through channels. It was rinsed by 1X PBS for 15min. Then cell-culture media was flowed in the device and it was allowed to stand for 30-60min before starting cell-based experiments. A solution containing 10µM Calcein-AM and 10µM PI was prepared in 1X PBS for labeling viable and non-viable cells. Cells were patterned as before. The cell-staining solution was flowed in the device and it was incubated for 15min at ambient temperature and fluorescence images were captured by using a fluorescence-microscope (Nikon Eclipse-80i). For time-based studies, after each time point, staining was performed. The culture-medium was flowed in the device at a flow-rate of $20\mu L min^{-1}$ for continuous flow of culture-media after patterning of cells. All cell-based experiments done on device were performed at room temperature. Cell viability was assessed by counting viable/non-viable cells on the device using imageJ software. For cell-counting in imageJ, 'thresholing' was applied, followed by applying 'watershed' to separate particles and finally 'analyze-particle' was applied. For cell-culture based studies, cells were recovered by back-flow of fluid which was centrifuged to get a pellet. The pellet was diluted in 1ml of media before putting it for culture at normal cell-culture conditions.

5.3 RESULTS AND DISCUSSION

5.3.1 CHARACTERIZATION OF THE MICRO-DEVICE

5.3.1.1 SIZE-CHARACTERIZATION OF 3D MICRO-TRAPS

The aforementioned micro-fluidic device has been used here for size-based separation and patterning of micro-beads as well as of cells. The dimension of each component in a single-trap has been presented in Fig.5.1. Each funnel-like pore consists of a conical and a cylindrical part. The cylindrical part of the pore has a diameter of 6µm and is 20µm deep (not shown here). The conical part is 6µm deep and has diameters of 10µm and 6µm at top and bottom respectively. The pyramidal structures are 10µm high and have a base-width of 10µm. The top of pyramidal-shaped structures is rounded. Center-to-center distance between nearest located pores is 14µm (not shown here). In a single trap, the center-to-center distance between a pair of oppositely located pyramids is approximately 20µm (not shown here). According to dimensions, each trap should be capable of holding particles in a size-range of 6µm-20µm. Particles less than 6µm should flow out of the device. To experimentally verify this hypothesis, different sizes of beads ranging from 5µm to 19µm have been used in this study. More than 90% of 5µm beads can be recovered from the device after passing it through the porous-membrane. About 2-3% of beads from clumps and cannot pass through whereas about 3-4% of beads are lost in sink or channel. Beads of size 7µm or more do not pass through pores and are patterned on the device at the flow-rate ($50\mu L min^{-1}$) used for experiments in this project. Cells can also be patterned on the device.

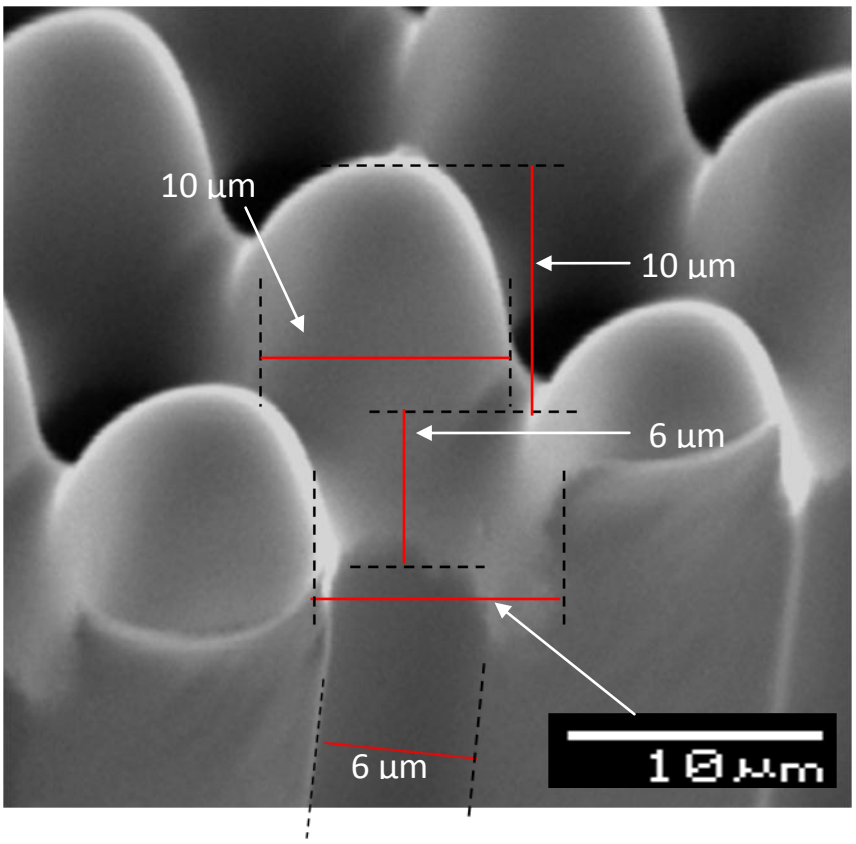

Fig. 5.1: The size characterization of features: The measurement of different features of a single trap is being presented here. The red lines indicate the distance whereas black dotted lines represent the line of feature between which distance is measured. White arrows indicate the distance measured by a red line.

5.3.1.2 SELECTION OF FLOW-RATE AND BEAD CONCENTRATION

The flow-rate and the bead-concentration for conducting this study have been chosen as $50\mu Lmin^{-1}$ and 10^5beads/mL, respectively. The appropriate value of flow-rate and appropriate number of beads for high patterning efficiency have been determined by conducting a study using different flow-rates and different number of beads. As a start,

beads (5µm) smaller than the pore size, have been used to study the passing-through of beads through the micro-filter at different flow-rates. Bead concentration has arbitrarily been chosen as a starting point. It can be observed from Fig.5.2a, that the percentage of beads passing through pores increases with increase in flow-rate in the beginning, but it becomes constant after 50µL/min. At lower flow-rate settling is more which can be the reason for this trend, but after certain point overall effect remains same. The flow-rate of $50\mu Lmin^{-1}$ has been selected as the starting point to study patterning. Using this flow-rate, patterning-efficiency has been studied for different bead concentrations. The patterning efficiency has been calculated according to the given formula for one time flow of bead solution. The bead concentration of 10^5beads/mL (100µL) has been chosen for further use as being suggested from the plot (Fig.5.2b). The number of pores (approx. $13x10^3$) is greater than the number of beads for optimal patterning (10^4). With increase in bead concentration more clustering has been observed. Fixing this concentration, patterning efficiency has been studied at different flow-rates. A flow-rate of $50\mu Lmin^{-1}$ has been selected for further studies as seen from the plot in Fig.5.2c. At lower flow-rates, more beads settle down in channels and at higher flow-rates more clustering of beads are observed in the micro-fluidic device.

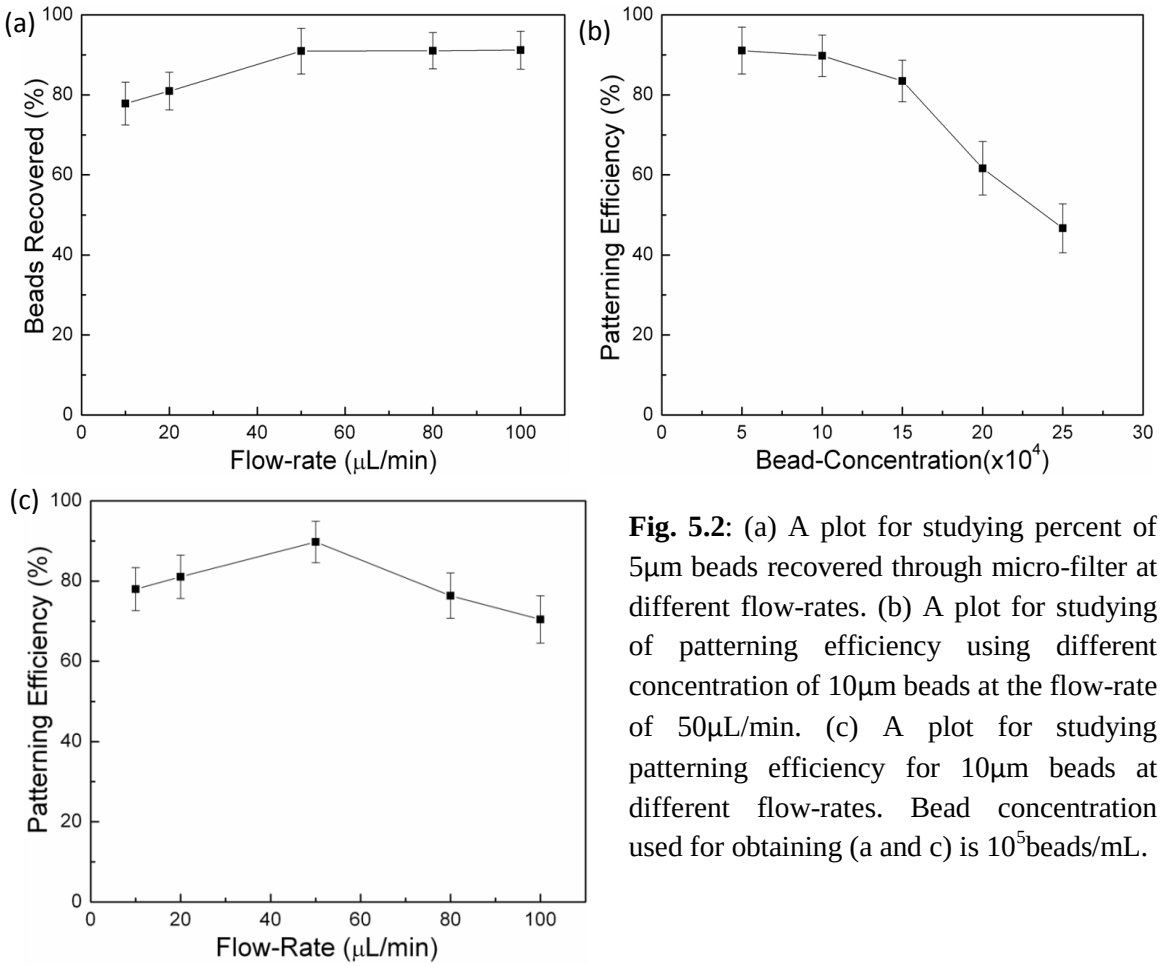

Fig. 5.2: (a) A plot for studying percent of 5μm beads recovered through micro-filter at different flow-rates. (b) A plot for studying of patterning efficiency using different concentration of 10μm beads at the flow-rate of 50μL/min. (c) A plot for studying patterning efficiency for 10μm beads at different flow-rates. Bead concentration used for obtaining (a and c) is 10^5beads/mL.

5.3.2 STUDY OF ANTI-CLOGGING CHARACTERISTICS

5.3.2.1 FLUID FLOW THROUGH INTERSTITIAL-GAPS

Computational study of anti-clogging: The anti-clogging porous membrane can be fundamentally significant for studying filtration process as well as for new applications. The 3DPPM should be considered anti-clogging, if fluid flow is maintained through interstitial-gaps after a micro-entity is trapped over a pore, even if many other pores remain empty (without any trapped micro-entities). Hence, a computational model has

been prepared, where micro-entities are trapped over some pores and the rest are left empty (Fig.5.3a). This model is solved for incompressible Newtonian fluid flow at steady state by solving Navier-stock's equation at different finite elements created by using COMSOL Multiphysics. Boundary conditions are defined as follows: 1.Inlet- Volumetric flow rate of $10^{-11}m^3$/sec, 2.Outlets: atmospheric pressure, 3.Walls: no-slip condition. Then, velocity field is obtained for the fluid flow as simulated in the software. Although, the flow-rate of fluid is reduced through interstitial gaps, the change is not drastic compared to the flow through empty pores in the model of membrane (Fig.5.3b). The result is reasonable as the pores are partially blocked by the trapped micro-entities and it indicates that fluid can pass through interstitial-gaps even if many pores are empty.

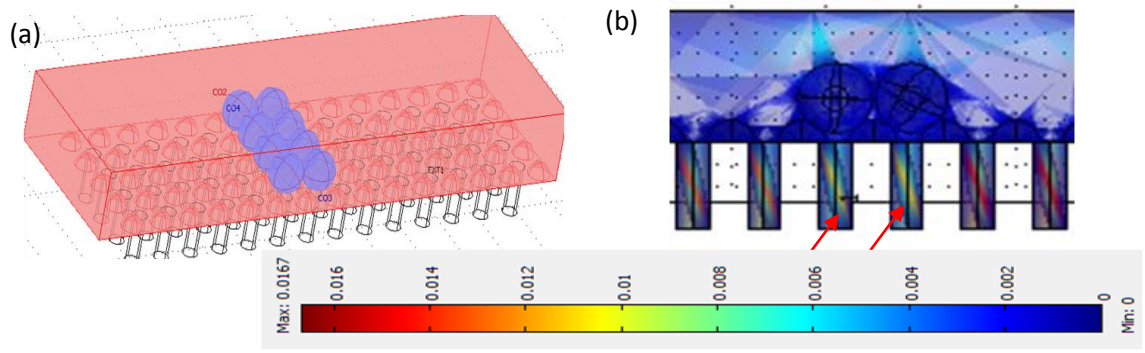

Fig. 5.3: **Modeling of Cell-trapping in the porous membrane:** A model is developed and solved for studying the fluid flow through pores by using COMSOL Multiphysics. a- the model containing an array of through-holes surrounded by 3D structures. Two columns in this array is filled with solid spheres representing beads (blue). b- the model is solved by the software and colored profile of velocity is obtained. The arrows indicate holes trapping beads. The figure shows that the flow rate is not reduced drastically by trapping beads and flow is maintained in the device.

Experimental study of fluid flow through interstitial-gaps: A magnified view of the interstitial-gap between a trapped bead and a pore can be seen in Figure-5.4(a-c). The fluid flow through these gaps in the 3DPPM has also been experimentally studied here.

The experimental study has been performed by comparing the fluid flow in the 3DPPM with that in a 2D porous membrane (membrane without any micro-structures). The reverse side of 3DPPM is used as 2D porous membrane to keep all other conditions (e.g. pore size) same for both types of membranes. A fixed number of beads (~10^4beads) are patterned on both types of membranes and fluid is then flowed in the device. Hypothetically, patterned beads would clog pores in 2D porous membrane but pores in 3DPPM would not be clogged. Thus, flow of fluid in the device would exert greater fluidic pressure over 2D porous membrane compared to the 3DPPM. Although, the fluidic pressure in the device may be a complex function of different parameters, the relative difference between these two types of membrane is useful to prove the concept. The relative difference can be measured by comparing the effect of increasing fluidic pressure on both membranes. The fluidic pressure can be increased by increasing the flow-rate of fluid. As pressure increases one of two possible effects may be observed; either the membrane is damaged at certain flow-rate or some trapped beads are pushed through pores in spite of their size being greater than pore size. The membrane has not been damaged even at very high flow-rates, instead some beads passed through pores in spite of their large size (10μm beads passed through 6μm pores). As PDMS is a rubber-like material, it is reasonable that larger beads are pushed through pores at high fluidic pressure (Fig.5.4d-f). As all other conditions are kept same for both of the membranes, the difference between the percent of beads passing through pores can indicate the relative difference in the fluidic pressure. This in turn can be related to the pore clogging. A plot between flow-rate and percentage of beads passing through the pores has been

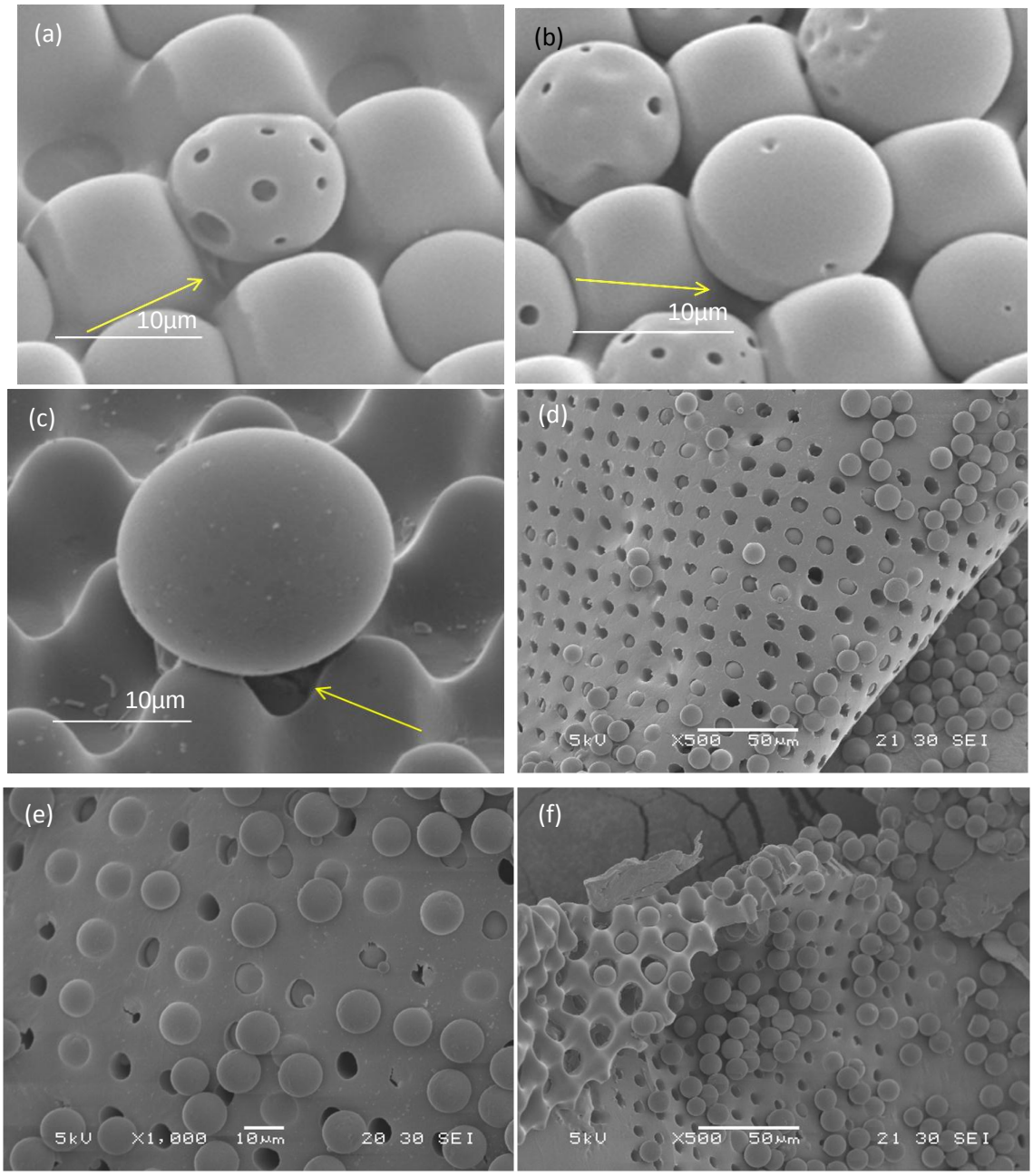

Fig. 5.4: Fluid flow through the interstitial gap: (a-c) are high-magnification SEM image for showing 'the Interstitial-Gap' between the pore and the trapped-bead. Arrows in the figure indicate the gap. Size of bead hanging over the indicated pore is about 10 µm in (a), 12µm in (b) and 20µm in (c). (d-f) are SEM-images 2-D porous membrane. (d) shows the filter with beads pushed in pores, (e) shows complete blocking of pores by beads and (f) shows beads coming out of the normal filter due to high pressure drop.

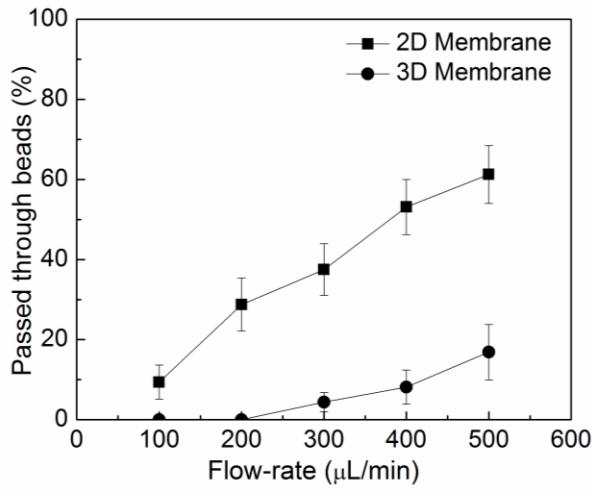

Fig.5.5: Comparison of bead flow through 2D and 3D porous membrane: a plot to compare the percent of beads that passed through 2D porous membrane and the 3DPPM at different flow-rates.

obtained for both types of membranes (Fig.5.5). The plot shows that the percentage of beads passing through 3DPPM is much smaller compared to 2D porous membrane. This indicates that fluid flow in the 3DPPM is less affected due to patterned beads compared to 2D porous membrane. This difference can only be caused due to fluid flow through interstitial-gaps present in 3DPPM. Hence, this proves the anti-clogging characteristic of 3DPPM. Also, it shows that the 3DPPM can be used at relatively high flow-rates (300-400µlmin^{-1}) compared to 2D porous membrane. This presents a clear improvement of 3DPPM over traditional membranes.

5.3.2.2 Flow of Micro-entities through interstitial-gaps

Flow of beads through interstitial-gaps: To prove that beads smaller than the interstitial-gap can pass through it, a movie has been captured using a high-speed camera and the

flow of smaller beads has been tracked in the movie by using a software, ImageJ (Fig.5.6). Bigger beads (12μm) are patterned on the 3DPPM keeping number of beads lesser than the approximate number of pores leaving many empty pores. Then smaller beads (2μm) are flowed in the device and the movie is captured (not provided with this thesis). Few representative frames from the movie have been shown in the Fig-5.6. As seen from the figure, a particle travels to a trapped particle, takes a turn perpendicular to the flow in main-channel and flows out. Since the flow in the channel is perpendicular to

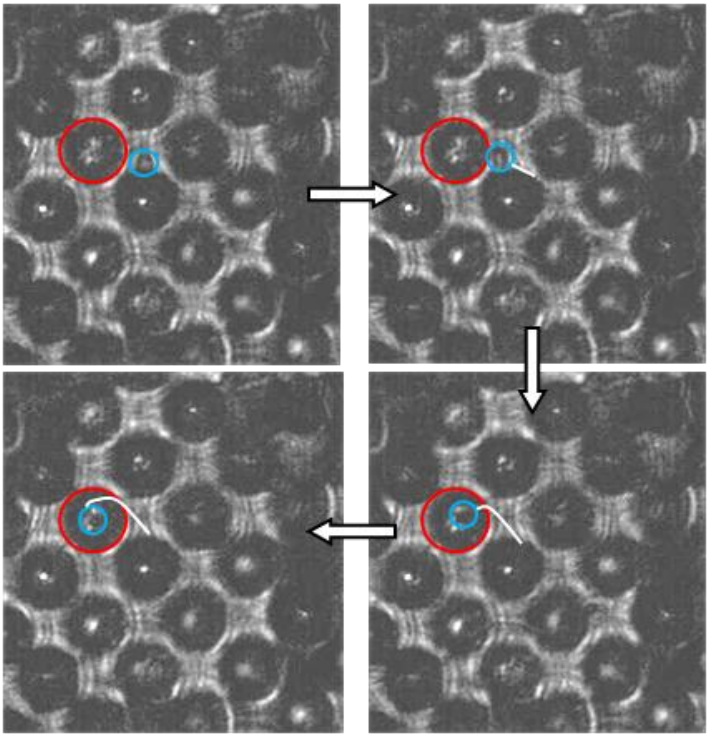

Fig. 5.6: Particle flow through interstitial-gap: Representative images taken from the movie to show the movement of the bead through the interstitial gap. The red and blue circles indicate the trapped large bead and the small bead to pass through the interstitial gap respectively. The white line shows the track of the small bead.

the flow in the sink, the smaller particle has passed through the interstitial-gap (which can be seen through the transparent beads) and has flowed out in the sink.

An experiment has also been performed to study the flow of beads through interstitial-gaps. To perform this experiment, a fixed number of beads of 12μm size are patterned on the 3DPPM and 2D porous membrane. Two different sizes of beads (1μm and 3μm), one smaller than and the other larger than interstitial-gaps, are flowed through 3DPPM as well as 2D porous membrane. The percent of beads passing through both membranes is calculated and compared. Hypothetically, if flow of fluid or beads is maintained through interstitial-gaps, then beads smaller than interstitial-gaps should pass through these gaps, whereas, beads bigger than interstitial-gaps should settle around patterned beads. In this case, there should be significant difference between the percent of these two types of beads passing through the membrane. If this is not the case i.e. none of beads pass through interstitial gaps or no such interstitial gap exists, then such difference should not surface. Thus, if 3DPPM is anti-clogging such difference should occur while it should not occur for 2D porous membrane.

Results obtained here support this hypothesis. For 3DPPM, 1μm beads are hardly seen whereas many 3μm beads can be seen trapped around patterned beads (Fig.5.7a, b) in SEM micrographs. For 2D porous-membrane, beads are scattered over the whole surface for both types of beads (Fig.5.7c, d). The plot in Fig.5.7e shows a significant difference between the percentage of 1μm and 3μm beads passing through the 3DPPM whereas this difference is not significant for 2D porous membrane. As both types of beads are smaller than pore-size (6μm), no such difference would occur if particles pass through empty pores. Also, all other conditions are kept same for both beads. Thus, such difference

should occur due to flow of beads through interstitial-gaps. Such difference does not occur for 2D porous membrane that does not have interstitial-gaps. Hence, this experiment proves that the smaller beads flows towards interstitial gaps even if all pores are not blocked. Now depending on their size, these beads either pass through or are stuck there. Thus, it can be concluded here that the 3DPPM is characteristically anti-clogging.

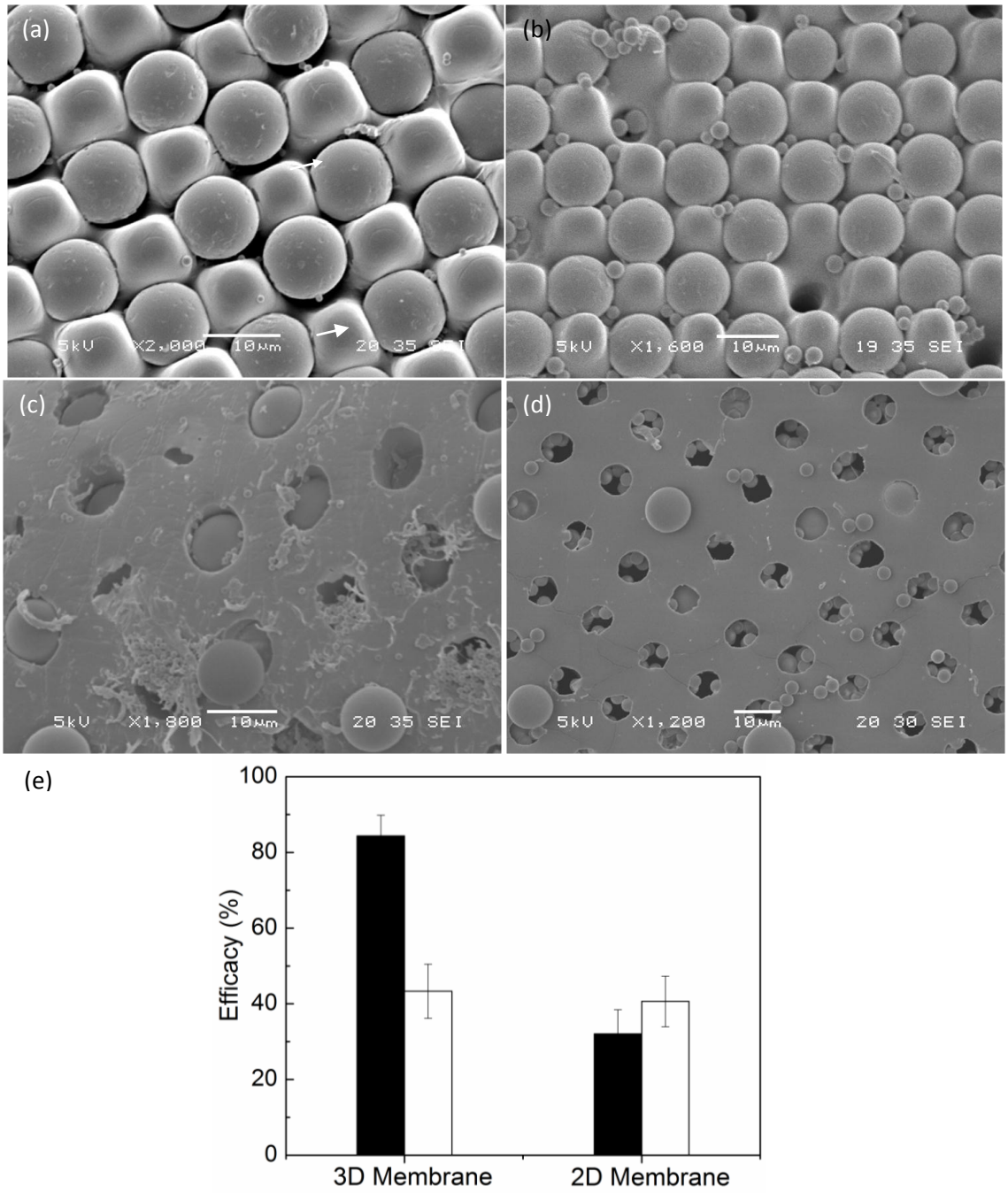

Fig. 5.7: Flow of smaller beads through the interstitial-gap: (a) and (b) are SEM-images which were captured after flowing 1µm and 3µm beads respectively through the 3DPPM patterned with 12µm. (c) and (d) are SEM-images which were captured after flowing 1µm and 3µm beads respectively through the 2D porous membrane patterned with 12µm beads. (e) is the bar chart for showing percentage of beads of size 1µm (black bar) and 3µm (white bar) passing through the 3DPPM and the 2D porous membrane.

Flow of beads through interstitial-gaps with patterned cells: Next, the anti-clogging of 3DPPM has been studied by using cells to prove that the 3DPPM is useful for cell-based applications. The cell-size within a batch varies, so it is difficult to ascertain the interstitial gaps. Also, the problem is complicated as cells are not rigid as beads. So, the anti-clogging should be determined by the experiment. To study this, cells (15-20µm) have been patterned in the device and smaller beads are flowed through the device. Beads of size 1µm, 3µm and 5µm have been used as smaller beads (all three are smaller than pores). It can be seen from the plot (Fig.5.8a) that high percentage of 1µm and 3µm beads have passed through 3DPPM while most of 5µm beads could not pass through it (Fig.5.8b). As all three types of beads can pass through pores, the significant difference here is caused due to ease with which 1µm and 3µm beads can pass through interstitial-gaps. This proves that 3DPPM can be used as anti-clogging membrane for cell-based experiments. Moreover, such differences are not observed for the 2D membrane which supports the conclusion.

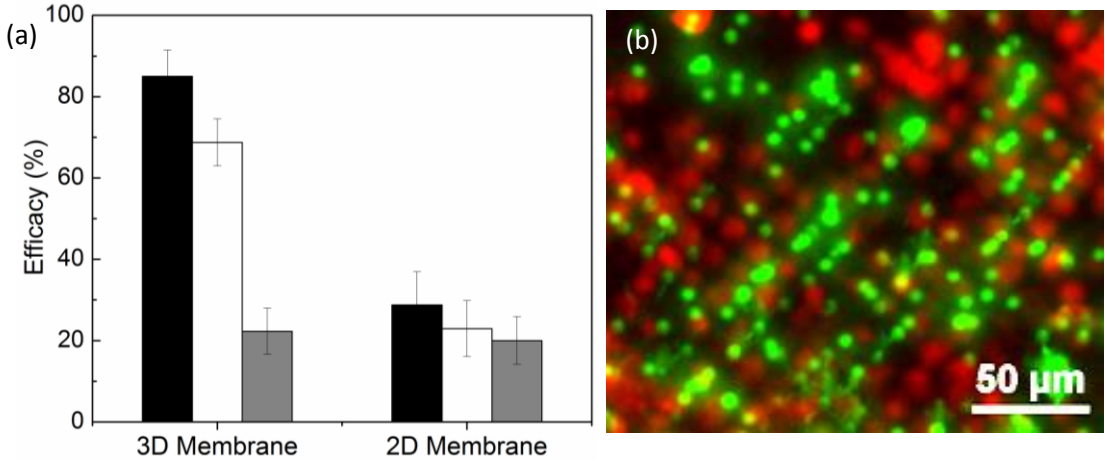

Fig. 5.8: Fluid flow through interstitial-gaps with patterned cells: (a) the plot showing percent of beads of size 1µm (black bar), 3µm (white bar) and 5µm (gray bar) that passed through the 3DPPM and 2D porous membrane with cells patterned on them. (b) the 5µm beads (green) are stuck around cells (red, labeled with CMPTX-a red fluorescent dye for staining live cells) on the device as fluid flows through pores.

5.3.3 SORTING AND PATTERNING BY THE 3DPPM

One of the major applications of the 3DPPM can be sorting and patterning of micro-entities besides being used as an anti-clogging porous membrane. As mentioned before, the 3DPPM is endowed with four main characteristics. The anti-clogging property of the 3DPPM has been studied in previous sections. Now, the study on other three characteristics is presented in this sub-section.

5.3.3.1 PATTERNING OF MICRO-ENTITIES OF DIFFERENT SIZES

Herein, patterning of beads with different sizes has been studied. Beads as well as cells of different sizes can be patterned on the 3DPPM (Fig.5.9). In this figure, different sizes can be seen to be trapped. The patterned cells look smaller than their normal size in Figure-5.9c. This can be due to shrinking of cells during sample preparation for SEM. The patterning of micro-entities has been quantitatively studied by obtaining Patterning efficiency for beads of different sizes (Fig.5.10a). The patterning efficiency is being defined here as,

$$Patterning\ Efficiency = \frac{No.of\ singly\ trapped\ beads\ \times 100}{Total\ no.of\ beads\ used}$$

The data shows beads of size 10µm and 12µm are patterned with high efficiency (~ 90%) which is expected for the given dimension of micro-traps. The 7µm and 15µm beads are patterned with slightly lower efficiency (~80% and ~70% respectively). Some of un-patterned 7µm beads get stuck between microstructures during washing, while some of 15µm beads leave their place during washing. The patterning efficiency for 19µm beads is low (~30%). The reason is the large size of these beads.

Although the maximum distance between pyramids in a single micro-trap is 20µm, the pore-to-pore distance is only 14µm. Hence, a trapped bead of large size prevents other beads to be trapped in its vicinity. The increase in patterning efficiency has been observed by decreasing the bead-concentration. Patterning efficiency of ~80% has been achieved for this size of beads (Fig.5.10b).

Living cells have also been used for this study. Cells have been successfully patterned on the device with an efficiency of ~85%.

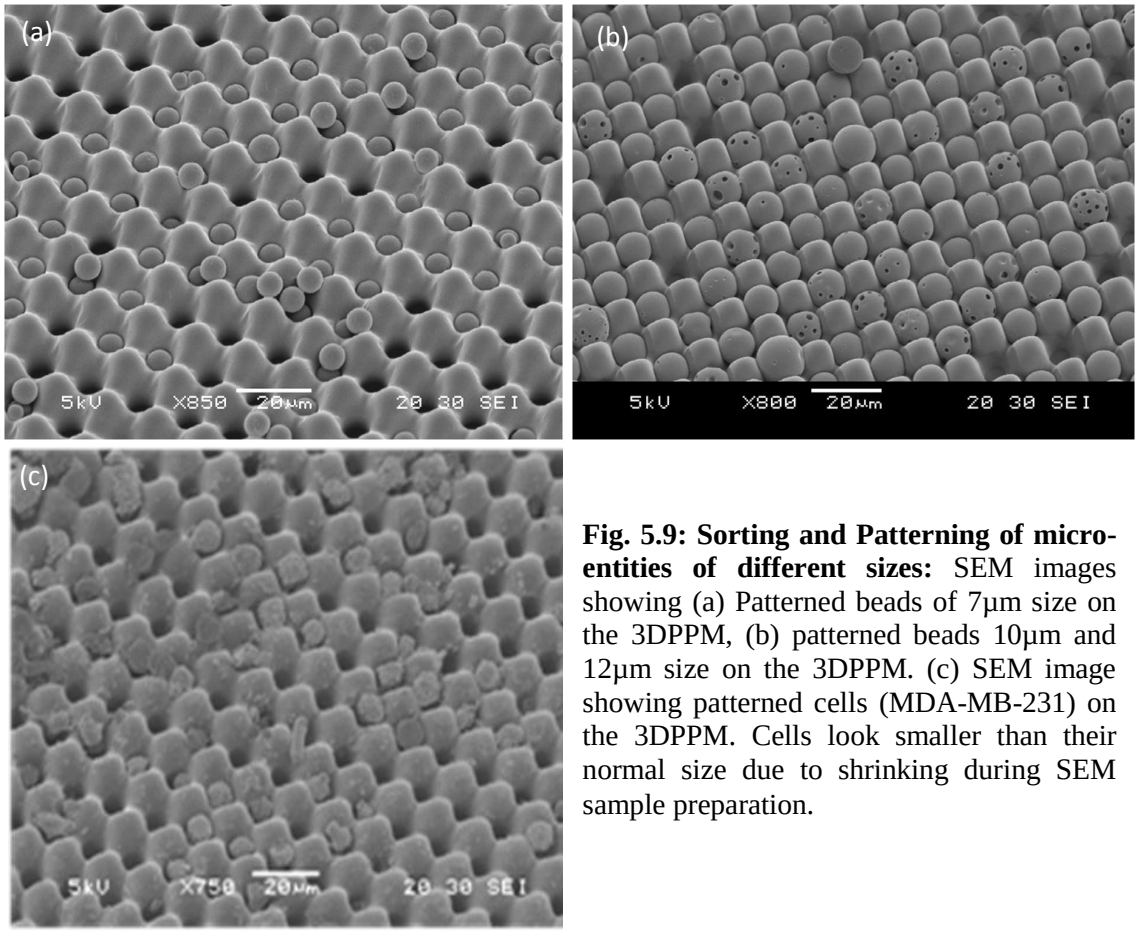

Fig. 5.9: Sorting and Patterning of micro-entities of different sizes: SEM images showing (a) Patterned beads of 7µm size on the 3DPPM, (b) patterned beads 10µm and 12µm size on the 3DPPM. (c) SEM image showing patterned cells (MDA-MB-231) on the 3DPPM. Cells look smaller than their normal size due to shrinking during SEM sample preparation.

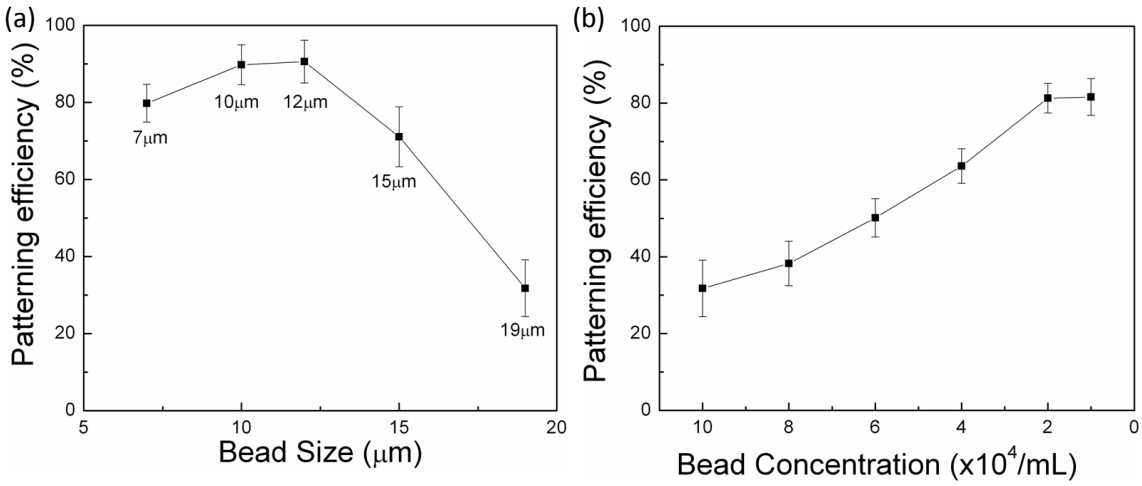

Fig. 5.10: Patterning efficiency: (a) The graph presenting the patterning efficiency of beads of different sizes on the device. (b) The graph presents the patterning efficiency of 19μm beads at different concentrations of beads.

5.3.3.2 Bi-directional sorting in 3DPPM

Next, bi-directional sorting of micro-entities in the 3DPPM has been studied. To perform this study, two sizes of beads have been chosen in such a way that smaller beads should pass through pores, but should not pass through interstitial-gaps while bigger beads are trapped over pores. This study has been performed to show the improved capability of 3DPPM as a micro-filter even without using its anti-clogging property. As discussed before, micro-entities can be separated in two directions, in the direction of fluid-flow in micro-channel (i.e. sorting in the main channel) as well as that perpendicular to it (i.e. through pores) (Scheme-S5.1b). This unique ability of the 3DPPM can be attributed to pyramidal microstructures that help in trapping of larger micro-entities. This allows washing of unsorted smaller micro-entities out of the main channel. Thus, apart from size-based sorting due to pores (like 2D porous membrane);

the in-channel sorting also takes place in 3DPPM (unlike 2D porous-membrane) which increases sorting efficiency. To verify this hypothesis, two different sizes of beads (5µm and 10µm) have been used in this study. A bead solution containing mixture of both types of beads is flowed through the device. A portion of 5µm beads (smaller beads) passes through the pores getting separated from the mixture as 10 µm beads (larger beads) are trapped. The unsorted smaller beads are then washed-off through outlet-1 without flushing away larger beads (Scheme-S5.1b). The washed-off solution mainly contains smaller beads with low number of bigger beads. The washed-off solution is re-flowed in the device to increase the purity of sorted beads. The sorting purity has been determined by calculating the percentage of smaller particles (5µm) in the fluid collected from the device. The sorting purity has been found to be more than 95% (98±2%) for the range of bead-ratio studied here (Fig.5.11a).

5.3.3.3 Simultaneous Sorting and Patterning in 3DPPM

The sorting as well as simultaneous patterning of micro-entities has been studied here. The respective efficiencies have also been calculated. For simplicity, sorting efficiency can be represented as the efficiency of the device in sorting smaller micro-entities from the mixture. It is also reasonable to consider that smaller micro-entities recovered from device are almost purely separated from the mixture (neglecting small number of larger particles for the ease of calculation). Thus, the patterning efficiency would simply mean the percentage of smaller micro-entities recovered from the device. Hence, a simple formula has been presented below for the calculation of

sorting efficiency which only contains terms for smaller beads. As larger micro-entities are patterned on the 3DPPM during sorting, the patterning efficiency can be calculated by another formula given below. Patterning efficiency is considered for larger micro-entities only and thus this formula contains the term for larger beads only. Using these formulae, simultaneous sorting and patterning efficiencies have been studied here for a range of bead-ratio (Fig.5.11a). Sorting and patterning efficiencies have been calculated as per the formulae given below.

$$Separation\ Efficiency = \frac{No.of\ smaller\ beads\ recovered\ \times 100}{Total\ no.of\ smaller\ beads\ used}$$

$$Patterning\ efficieny = \frac{No.of\ singly\ trapped\ big\ beads\ \times 100}{Total\ no.of\ big\ beads\ in\ the\ mixture}$$

As it can be seen from the plot in Fig.5.11a, there is no significant change in sorting or patterning efficiency with change in beads-ratio which can be attributed to the bi-directional sorting mechanism of 3DPPM. The smaller particles (5µm) cannot pass through interstitial-gaps, so they tend to settle around the larger particles (10µm). As beads-ratio is increased, number of smaller beads settling around larger beads also increases, but the smaller beads settled on the membrane can be washed-off. Hence, even though the beads-ratio is changed, the sorting and patterning efficiency is not changed.

Simultaneous sorting and patterning of cells have also been performed. Human cancer cells (~15-20µm) have been sorted from yeast cells (~5µm) and have been patterned on 3DPPM with reasonably high efficiency (Fig.5.11d).

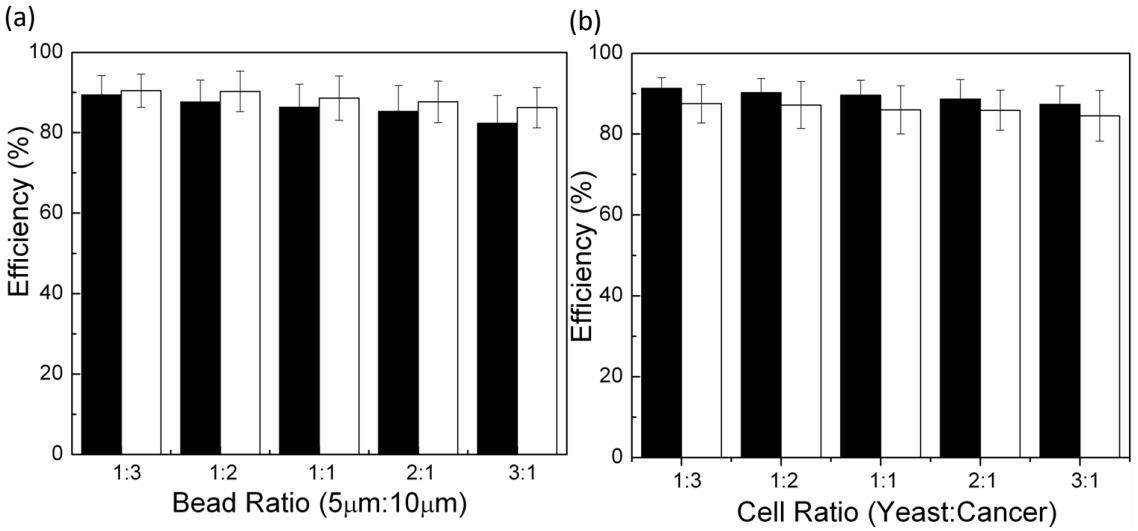

Fig. 5.11: **Separation and simultaneous patterning efficiencies:** (a) the graph presenting the separation efficiency of device in separating 5μm beads from 10μm beads and simultaneous patterning efficiency for patterning 10μm beads on the device. (b) the graph presenting the separation efficiency of device in separating yeast cells (smaller) from cancer cells (bigger) and simultaneous patterning efficiency for patterning of cancer cells. Black and white bars represent separation and patterning, respectively, in (a) and (b).

5.3.3.5 USE OF 3DPPM FOR OTHER SHAPE OF MICRO-ENTITIES

In this project it has been demonstrated that the 3DPPM is suitable for sorting and patterning of spherical micro-entities. It is difficult to predict how the 3DPPM would behave for non-spherical micro-entities. It would depend on many characteristics of such micro-entities, such as rigidity. As most of the micro-entities like beads or cells (in solution) remain spherical or nearly spherical, the 3DPPM should be useful in most of the cases. However, for some special micro-entities like blood cells, the 3DPPM may not be suitable.

5.3.4 CELL VIABILITY ON THE DEVICE

The micro-filter device presented here can be a useful tool for cell-based applications as cells can be separated and patterned on the device with high efficiency. Also, it has been proved that trapped-cells do not block pores. Now, it is important to study if the filtration process can cause significant decrease in cell-viability or cell-functionality. To study the cell viability on the device, a combination of two fluorescent-dyes Calcein-AM and Propidium Iodide (PI) have been used. Calcein-AM (green fluorescence) labels live-cells only whereas PI (red fluorescence) labels dead-cells only. To perform this experiment, cells (MDA-MB-231, breast cancer cell-line, average size=16μm) are patterned on the same device and cell- viability is assessed at different time–intervals by using the above mentioned dyes. Cell viability does not change significantly even after five hours of incubation (Fig.5.12a-c) which proves that filtration process does not affect cell-viability significantly.

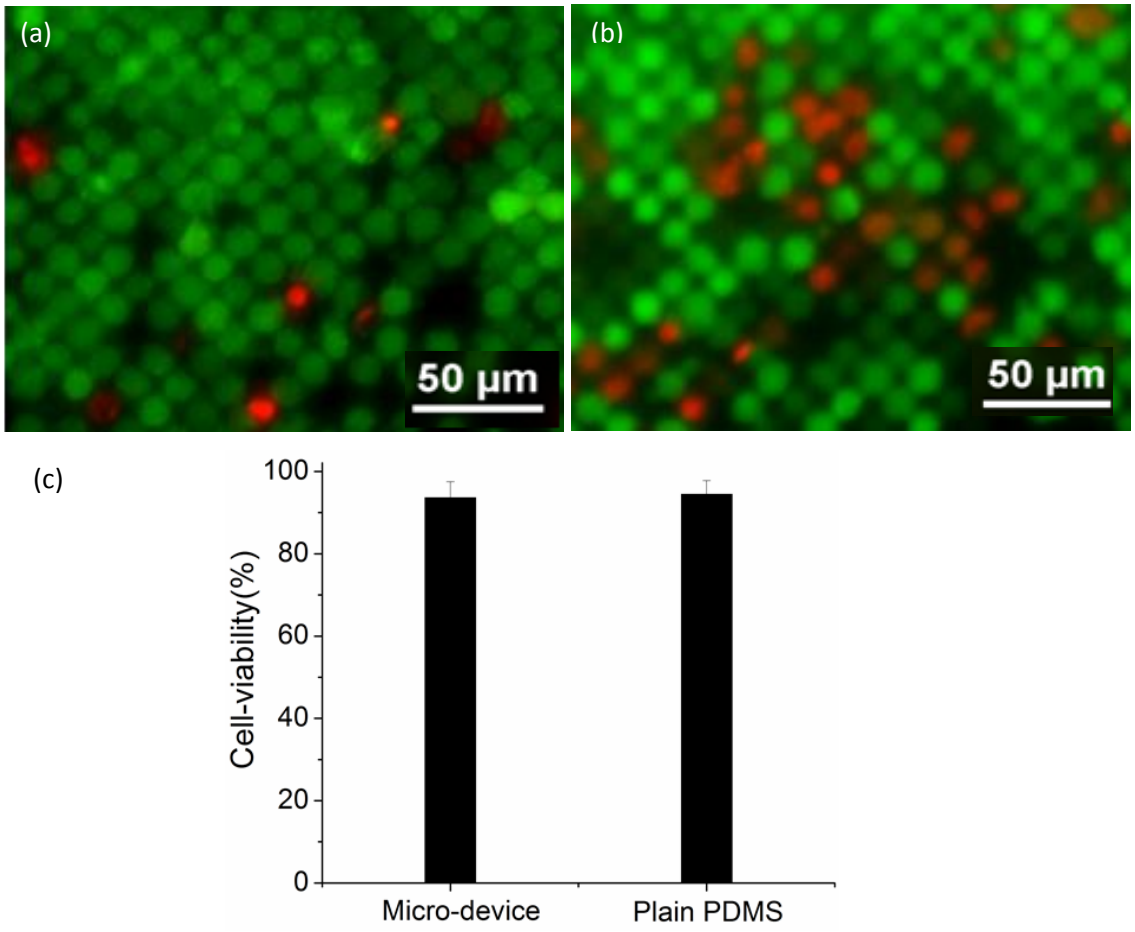

Fig. 5.12: Cell-viability in the device: (a) and (b) are obtained from the cell-viability study on the device. Green fluorescence indicates viable cells and red fluorescence indicates non-viable cells. (a) Cells just after patterning and (b) after 5hr of incubation in the device. (c) a plot showing cell-viability studied over 5hrs of incubation in comparison to the plain PDMS surface.

To further confirm the finding and to prove that cells remain functional, another experiment has been performed. Cells are flushed-out from the device after patterning by using back-flow of fluid. The recovered cells are then cultured and cell-culture is compared to the normal cell-culture. The cells have been found to grow normally and are morphologically similar to cells from normal culture (Fig.5.13a and b). This experiment shows that cells remain viable and functional after filtration process.

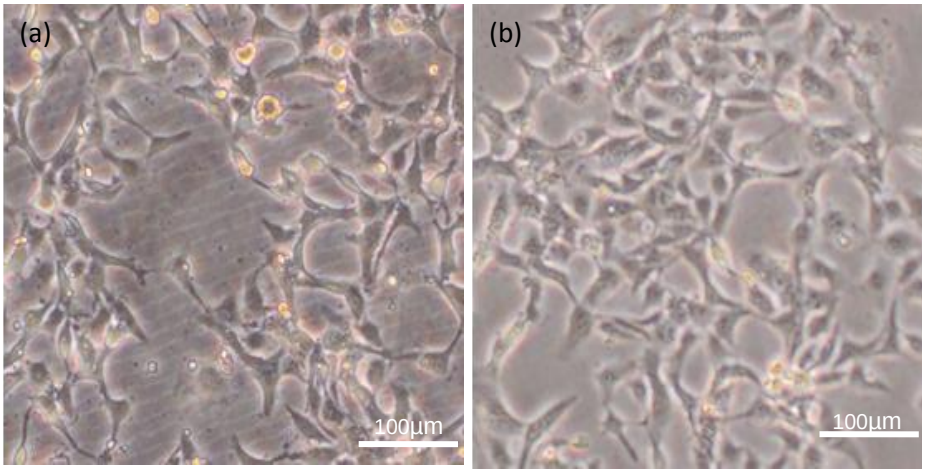

Fig. 5.13: (a) shows culture of cells recovered from device after filtration process and (b) culture of cells under normal conditions

5.4 CONCLUSIONS

A unique 3D pyramidal porous membrane has been integrated in a functional micro-device which has been used here for simultaneous separation and patterning of cells/beads. The anti-clogging nature has been studied in detail. The membrane also exhibits an interesting separation mechanism, i.e. bi-directional separation. It has been proved here that the high efficiency of separation and patterning of cells/beads can be achieved by the bi-directional separation mechanism. The micro-device used here is compatible for the cell-trapping and can be used for the cell-based applications. Anti-clogging porous membrane has not been reported in the past.

Chapter-6: Conclusion and Future Work

Chapter-6: Conclusion and Future Work

6.1 CONCLUSIONS

A novel 3D microfabrication technique has been developed in this project. This technique is simple, inexpensive and has high throughput. It does not require any sophisticated equipment or facilities for adopting this technology. This technique is based on an approach different from other approaches used in existing 3D microfabrication techniques. In the most of the existing techniques, exposure of light on a photosensitive material is highly controlled or localized, whereas the cross-linking of the material is controlled in this newly developed technique. A new concept of material cross-linking termed as 'Partial activation' (PA) has been introduced in this project, which helps in controlling the cross-linking of the material. The cross-linking properties of PA have been found to be different from normal complete cross-linked state. The PA is a flexible state of cross-linking which can be modulated to control the cross-linking of the material. It has been interesting to study anisotropic cross-linking within the PA. This property has been studied by using an optical imaging as well as a molecular spectroscopy technique (FTIR). Results from both of these techniques have confirmed the re-arrangement within PA. Such re-arrangement has endowed the ability to fabricate different 3D microstructures. Based on this understanding, the novel 3D microfabrication technique has been developed. A single inexpensive plastic photo-mask has been used here for the fabrication of various 3D microstructures. The shape and size of these microstructures can be modulated by exposure energy and PEB temperature. To the best of our

knowledge, the study on PA as well as the 3D microfabrication based on materials' properties has not been reported in past.

The 3D microfabrication technique developed in this project has been applied for the fabrication of a unique anti-clogging 3D pyramidal porous membrane (3DPPM). A master-mold is fabricated in SU-8 which is used several times for the fabrication of 3DPPM in PDMS. The anti-shape of the desired 3D microstructures is fabricated in the master-mold which is replicated in PDMS. These micro-structures are fabricated on a replica of micro-channel. This allows integration of 3D microstructures in a micro-fluidic device. The fabrication of such master-mold requires integration of different 3D microstructures. Such integration is challenging as complex 3D microstructures are desired. In this project, the 3D microstructures with positive and negative relief features are required to be integrated together, which also need to be integrated with micro-pillars. Such integration has been found to be challenging due to use of multiple layers and instability of micro-pillars in standing over 3D microstructures. To overcome this problem, the PA and its molecular re-arrangement has been harnessed to develop two methods for such integration of microstructures. Both of these methods depend on generation of the PA. In one of these methods it is generated by exposing SU-8 to low dose of exposure energy ('Low dose exposure energy' method), while in other method it is generated by diffusion of activated cross-linking species from exposed region to unexposed region ('Diffusion' method). 'Low dose exposure energy' method is simpler while 'Diffusion' method is more versatile. Both methods have been demonstrated for the fabrication of the master-mold. The master-mold has been used for fabrication of the 3DPPM. The 3D microstructures are replicated while micro-pillars are utilized for

fabrication of pores (through-holes). It is accomplished by coating a thin layer of PDMS over microstructures. However, it has been found that PDMS is accumulated over these microstructures and prevent formation of through-holes. Hence, a weight extrusion method has been developed in this project to overcome this problem. Furthermore, peeling the membrane off the master-mold has been found to damage the membrane. To overcome this problem, a solvent based approach has been developed for easy and automatic release of porous membrane from the master-mold. The 3DPPM membrane has been successfully fabricated in this project, which consists of 'funnel-like' pores surrounded by 3D pyramidal microstructures. The 3DPPM has been integrated in a micro-fluidic device by integrating it to a layer containing sink for collecting fluid passing through it. The 3DPPM has been supported by using unique 'Doll-like' microstructures in the sink. These structures have been fabricated by the newly developed 3D microfabrication technique in this project. The micro-device consisting 3D PPM has been found to be stable at high flow-rates and thus can be used for various applications.

The 3DPPM confers four characteristics to the micro-fluidic device developed in this project, which has been applied for sorting and patterning of micro-entities such as cells and beads. These characteristics are: 1) It is anti-clogging and therefore allows uninterrupted sorting of micro-entities continuously; 2) Simultaneous sorting and patterning of micro-entities has been achieved; 3) Micro-entities of different sizes has been patterned or trapped between the 3D microstructures; 4) Bi-directional sorting has been achieved, both in the direction of fluid-flow through the pores as well as that perpendicular to it, for high sorting efficiency. The anti-clogging of the 3DPPM has been studied using computational technique as well as by experimental method. It has been

found from these studies that fluid as well as micro-entities can pass through interstitial-gaps between trapped micro-entities and pores. The bi-directional sorting of micro-entities has led to high purity of sorting and sorted micro-entities have been found to contain negligible amount of contamination by other micro-entities present in the mixture. The 3DPPM has been found to perform simultaneous sorting and patterning of micro-entities at high efficiencies which remain unaffected by change in ratio of micro-entities. These studies have also been performed by using living cells. The cell-viability and cell-functionality has also been studied to assess effect of sorting and patterning process on cells. It has been found that cells remain viable and functional in the micro-device. Hence, the micro-device developed here can be useful for cell-based studies and for biomedical applications.

6.2 FUTURE WORKS

Future work for 3D microfabrication technique: The lack of simple 3D microfabrication technique fuels a strong need for developing a simple, inexpensive and versatile technique for this purpose. Also, possible applications and potentials of 3D microstructures or topographies might not been fully explored. One of the examples from the past developments can be taken for the introduction of three-dimensional cell-culture techniques. Though the 2D cell culture has been well established, the introduction of 3D cell-culture techniques has greatly increased the understanding of cell-behavior and has increased the attention of biologist to study cell in a 3D environment which resembles more to their natural environment. The concept has radically changed the view about cell-culture, cell-behavior and cell-based applications. Similarly, many possible applications can be conceptualized from the use of 3D topographies. For example, cells are trapped by using micro-wells for single-cell studies in some of the existing techniques. Usually, vertical dimensions of these wells do not vary which provides a strict dimensional restriction for capturing cells. Dimensions of cells (even from the same batch) vary and cells of different sizes can be found from the same batch of cell culture. So, capturing cells using such wells produces biasness for capturing cells of particular size only that may not represents the true stochasticity in the single-cell analysis. The use of 3D microstructures with varying vertical dimension may represent better system by accommodating cells of different sizes. Another example can come from high-aspect ratio microfabrication. High-aspect ratio of microstructures decreases their stability. The simple solution to this problem can be using conical structures with broader base and slimmer top. There can be many such examples and applications where 3D

microstructures can be used to add more functionality or to improve the current functionality of a system apart from being used for unique and specialized purposes. Thus, it is important to develop simple techniques for 3D microfabrication. This project is an effort in this direction. However, this is not end in itself and provides wide scope for future exploration to tailor this technique according to needs for various scientists. Following works can be undertaken in future to extend this project:

- The 3D microfabrication technique developed here has been demonstrated only for SU-8 that is a negative photoresist. The work can be extended for other types of negative photoresists available in market, e.g. Negative photoresist (AL-217) from Sigma-Aldrich.
- The concept of the PA should be explored more for other polymeric material. It would be interesting to explore if other material shows "molecular re-arrangement" too. It would also be useful to study if PA in other material can be used for developing other important techniques. A deeper research in this area should be undertaken.
- The 3D microstructures developed in this project should be explored for different applications such as fabrication of different types of micro-lens array, moving parts in MEMS system.
- Array of pillar arranged in particular fashion has been recently used for sorting micro-entities. This technique has been reported to be quite efficient. However, it is only limited to size based separation, whereas many micro-filtration techniques can sort micro-entities based on size and defromability of micro-entities. Hence, it can be an interesting exploration to use 3D micro-pillars in

such application as these microstructures may modulate movement of micro-entities in different way. Moreover, if such microstructures are flexible, sorting of micro-entities based on defromability may also be achieved. This can be interesting new addition to the existing tools for sorting of micro-entities.

Future work for the 3D porous membrane: No doubt, porous membranes are one of the most traditional tools that are essential components of many advanced industrial and research applications. However, the basic architecture (2D) and the major drawback (pore clogging) of porous membranes have not seen much advancement in long history of their use. Herein, we intend to add a new dimension in this technology by presenting the 3DPPM with anti-clogging characteristics. The purpose of this research is two-fold: 1) to introduce the concept of anti-clogging 3D porous membrane and 2) to present a new tool for biomedical applications. In future, further study would be required for using this technology for many applications. Following are some suggested future works:

- The anti-clogging is a new concept for filtration by using porous membrane. Hence, it should be important to understand the fundamental aspects of this concept. Such understanding may lead to develop similar anti-clogging porous membrane used for different industrial application.
- *Infectious Disease Diagnosis:* Bacterial identification from pathological samples is clinically very important. Although bacterial disease diagnosis is clinically important and commercially lucrative, existing techniques are either slow (mainly based on bacterial culture) or require stringent sample preparation (based on PCR). Hence there is a need to develop a new technique for fast, efficient and sensitive detection of bacteria.

The 3DPPM patterned with functionalized beads (with antibodies or other capturing molecules specific for bacterial capture) may solve this problem. Patterned beads do not block holes/pores leaving interstitial-gaps which allow fluid to pass through (Due to anti-clogging property of the membrane). The bacteria from the sample would be forced to pass through these gaps. During this process they would interact with functional moieties on beads and may get trapped. Moreover, the device can be used for multiplex detection as an array of beads functionalized with different antibodies may be used. It may also be developed for testing antibiotics against trapped bacteria. If successful, the device can replace the age-old bacterial culture based diagnosis system. Based on this idea, we plan to develop a point-of-care bacterial diagnosis system for fast and sensitive detection of bacteria. Recently, a grant (Biomedial Engineering Programme (**BEP**) under A-star grant) has been secured for his purpose.

- *Disease Treatment:* Leukemia is a serious clinical problem in which number of cancerous cells increases in the blood which makes it more viscous. The increased viscosity can cause failure of vital organs like heart. One of the current treatments for Leukemia is called Leukapheresis whereby cancerous cells are removed from the body by separation of cancerous cells using big and bulky equipment. It is a tedious process and needs hospitalization. Miniaturized equipment using anti-clogging filtration system can be developed in future to solve this problem. The 3DPPM can be integrated in such equipment for continuous separation of cancerous cells from blood. The system would be

expected to clear out cancerous blood and supply back the normal blood. The system would contain circulation system for continuous separation without the need for hospitalization.

- *Support System for Disease management:* The failure of insulin production from beta-cells cause diabetes which is one of the silent killers that affects human lives world-wide. Conventional therapy consists of direct insulin injection based on the physician's recommendation about the amount and number of dosage. The conventional technique is difficult to regulate and is inefficient in regulating blood-glucose concentration.

  A "pancreas-mimic micro-device (PMMD)" using encapsulated β-cells can be used to solve this problem. The goal would be to mimic the pancreas function in a micro-device. The 3DPPM can be used as an anti-clogging porous membrane for continuous interaction of blood with encapsulated cells. A number of β-cells can be encapsulated (by established methods of micro-encapsulation) to make small beads containing cells. Beads of different sizes can be trapped in the membrane avoiding the need for strictly controlling the bead-size. Blood can continuously be flowed in the device without cells being washed-off due to anti-clogging property of the membrane. Blood flow around each encapsulated beads would allow cells to access blood-glucose correctly which in turn would help β-Cells to sense blood-glucose accurately and release correct amount of insulin in response. This would also provide nutrient and gases from blood for cell survival.

The device may mimic the Pancreas. Pancreas contains β-cells for insulin release with high perfusion of blood-flow, as may be in this micro-device. Finally, stem-cells or engineered-cells can be used for long-term release of insulin as it is an external device.

References

References

1. Del Campo, A. and E. Arzt, *Fabrication approaches for generating complex micro- and nanopatterns on polymeric surfaces.* Chemical Reviews, 2008. **108**(3): p. 911-945.
2. Geissler, M. and Y.N. Xia, *Patterning: Principles and some new developments.* Advanced Materials, 2004. **16**(15): p. 1249-1269.
3. Pollice, A., et al., *Sub-critical flux fouling in membrane bioreactors--a review of recent literature.* Desalination, 2005. **174**(3): p. 221-230.
4. Zularisam, A., A. Ismail, and R. Salim, *Behaviours of natural organic matter in membrane filtration for surface water treatment--a review.* Desalination, 2006. **194**(1-3): p. 211-231.
5. Chang, I.S., et al., *Membrane fouling in membrane bioreactors for wastewater treatment.* Journal of environmental engineering, 2002. **128**: p. 1018.
6. Popovic, Z., R. Sprague, and G. Connell, *Technique for monolithic fabrication of microlens arrays.* Applied optics, 1988. **27**(7): p. 1281-1284.
7. Chen, J., et al., *Variable-focusing microlens with microfluidic chip.* Journal of Micromechanics and Microengineering, 2004. **14**: p. 675.
8. Orhan, J.B., et al., *Fabrication and characterization of three-dimensional microlens arrays in sol-gel glass.* Journal of Microelectromechanical Systems, 2006. **15**(5): p. 1159-1164.
9. Lim, T.W., et al., *Direct single-layered fabrication of 3D concavo–convex patterns in nano-stereolithography.* Applied Physics A: Materials Science & Processing, 2006. **84**(4): p. 379-383.
10. Yang, R., W. Wang, and S. Soper, *Out-of-plane microlens array fabricated using ultraviolet lithography.* Applied Physics Letters, 2005. **86**: p. 161110.
11. Jeong, K.-H., J. Kim, and L.P. Lee, *Biologically Inspired Artificial Compound Eyes.* Science, 2006. **312**(5773): p. 557-561.
12. Cuisin, C., et al., *Fabrication of three-dimensional photonic structures with submicrometer resolution by x-ray lithography.* Journal of Vacuum Science & Technology B: Microelectronics and Nanometer Structures, 2000. **18**: p. 3505.
13. Kawashima, S., K. Ishizaki, and S. Noda, *Light propagation in three-dimensional photonic crystals.* Optics Express. **18**(1): p. 386-392.
14. Yao, P., et al., *Fabrication of three-dimensional photonic crystals with multilayer photolithography.* Optics Express, 2005. **13**(7): p. 2370-2376.
15. Lin, S.Y., et al., *A three-dimensional photonic crystal operating at infrared wavelengths.* Nature, 1998. **394**(6690): p. 251-253.
16. Nakano, M., et al., *Three-dimensional patterned media for ultrahigh-density optical memory.* Applied Physics Letters, 2004. **85**(2): p. 176-178.
17. Sato, H., et al., *In-channel 3-D micromesh structures using maskless multi-angle exposures and their microfilter application.* Sensors and Actuators a-Physical, 2004. **111**(1): p. 87-92.
18. Nock, V. and R.J. Blaikie, *Fabrication of optical grayscale masks for tapered microfluidic devices.* Microelectronic Engineering, 2008. **85**(5-6): p. 1077-1082.
19. Hoi, S.K., et al., *Microfluidic sorting system based on optical force switching.* Applied Physics B-Lasers and Optics, 2009. **97**(4): p. 859-865.

20. Wang, L., et al., *SU-8 microstructure for quasi-three-dimensional cell-based biosensing.* Sensors and Actuators B-Chemical, 2009. **140**(2): p. 349-355.
21. Tian, C., et al., *Microfabrication of chamber-type microchips and its applications for chemical sensors.* Sensors and Actuators B: Chemical, 1998. **52**(1-2): p. 119-124.
22. Sugioka, K., Y. Hanada, and K. Midorikawa, *3D integration of microcomponents in a single glass chip by femtosecond laser direct writing for biochemical analysis.* Applied Surface Science, 2007. **253**(15): p. 6595-6598.
23. Popov, V.K., et al., *Laser stereolithography and supercritical fluid processing for custom-designed implant fabrication.* Journal of Materials Science: Materials in Medicine, 2004. **15**(2): p. 123-128.
24. Liu, Y., et al., *3D femtosecond laser patterning of collagen for directed cell attachment.* Biomaterials, 2005. **26**(22): p. 4597-4605.
25. Motlagh, D., et al., *Microtextured substrata alter gene expression, protein localization and the shape of cardiac myocytes.* Biomaterials, 2003. **24**(14): p. 2463-2476.
26. Altomare, L. and S. Fare, *Cells response to topographic and chemical micropatterns.* Journal of Applied Biomaterials & Biomechanics, 2008. **6**(3): p. 132-143.
27. Perennes, F., et al., *Sharp beveled tip hollow microneedle arrays fabricated by LIGA and 3D soft lithography with polyvinyl alcohol.* Journal of Micromechanics and Microengineering, 2006. **16**: p. 473.
28. Wang, P., et al. *Hollow polymer microneedle array fabricated by photolithography process combined with micromolding technique*. 2009. IEEE.
29. Hoipkemeier-Wilson, L., et al., *Antifouling Potential of Lubricious, Micro-engineered, PDMS Elastomers against Zoospores of the Green Fouling Alga Ulva (Enteromorpha).* Biofouling: The Journal of Bioadhesion and Biofilm Research, 2004. **20**(1): p. 53 - 63.
30. M. Geissler, Y.X., *Patterning: Principles and Some New Developments.* Advanced Materials, 2004. **16**(15): p. 1249-1269.
31. Kley, E.-B., *Continuous profile writing by electron and optical lithography.* Microelectronic Engineering, 1997. **34**(3-4): p. 261-298.
32. Gimkiewicz, C., et al., *Fabrication of microprisms for planar optical interconnections by use of analog gray-scale lithography with high-energy-beam-sensitive glass.* Applied optics, 1999. **38**(14): p. 2986-2990.
33. Dillon, T., et al. *Process development and application of grayscale lithography for efficient three-dimensionally profiled fiber-to-waveguide couplers*. 2003.
34. Oppliger, Y., et al., *One-step 3D shaping using a gray-tone mask for optical and microelectronic applications.* Microelectronic Engineering, 1994. **23**(1-4): p. 449-454.
35. Daschner, W., et al. *Fabrication of diffractive optical elements using a single optical exposure with a gray level mask*. 1995. Scottsdale, Arizona (USA): AVS.
36. Hanai, K. and Y. Matsumoto, *Comparison of micro chrome patterns in gray scale lithography*, in *Micromachining and Microfabrication Process Technology Ix*, M.A. Maher and J.F. Jakubczak, Editors. 2004. p. 221-228.
37. Qiu, C.K., et al., *Continuous micro-optics fabrication using half tone masks and proximity printing*, in *Holography, Diffractive Optics, and Applications II, Pts 1 and 2*, Y.L. Sheng, et al., Editors. 2005. p. 712-716.
38. Wang, C.T. and C.L. Du, *Rings coded half tone masks for the fabrication of circular micro optical elements*, in *Lithographic and Micromachining Techniques for Optical Component Fabrication Ii*, E.B. Kley and H.P. Herzig, Editors. 2003. p. 199-206.

39. Claydon, G.S. and E.W. Balch, *Design rules for fabrication of binary half tone masks used for MEMS and photonic devices*, in *Micromachining and Microfabrication Process Technology Viii*, J.A. Yasaitis, M.A. PerezMaher, and J.M. Karam, Editors. 2003. p. 337-352.
40. Kalus, M., et al., *Free 3D shaping with grey-tone lithography and multidose e-beam writing.* Microelectronic Engineering, 1998. **41-42**: p. 461-464.
41. Dillon, T., et al., *Continuous-tone grayscale mask fabrication using high-energy-beam-sensitive glass.* Journal of Microlithography Microfabrication and Microsystems, 2004. **3**(4): p. 550-554.
42. Sure, A., et al., *Fabrication and characterization of three-dimensional silicon tapers.* Optics Express, 2003. **11**(26): p. 3555-3561.
43. Dillon, T., et al., *Microlens fabrication using HEBS glass for compact high-resolution IR imaging system - art. no. 63270B.* Nanoengineering: Fabrication, Properties, Optics, and Devices III, 2006. **6327**: p. B3270-B3270.
44. Kim, W.C., et al., *Fabrication of diffractive optical elements with grayscale photo-lithography.* Optical Data Storage 2004, 2004. **5380**: p. 686-696.
45. Sure, A., et al., *Fabrication and characterization of three-dimensional silicon tapers.* Optics Express, 2003. **11**(26): p. 3555-3561.
46. Wang, J., et al., *Bimetallic thin film grayscale photomasks for complex 3D microstructure creation in SU-8.* 2007 Canadian Conference on Electrical and Computer Engineering, Vols 1-3, 2007: p. 959-962.
47. Guo, C.F., et al., *Grayscale photomask fabricated by laser direct writing in metallic nano-films.* Optics Express, 2009. **17**(22): p. 19981-19987.
48. Wu, M.H., C. Park, and G.M. Whitesides, *Fabrication of arrays of microlenses with controlled profiles using gray-scale microlens projection photolithography.* Langmuir, 2002. **18**(24): p. 9312-9318.
49. Chen, C.C., D. Hirdes, and A. Folch, *Gray-scale photolithography using microfluidic photomasks.* Proceedings of the National Academy of Sciences of the United States of America, 2003. **100**(4): p. 1499-1504.
50. McKechnie, J. and D. Sinton, *Dynamic microfluidic photomasking.* Journal of Microelectromechanical Systems, 2007. **16**(5): p. 1145-1151.
51. Hayashia, T., et al., *Photolithography system with liquid crystal display as active gray-tone mask for 3D structuring of photoresist.* Sensors and Actuators a-Physical, 2008. **144**(2): p. 381-388.
52. Lee, S.Y., et al., *Spatial dose control for fabrication of saw-tooth structures.* Journal of Vacuum Science & Technology B, 2009. **27**(6): p. 2580-2584.
53. Yamazaki, K., H. Namatsu, and Ieee, *Three-dimensional nanofabrication (3D-NANO) down to 10-nm order using electron-beam lithography*, in *Mems 2004: 17th Ieee International Conference on Micro Electro Mechanical Systems, Technical Digest*2004, Ieee: New York. p. 609-612.
54. Koller, D.M., et al., *Three-dimensional SU-8 sub-micrometer structuring by electron beam lithography.* Microelectronic Engineering, 2008. **85**(7): p. 1639-1641.
55. van Kan, J.A., A.A. Bettiol, and F. Watt, *Proton Beam Writing of Three-Dimensional Nanostructures in Hydrogen Silsesquioxane.* Nano Letters, 2006. **6**(3): p. 579-582.
56. Van Kan, J., A. Bettiol, and F. Watt, *Three-dimensional nanolithography using proton beam writing.* Applied Physics Letters, 2003. **83**: p. 1629.

57. Yu, H., et al., *Fabrication of three-dimensional microstructures based on singled-layered SU-8 for lab-on-chip applications.* Sensors and Actuators A: Physical, 2006. **127**(2): p. 228-234.
58. Totsu, K., et al., *Fabrication of three-dimensional microstructure using maskless gray-scale lithography.* Sensors and Actuators A: Physical, 2006. **130**: p. 387-392.
59. Maruo, S. and K. Ikuta, *Submicron stereolithography for the production of freely movable mechanisms by using single-photon polymerization.* Sensors and Actuators A: Physical, 2002. **100**(1): p. 70-76.
60. Bärsch, N., et al., *Ablation and cutting of planar silicon devices using femtosecond laser pulses.* Applied Physics A: Materials Science & Processing, 2003. **77**(2): p. 237-242.
61. Lehmann, O. and M. Stuke, *Laser-Driven Movement of Three-Dimensional Microstructures Generated by Laser Rapid Prototyping.* Science, 1995. **270**(5242): p. 1644-1646.
62. Lee, K.-S., et al., *Advances in 3D nano/microfabrication using two-photon initiated polymerization.* Progress in Polymer Science, 2008. **33**(6): p. 631-681.
63. Lee, K.-S., et al., *Recent developments in the use of two-photon polymerization in precise 2D and 3D microfabrications.* Polymers for Advanced Technologies, 2006. **17**(2): p. 72-82.
64. Sun, H. and S. Kawata, *Two-photon laser precision microfabrication and its applications to micro-nano devices and systems.* Journal of lightwave technology, 2003. **21**(3): p. 624.
65. Liu, Y.H., D.D. Nolte, and L.J. Pyrak-Nolte, *Large-format fabrication by two-photon polymerization in SU-8.* Applied Physics a-Materials Science & Processing, 2010. **100**(1): p. 181-191.
66. Malinauskas, M., et al., *A femtosecond laser-induced two-photon photopolymerization technique for structuring microlenses.* Journal of Optics, 2010. **12**(3).
67. Kim, D.Y., et al., *Laser-induced holographic surface relief gratings on nonlinear optical polymer films.* Applied Physics Letters, 1995. **66**(10): p. 1166-1168.
68. Jang, J.H., et al., *3D Micro- and Nanostructures via Interference Lithography.* Advanced Functional Materials, 2007. **17**(16): p. 3027-3041.
69. Campbell, M., et al., *Fabrication of photonic crystals for the visible spectrum by holographic lithography.* Nature, 2000. **404**(6773): p. 53-56.
70. Lin, S., et al., *A three-dimensional photonic crystal operating at infrared wavelengths.* Nature, 1998. **394**(6690): p. 251-253.
71. Lee, K.S., R.H. Kim, and P. Prabhakaran, *Two-photon stereolithography.* Journal of Nonlinear Optical Physics & Materials, 2007. **16**: p. 59-73.
72. Park, S.H., D.Y. Yang, and K.S. Lee, *Two-photon stereolithography for realizing ultraprecise three-dimensional nano/microdevices.* Laser & Photonics Reviews, 2009. **3**(1-2): p. 1-11.
73. Bertsch, A., H. Lorenz, and P. Renaud, *3D microfabrication by combining microstereolithography and thick resist UV lithography.* Sensors and Actuators A: Physical, 1999. **73**(1-2): p. 14-23.
74. Choi, J.W., E. MacDonald, and R. Wicker, *Multi-material microstereolithography.* International Journal of Advanced Manufacturing Technology, 2010. **49**(5-8): p. 543-551.
75. Smay, J.E., et al., *Directed colloidal assembly of 3D periodic structures.* Advanced Materials, 2002. **14**(18): p. 1279-1283.
76. Smay, J.E., J. Cesarano III, and J.A. Lewis, *Colloidal inks for directed assembly of 3-D periodic structures.* Langmuir, 2002. **18**(14): p. 5429-5437.

77. Vlasov, Y.A., et al., *On-chip natural assembly of silicon photonic bandgap crystals.* Nature, 2001. **414**(6861): p. 289-293.
78. Xia, Y., B. Gates, and Z.Y. Li, *Self-assembly approaches to three-dimensional photonic crystals.* Advanced Materials, 2001. **13**(6): p. 409-413.
79. Han, M., et al., *3D microfabrication with inclined/rotated UV lithography.* Sensors and Actuators A: Physical, 2004. **111**(1): p. 14-20.
80. You, H., et al., *Deep X-ray exposure system with multistage for 3D microfabrication.* Journal of Micromechatronics, 2002. **2**(1): p. 1-11.
81. Teo, E., et al., *Three-dimensional microfabrication in bulk silicon using high-energy protons.* Applied Physics Letters, 2004. **84**: p. 3202.
82. Murali, R., et al., *Process optimization and proximity effect correction for gray scale e-beam lithography.* Journal of Vacuum Science & Technology B, 2006. **24**(6): p. 2936-2939.
83. Adams, J.D. and H.T. Soh, *Perspectives on Utilizing Unique Features of Microfluidics Technology for Particle and Cell Sorting.* Jala, 2009. **14**(6): p. 331-340.
84. Gossett, D., et al., *Label-free cell separation and sorting in microfluidic systems.* Analytical and Bioanalytical Chemistry, 2010. **397**(8): p. 3249-3267.
85. Lim, C. and Y. Zhang, *Bead-based microfluidic immunoassays: the next generation.* Biosensors and Bioelectronics, 2007. **22**(7): p. 1197-1204.
86. Ling, M.M., C. Ricks, and P. Lea, *Multiplexing molecular diagnostics and immunoassays using emerging microarray technologies.* Expert Review of Molecular Diagnostics, 2007. **7**(1): p. 87-98.
87. Mohamed, H., et al., *Isolation of tumor cells using size and deformation.* Journal of Chromatography A, 2009. **1216**(47): p. 8289-8295.
88. Tan, S.J., et al., *Microdevice for the isolation and enumeration of cancer cells from blood.* Biomedical Microdevices, 2009. **11**(4): p. 883-892.
89. Fernandez, M.J.S., et al., *Clinical relevance associated to the analysis of circulating tumour cells in patients with solid tumours.* Clinical & Translational Oncology, 2009. **11**(10): p. 659-668.
90. Boos, C.J., G.Y.H. Lip, and A.D. Blann, *Circulating endothelial cells in cardiovascular disease.* Journal of the American College of Cardiology, 2006. **48**(8): p. 1538-1547.
91. Wu, H.W., et al., *A microfluidic device for separation of amniotic fluid mesenchymal stem cells utilizing louver-array structures.* Biomedical Microdevices, 2009. **11**(6): p. 1297-1307.
92. Sethu, P., A. Sin, and M. Toner, *Microfluidic diffusive filter for apheresis (leukapheresis).* Lab on a Chip, 2006. **6**(1): p. 83-89.
93. Di Carlo, D., L.Y. Wu, and L.P. Lee, *Dynamic single cell culture array.* Lab on a Chip, 2006. **6**(11): p. 1445-1449.
94. Charnley, M., et al., *Integration column: microwell arrays for mammalian cell culture.* Integrative Biology, 2009. **1**(11-12): p. 625-634.
95. Pethig, R., *Review Article-Dielectrophoresis: Status of the theory, technology, and applications.* Biomicrofluidics, 2010. **4**(2).
96. Pohl, H.A., *The motion and precipitation of suspensoids in divergent electric fields.* Journal of Applied Physics, 1951. **22**(7): p. 869-871.
97. Barrett, L.M., et al., *Dielectrophoretic Manipulation of Particles and Cells Using Insulating Ridges in Faceted Prism Microchannels.* Analytical Chemistry, 2005. **77**(21): p. 6798-6804.

98. Barbulovic-Nad, I., et al., *DC-dielectrophoretic separation of microparticles using an oil droplet obstacle.* Lab on a Chip, 2006. **6**(2): p. 274-279.
99. Kang, K.H., et al., *Continuous separation of microparticles by size with Direct current-dielectrophoresis.* ELECTROPHORESIS, 2006. **27**(3): p. 694-702.
100. Cummings, E.B. and A.K. Singh, *Dielectrophoresis in Microchips Containing Arrays of Insulating Posts: Theoretical and Experimental Results.* Analytical Chemistry, 2003. **75**(18): p. 4724-4731.
101. Gonzalez, C.F. and V.T. Remcho, *Harnessing dielectric forces for separations of cells, fine particles and macromolecules.* Journal of Chromatography A, 2005. **1079**(1-2): p. 59-68.
102. Doh, I. and Y.H. Cho, *A continuous cell separation chip using hydrodynamic dielectrophoresis (DEP) process.* Sensors and Actuators A: Physical, 2005. **121**(1): p. 59-65.
103. Markx, G.H., M.S. Talary, and R. Pethig, *Separation of viable and non-viable yeast using dielectrophoresis.* Journal of biotechnology, 1994. **32**(1): p. 29-37.
104. Gascoyne, P., et al., *Microsample preparation by dielectrophoresis: isolation of malaria.* Lab on a Chip, 2002. **2**(2): p. 70-75.
105. Becker, F.F., et al., *Separation of human breast cancer cells from blood by differential dielectric affinity.* Proceedings of the National Academy of Sciences of the United States of America, 1995. **92**(3): p. 860-864.
106. Becker, F. and X. Wang, *The removal of human leukaemia cells from blood using interdigitated microelectrodes.* Journal of Physics D: Applied Physics, 1994. **27**: p. 2659.
107. Talary, M., et al., *Dielectrophoretic separation and enrichment of CD34+ cell subpopulation from bone marrow and peripheral blood stem cells.* Medical and Biological Engineering and Computing, 1995. **33**(2): p. 235-237.
108. Borgatti, M., et al., *Separation of white blood cells from erythrocytes on a dielectrophoresis (DEP) based'Lab-on-a-chip'device.* International journal of molecular medicine, 2005. **15**(6): p. 913.
109. Talary, M., et al., *Dielectrophoretic separation and enrichment of CD34+cell subpopulation from bone marrow and peripheral blood stem cells.* Medical and Biological Engineering and Computing, 1995. **33**(2): p. 235-237.
110. Pamme, N., *Magnetism and microfluidics.* Lab on a Chip, 2006. **6**(1): p. 24-38.
111. Xia, N., et al., *Combined microfluidic-micromagnetic separation of living cells in continuous flow.* Biomedical Microdevices, 2006. **8**(4): p. 299-308.
112. Smistrup, K., et al., *Magnetic separation in microfluidic systems using microfabricated electromagnets--experiments and simulations.* Journal of Magnetism and Magnetic Materials, 2005. **293**(1): p. 597-604.
113. Pamme, N. and A. Manz, *On-Chip Free-Flow Magnetophoresis: Continuous Flow Separation of Magnetic Particles and Agglomerates.* Analytical Chemistry, 2004. **76**(24): p. 7250-7256.
114. Ramadan, Q., et al., *Magnetic-based microfluidic platfrom for biomolecular separation.* Biomedical Microdevices, 2006. **8**(2): p. 151-158.
115. Gijs, M.A.M., *Magnetic bead handling on-chip: new opportunities for analytical applications.* Microfluidics and Nanofluidics, 2004. **1**(1): p. 22-40.
116. Zaytseva, N.V., et al., *Development of a microfluidic biosensor module for pathogen detection.* Lab on a Chip, 2005. **5**(8): p. 805-811.
117. Yung, C.W., et al., *Micromagnetic-microfluidic blood cleansing device.* Lab on a Chip, 2009. **9**(9): p. 1171-1177.

118. Pamme, N. and C. Wilhelm, *Continuous sorting of magnetic cells via on-chip free-flow magnetophoresis.* Lab on a Chip, 2006. **6**(8): p. 974-980.
119. Furdui, V.I. and D.J. Harrison, *Immunomagnetic T cell capture from blood for PCR analysis using microfluidic systems.* Lab on a Chip, 2004. **4**(6): p. 614-618.
120. Han, K.-H. and A.B. Frazier, *Paramagnetic capture mode magnetophoretic microseparator for high efficiency blood cell separations.* Lab on a Chip, 2006. **6**(2): p. 265-273.
121. Dholakia, K., P. Reece, and M. Gu, *Optical micromanipulation.* Chemical Society Reviews, 2008. **37**(1): p. 42-55.
122. Ashkin, A., *Optical trapping and manipulation of neutral particles using lasers.* Proceedings of the National Academy of Sciences of the United States of America, 1997. **94**(10): p. 4853-4860.
123. Ashkin, A., *Acceleration and trapping of particles by radiation pressure.* Physical Review Letters, 1970. **24**(4): p. 156-159.
124. Ashkin, A. and J. Dziedzic, *Optical trapping and manipulation of viruses and bacteria.* Science, 1987. **235**(4795): p. 1517-1520.
125. Ashkin, A. and J.M. Dziedzic, *Optical trapping and manipulation of single living cells using infra-red laser beams.* Berichte der Bunsengesellschaft für physikalische Chemie, 1989. **93**(3): p. 254-260.
126. Wang, M.M., et al., *Microfluidic sorting of mammalian cells by optical force switching.* Nat Biotech, 2005. **23**(1): p. 83-87.
127. Perroud, T.D., et al., *Microfluidic-Based Cell Sorting of Francisella tularensis Infected Macrophages Using Optical Forces.* Analytical Chemistry, 2008. **80**(16): p. 6365-6372.
128. Dao, M., C. Lim, and S. Suresh, *Mechanics of the human red blood cell deformed by optical tweezers.* Journal of the Mechanics and Physics of Solids, 2003. **51**(11-12): p. 2259-2280.
129. Brandao, M., et al., *Optical tweezers for measuring red blood cell elasticity: application to the study of drug response in sickle cell disease.* European journal of haematology, 2003. **70**(4): p. 207-211.
130. Laurell, T., F. Petersson, and A. Nilsson, *Chip integrated strategies for acoustic separation and manipulation of cells and particles.* Chemical Society Reviews, 2007. **36**(3): p. 492-506.
131. Terence Coakley, W., *Ultrasonic separations in analytical biotechnology.* Trends in biotechnology, 1997. **15**(12): p. 506-511.
132. Hawkes, J.J. and W.T. Coakley, *Force field particle filter, combining ultrasound standing waves and laminar flow.* Sensors and Actuators B: Chemical, 2001. **75**(3): p. 213-222.
133. Nilsson, A., et al., *Acoustic control of suspended particles in micro fluidic chips.* Lab on a Chip, 2004. **4**(2): p. 131-135.
134. Petersson, F., et al., *Free Flow Acoustophoresis: Microfluidic-Based Mode of Particle and Cell Separation.* Analytical Chemistry, 2007. **79**(14): p. 5117-5123.
135. Petersson, F., et al., *Continuous separation of lipid particles from erythrocytes by means of laminar flow and acoustic standing wave forces.* Lab on a Chip, 2005. **5**(1): p. 20-22.
136. Giddings, J.C., *A System Based on Split-Flow Lateral-Transport Thin (SPLITT) Separation Cells for Rapid and Continuous Particle Fractionation.* Separation Science and Technology, 1985. **20**(9): p. 749 - 768.

137. Yamada, M., M. Nakashima, and M. Seki, *Pinched Flow Fractionation: Continuous Size Separation of Particles Utilizing a Laminar Flow Profile in a Pinched Microchannel.* Analytical Chemistry, 2004. **76**(18): p. 5465-5471.
138. Zhang, X., et al., *Continuous flow separation of particles within an asymmetric microfluidic device.* Lab on a Chip, 2006. **6**(4): p. 561-566.
139. Takagi, J., et al., *Continuous particle separation in a microchannel having asymmetrically arranged multiple branches.* Lab on a Chip, 2005. **5**(7): p. 778-784.
140. Chen, X., et al., *Continuous flow microfluidic device for cell separation, cell lysis and DNA purification.* Analytica Chimica Acta, 2007. **584**(2): p. 237-243.
141. Zheng, S., et al., *Membrane microfilter device for selective capture, electrolysis and genomic analysis of human circulating tumor cells.* Journal of Chromatography A, 2007. **1162**(2): p. 154-161.
142. Chen, Z.Z., et al., *Pool-dam structure based microfluidic devices for filtering tumor cells from blood mixtures.* Surface and Interface Analysis, 2006. **38**(6): p. 996-1003.
143. Wilding, P., et al., *Integrated cell isolation and polymerase chain reaction analysis using silicon microfilter chambers.* Analytical Biochemistry, 1998. **257**(2): p. 95-100.
144. Zhu, L., et al., *Cell loss in integrated microfluidic device.* Biomedical Microdevices, 2007. **9**(5): p. 745-750.
145. Chandler, M. and A. Zydney, *Effects of membrane pore geometry on fouling behavior during yeast cell microfiltration.* Journal of Membrane Science, 2006. **285**(1-2): p. 334-342.
146. Ji, H.M., et al., *Silicon-based microfilters for whole blood cell separation.* Biomedical Microdevices, 2008. **10**(2): p. 251-257.
147. VanDelinder, V. and A. Groisman, *Separation of Plasma from Whole Human Blood in a Continuous Cross-Flow in a Molded Microfluidic Device.* Analytical Chemistry, 2006. **78**(11): p. 3765-3771.
148. Yamada, M. and M. Seki, *Hydrodynamic filtration for on-chip particle concentration and classification utilizing microfluidics.* Lab on a Chip, 2005. **5**(11): p. 1233-1239.
149. Yamada, M. and M. Seki, *Microfluidic Particle Sorter Employing Flow Splitting and Recombining.* Analytical Chemistry, 2006. **78**(4): p. 1357-1362.
150. Jäggi, R., R. Sandoz, and C. Effenhauser, *Microfluidic depletion of red blood cells from whole blood in high-aspect-ratio microchannels.* Microfluidics and Nanofluidics, 2007. **3**(1): p. 47-53.
151. Shevkoplyas, S.S., et al., *Biomimetic Autoseparation of Leukocytes from Whole Blood in a Microfluidic Device.* Analytical Chemistry, 2004. **77**(3): p. 933-937.
152. Yang, S., A. Undar, and J.D. Zahn, *A microfluidic device for continuous, real time blood plasma separation.* Lab on a Chip, 2006. **6**(7): p. 871-880.
153. Sim, T.S., et al., *Multistage-multiorifice flow fractionation (MS-MOFF): continuous size-based separation of microspheres using multiple series of contraction/expansion microchannels.* Lab on a Chip, 2011. **11**(1): p. 93-99.
154. Huang, L.R., et al., *Continuous Particle Separation Through Deterministic Lateral Displacement.* Science, 2004. **304**(5673): p. 987-990.
155. Inglis, D.W., et al., *Critical particle size for fractionation by deterministic lateral displacement.* Lab on a Chip, 2006. **6**(5): p. 655.
156. Davis, J.A., et al., *Deterministic hydrodynamics: Taking blood apart.* Proceedings of the National Academy of Sciences, 2006. **103**(40): p. 14779-14784.

157. Zheng, S., et al. *Deterministic lateral displacement MEMS device for continuous blood cell separation*. 2005. IEEE.
158. Green, J.V., M. Radisic, and S.K. Murthy, *Deterministic Lateral Displacement as a Means to Enrich Large Cells for Tissue Engineering.* Analytical Chemistry, 2009. **81**(21): p. 9178-9182.
159. Inglis, D.W., et al., *Determining blood cell size using microfluidic hydrodynamics.* Journal of Immunological Methods, 2008. **329**(1-2): p. 151-156.
160. Choi, S. and J.-K. Park, *Continuous hydrophoretic separation and sizing of microparticles using slanted obstacles in a microchannel.* Lab on a Chip, 2007. **7**(7): p. 890-897.
161. Choi, S., et al., *Continuous blood cell separation by hydrophoretic filtration.* Lab on a Chip, 2007. **7**(11): p. 1532-1538.
162. Di Carlo, D., *Inertial microfluidics.* Lab on a Chip, 2009. **9**(21): p. 3038-3046.
163. Bhagat, A.A.S., S.S. Kuntaegowdanahalli, and I. Papautsky, *Continuous particle separation in spiral microchannels using dean flows and differential migration.* Lab on a Chip, 2008. **8**(11): p. 1906-1914.
164. Johann, R.M., *Cell trapping in microfluidic chips.* Analytical and Bioanalytical Chemistry, 2006. **385**(3): p. 408-412.
165. Sangeeta N. Bhatia, M.L.Y., Mehmet Toner,, *Controlling cell interactions by micropatterning in co-cultures: Hepatocytes and 3T3 fibroblasts.* Journal of Biomedical Materials Research, 1997. **34**(2): p. 189-199.
166. Wang, L., et al., *Patterning bio-molecules for cell attachment at single cell levels in PDMS microfluidic chips.* Microelectronic Engineering, 2009. **86**(4-6): p. 1462-1464.
167. Xia, Y.N. and G.M. Whitesides, *Soft lithography.* Annual Review of Materials Science, 1998. **28**: p. 153-184.
168. Kim, E., Y. Xia, and G.M. Whitesides, *Polymer microstructures formed by moulding in capillaries.* Nature, 1995. **376**(6541): p. 581-584.
169. Jackman, R., J. Wilbur, and G. Whitesides, *Fabrication of submicrometer features on curved substrates by microcontact printing.* Science, 1995. **269**(5224): p. 664-666.
170. Albert Folch, M.T., *Cellular Micropatterns on Biocompatible Materials.* Biotechnology Progress, 1998. **14**(3): p. 388-392.
171. Folch, A., et al., *Microfabricated elastomeric stencils for micropatterning cell cultures.* Journal of Biomedical Materials Research, 2000. **52**(2): p. 346-353.
172. Takayama, S., et al., *Patterning cells and their environments using multiple laminar fluid flows in capillary networks.* Proceedings of the National Academy of Sciences of the United States of America, 1999. **96**(10): p. 5545-5548.
173. Takayama, S., et al. *Patterning the topographical environment for mammalian cell culture using laminar flows in capillaries*. in *1st Annual International IEEE-EMBS Special Topic Conference on Microtechnologies in Medicine & Biology*. 2000. Lyon, France.
174. Hong, J., J.B. Edel, and A.J. deMello, *Micro- and nanofluidic systems for high-throughput biological screening.* Drug Discovery Today, 2009. **14**(3-4): p. 134-146.
175. Ito, Y., *Surface micropatterning to regulate cell functions.* Biomaterials, 1999. **20**(23-24): p. 2333-2342.
176. Ashkin, A., *Acceleration and trapping of particles by radiation pressure.* **physical review letters** 1970. **4**: p. 156-59.
177. Desai, J.P., A. Pillarisetti, and A.D. Brooks, *Engineering approaches to biomanipulation.* Annual Review of Biomedical Engineering, 2007. **9**: p. 35-53.

178. Kimura, T., et al., *Micropatterning of Cells Using Modulated Magnetic Fields.* Langmuir, 2005. **21**(3): p. 830-832.
179. Di Carlo, D., N. Aghdam, and L.P. Lee, *Single-Cell Enzyme Concentrations, Kinetics, and Inhibition Analysis Using High-Density Hydrodynamic Cell Isolation Arrays.* Analytical Chemistry, 2006. **78**(14): p. 4925-4930.
180. Deutsch, M., et al., *A novel miniature cell retainer for correlative high-content analysis of individual untethered non-adherent cells.* Lab on a Chip, 2006. **6**(8): p. 995-1000.
181. Braschler, T., et al., *Gentle cell trapping and release on a microfluidic chip by in situ alginate hydrogel formation.* Lab on a Chip, 2005. **5**(5): p. 553-559.
182. Pishko, M.V. and Ieee. *Microfabricated cell-based biosensor arrays*. in *27th Annual International Conference of the IEEE-Engineering-in-Medicine-and-Biology-Society*. 2005. Shanghai, PEOPLES R CHINA.
183. del Campo, A. and C. Greiner, *SU-8: a photoresist for high-aspect-ratio and 3D submicron lithography.* Journal of Micromechanics and Microengineering, 2007. **17**(6): p. R81-R95.
184. Campo, A. and C. Greiner, *SU-8: a photoresist for high-aspect-ratio and 3D submicron lithography.* Journal of Micromechanics and Microengineering, 2007. **17**: p. R81.
185. Liu, J., et al., *Process research of high aspect ratio microstructure using SU-8 resist.* Microsystem Technologies, 2004. **10**(4): p. 265-268.
186. Becnel, C. and et al., *Ultra-deep x-ray lithography of densely packed SU-8 features: I. An SU-8 casting procedure to obtain uniform solvent content with accompanying experimental results.* Journal of Micromechanics and Microengineering, 2005. **15**(6): p. 1242.
187. Tan, T.L., et al., *Study of a Chemically Amplified Resist for X-ray Lithography by Fourier Transfrom Infrared Spectroscopy.* Appl. Spectrosc., 2004. **58**(11): p. 1288-1294.
188. Smith, B., *Infrared Spectral Interpretation, a systematic approach*1999, New York: CRC Press. p. 75-81.
189. Shaw, J.M., et al., *Negative photoresists for optical lithography.* Ibm Journal of Research and Development, 1997. **41**(1-2): p. 81-94.
190. Nagrath, S., et al., *Isolation of rare circulating tumour cells in cancer patients by microchip technology.* Nature, 2007. **450**(7173): p. 1235-U10.
191. Talasaz, A.H., et al., *Isolating highly enriched populations of circulating epithelial cells and other rare cells from blood using a magnetic sweeper device.* Proceedings of the National Academy of Sciences, 2009. **106**(10): p. 3970-3975.
192. Toner, M. and D. Irimia, *Blood-on-a-chip.* Annual Review of Biomedical Engineering, 2005. **7**: p. 77-103.
193. Hu, X., et al., *Marker-specific sorting of rare cells using dielectrophoresis.* Proceedings of the National Academy of Sciences of the United States of America, 2005. **102**(44): p. 15757-15761.
194. Adams, J.D., U. Kim, and H.T. Soh, *Multitarget magnetic activated cell sorter.* Proceedings of the National Academy of Sciences, 2008. **105**(47): p. 18165-18170.
195. Ramser, K. and D. Hanstorp, *Optical manipulation for single-cell studies.* Journal of Biophotonics, 2010. **3**(4): p. 187-206.
196. Zheng, S., et al., *Membrane microfilter device for selective capture, electrolysis and genomic analysis of human circulating tumor cells.* Journal of Chromatography A, 2007. **1162**(2): p. 154-161.

197. Lewis, S.R., et al., *Reactive nanostructured membranes for water purification.* Proceedings of the National Academy of Sciences, 2011. **108**(21): p. 8577-8582.
198. Ozdemir, S.S., M.G. Buonomenna, and E. Drioli, *Catalytic polymeric membranes: Preparation and application.* Applied Catalysis a-General, 2006. **307**(2): p. 167-183.
199. Sheridan, S.D., et al., *Microporous membrane growth substrates for embryonic stem cell culture and differentiation*, in *Stem Cell Culture*2008, Elsevier Academic Press Inc: San Diego. p. 29-+.
200. Higuchi, A. and Y. Tsukamoto, *Cell separation of hepatocytes and fibroblasts through surface-modified polyurethane membranes.* Journal of Biomedical Materials Research Part A, 2004. **71A**(3): p. 470-479.
201. Wei, H., et al., *Particle sorting using a porous membrane in a microfluidic device.* Lab on a Chip, 2011. **11**(2): p. 238-245.
202. Dai, J., G.L. Baker, and M.L. Bruening, *Use of Porous Membranes Modified with Polyelectrolyte Multilayers as Substrates for Protein Arrays with Low Nonspecific Adsorption.* Analytical Chemistry, 2005. **78**(1): p. 135-140.
203. Nabatiyan, A., et al., *Membrane-based plasma collection device for point-of-care diagnosis of HIV.* Journal of Virological Methods, 2011. **173**(1): p. 37-42.
204. Stromberg, R.R., et al., *Membrane technology applied to donor plasmapheresis.* Journal of Membrane Science, 1989. **44**(1): p. 131-143.
205. Choi, H., et al., *Influence of cross-flow velocity on membrane performance during filtration of biological suspension.* Journal of Membrane Science, 2005. **248**(1-2): p. 189-199.
206. Sims, C.E. and N.L. Allbritton, *Analysis of single mammalian cells on-chip.* Lab on a Chip, 2007. **7**(4): p. 423-440.
207. Saliba, A.-E., et al., *Microfluidic sorting and multimodal typing of cancer cells in self-assembled magnetic arrays.* Proceedings of the National Academy of Sciences, 2010. **107**(33): p. 14524-14529.